

POLITECNICO DI TORINO



**Politecnico
di Torino**

MASTER DEGREE THESIS

A.Y. 2022/2023

Design of Metasurface Antennas.

Supervisor:

Prof. Giuseppe VECCHI

**Co-supervisor and
tutor:**

Giorgio GIORDANENGO

Marcello ZUCCHI

Lucia TEODORANI

Candidate:

Antonino Samuele Giuseppe

CUCINOTTA

286274

Contents

Acknowledgments	5
Abstract	5
Introduction	5
Significance of the Study	5
Thesis organization	5
1 Metasurface antennas	9
1.1 Metasurface overview and general attributes	9
1.2 Metasurface antennas	11
1.2.1 State of the art	11
1.2.2 Current developments	14
2 Numerical simulation	16
2.1 Equations and parameters involved	16
2.1.1 Maxwell's equations	16
2.1.2 Helmholtz equation	17
2.1.3 Plane wave propagation	17
2.1.4 Wavelength	18
2.1.5 Far-Field conditions	19
2.1.6 Field polarization	20
2.1.7 Antenna directivity	20
2.1.8 Antenna gain	21
2.1.9 Radiation pattern	21
2.1.10 Link budget, Friis formula	22
2.1.11 Scattering parameters	23
2.1.12 Leaky-wave antennas	24
2.1.13 Electromagnetic modeling	25
2.2 CST software	28
2.2.1 CST environment	29
2.2.2 Time Domain solver	29
2.2.3 Frequency Domain solver	30
2.2.4 Matlab-CST interface	31
3 Automatic code development for Metasurface antenna design	32
3.1 Possible approaches	32
3.2 Automatic structure generation	32
3.2.1 Dielectric substrate and ground plane generation	35
3.2.2 Feeding element generation	37
3.2.3 Radiating elements generation	39
3.2.4 VBA scripting examples	41
3.2.5 Matlab scripting examples	42

3.3	Creating Matlab functions	44
3.3.1	Circular substrate generation	44
3.3.2	Circular GND plane generation	46
3.3.3	Coax cable feeder generation	46
3.3.4	Circular patches generation	47
3.3.5	Elliptical patches generation	48
3.3.6	Coffee bean generation	49
3.3.7	Double anchors generation	50
3.4	VBA functions	54
3.5	Parameters extraction	58
3.6	Feeder optimization	58
3.7	Impedance reconstruction comparisons	64
3.8	MTS and feeder simulations	65
4	Numerical results	67
4.1	Automatic modelling of MTS antenna	67
4.2	Feeder design and optimization	68
4.3	Feed efficiency optimization	73
4.4	Simulation results and performance of complete MTS structure	76
4.4.1	Impedance reconstruction results	82
4.5	Discussion on improvements	91
5	Conclusions	93
	Bibliography	94

List of Figures

1	Curved wavefront supported by impedance modulation [2].	9
2	Isotropic and anisotropic MTS examples.	10
3	Gain over relative bandwidth trend for different antenna systems. . .	12
4	Different designs for multibeam purposes.	13
5	Top view of the MTS structure, emphasis on square patches modulation and ports disposition.	14
6	Generic traveling plane wave.	18
7	Transmitting antenna example.	19
8	Radiation pattern examples. (a) shows an example of antenna radiation pattern in Cartesian form and (b) shows a polar representation (of a radiation pattern different from the previous one).	22
9	Multiscale problem. (a) shows the <i>macroscale</i> related to antenna total dimensions; (b) shows <i>mesoscale</i> related to local lattice dimensions; (c) shows <i>microscale</i> related to patches and mesh dimensions.	26
10	MTS modeling approach.	27
11	Examples of physically realized MTS antenna.	28
12	CST examples of MTS antennas. (a) shows a structure with variable-size circular patches as radiating elements; (b) shows a structure with double anchors shapes as radiating elements.	28
13	Finite domain discretization of Maxwell's equations.	30
14	CST implementation of general MTS (not complete) structures. (a) shows a circular antenna geometry; (b) shows a square antenna geometry.	33
15	First example of MTS antenna complete structure with circular patches as radiating elements. CST implementation.	34
16	Detailed CST views of the square dielectric structure.	36
17	Detailed CST views of the circular dielectric structure.	37
18	Detailed CST views of the coaxial feeding system.	38
19	Isolated CST views of the coaxial feeding system.	39
20	Radiating elements examples [4].	40
21	Automatic generation of a cylinder in VBA.	42
22	Coffee bean shape, step-by-step CST implementation.	50
23	Double anchor shape, step-by-step CST implementation.	54
24	Generic triangular polygon generation.	55
25	Generic triangular polygon generation.	56
26	Geometric form obtained by exploiting mirroring function.	57
27	Power contributes of a generic MTS antenna. Taken from [17].	59
28	Zoomed view of the feeding annular termination of a practical MTS antenna. Taken from [4].	61
29	Zoomed view of the feeding annular termination of a MTS antenna implemented in CST environment.	61
30	Intuitive feeder termination structures.	63

31	Partitioning of the MTS domain.	64
32	CST designs of the feeding design before and after the optimization. . .	69
33	CST implementation of the complete structure simulated for the feeder optimization. Just the dielectric slab is considered at this level. . . .	70
34	Performance comparisons between optimized and non-optimized feeder. Blue curves report the non-optimized feeder trends, red curves report the optimized feeder trends.	71
35	S_{11} comparison between optimized feeder structures.	72
36	Comparison of input impedance values between the only substrate and complete MTS structure. The blue curve reports the reference impedance value for a structure made only by a dielectric substrate, red curve reports the reference impedance value for a complete MTS antenna structure with a random Metasurface distribution.	73
37	CST 3D perspective view of the model used for feed efficiency op- timization. Red elements are the waveguide ports implemented to measure the surface wave power propagating through the dielectric substrate.	74
38	Comparison between SW and input power trends. Red curve shows the input power, blue curve shows the SW power.	75
39	CST implementation of the complete MTS antenna with double an- chors elements. The pane shows the zoomed view of radiating ele- ments and the feeding system exploited for the considered design. . .	77
40	Reactance and optimized current distributions for the complete dou- ble anchors MTS antenna. Patterns are exploited to synthesized the MTS lattice.	78
41	Perspective CST view of the FF radiation of the complete MTS an- tenna structure with double anchor elements.	79
42	Lateral CST view of the FF radiation of the complete MTS antenna structure with double anchor elements.	80
43	Simulation results, FF Directivity Co-Polarization components of the designed MTS antenna for different plane cuts.	81
44	Current density distributions for isolated and continuous MTS cells partitioning.	83
45	Current density and synthesized reactance profiles for square and hexagonal MTS partitioning.	84
46	CST view of MTS circular antenna with circular patches designed exploiting square cells.	85
47	CST view of MTS circular antenna with circular patches designed exploiting hexagonal cells.	86
48	Comparisons of FF Directivity plane cut $\phi = 0^\circ$ and $\phi = 90^\circ$ for square isolated and continuous MTS partitioning.	87
49	Comparisons of FF Directivity plane cut $\phi = 0^\circ$ and $\phi = 90^\circ$ for hexagonal isolated and continuous MTS partitioning.	88
50	3D FF Directivity for each designed MTS antenna.	90

Acknowledgments

Firstly I would like to say that I'm really grateful to Professor Giuseppe Vecchi who gave me the opportunity to develop this thesis and to approach the working world allowing me to spend my traineeship at *Fondazione LINKS*. In this regard, I would also like to extend my deepest gratitude and appreciation to Giorgio Giordanengo, Marcello Zucchi, Lucia Teodorani, and to all the components of *Fondazione LINKS* who shared with me any kind of tips or help from their experience background. This was fundamental for me to make steps forward in front of the various tasks that came out during the development of this work.

Finally, I express my special thanks to my family and friends whose support and appreciation were, from the beginning, essential to carry out my assignments in any kind of context.

Abstract

Metamaterials are artificial materials composed of various inclusion types embedded in a host medium in specific arrangements. These materials are often exploited because their macroscopic characteristics are not just related to the molecular structure but to their building geometry. This aspect allows one to work on the properties of a certain Metamaterial starting from its structure instead of its chemical composition. A *metasurface* (*MTS*) is a thin metamaterial layer (2D metamaterial). MTSs can be designed to provide engineered boundary conditions for controlling the propagation of surface waves and radiation.

Considering this, the use of metasurfaces can be extremely helpful in order to create antennas whose properties can be “easier” controlled by exploiting more degrees of freedom compared to commonly used materials.

This thesis work aims at the creation of a *scripting code* able to provide the automatic generation of complete MTS antenna structures exploiting commercial software environments (Microwave Studio and Matlab, as properly described in the following chapters), at the validation of designed models through numerical simulations and at the model optimizations in order to improve performances for new possible scenarios.

Introduction

Significance of the Study

Antenna systems are widely used by a large kind of communication links in order to act as transmitting and/or receiving equipment. Due to its principal purpose, antenna developments and improvements are highly promoted by research.

Considering the critical role that free space signal propagation carries out for communication intents, to correctly satisfy communication link requirements, an antenna (both receiving or transmitting) must be quite consistent with directional performance constraints, ruled by the application they are involved in.

Array-antennas, composed of sets of electromagnetic emitters, are able to produce a radiation beam with precise directional characteristics exploiting single radiating element properties, such as their relative position or phase differences of the relative signals (phased array).

Array-based antennas are therefore, theoretically, able to respect high performance requirements, but it must be considered that they are inherently limited by some restrictions like the segmentation of the aperture, the size of their elements, and the feeding complexity that typically ends in a complex and expensive implementation of the antenna itself.

Hence, there is a need for some engineered design able to provide the desired characteristics at an acceptable level of complexity and cost.

For this purpose, Metasurface antennas play a key role. These kinds of antenna are realized by using sheet materials that are usually composed of metallic patches or dielectric etchings in planar or multi-layer configurations with sub-wavelength thickness. They have the advantages of light weight, ease of fabrication, and the ability to control wave propagation both on the surface (*surface wave propagations* and in the surrounding free space (radiated field) [1].

Thesis organization

This document is organized as follows:

- *Chapter 1*: overview and description of Metasurface antennas by characterizing attributes and operations.
- *Chapter 2*: introduction to numerical simulations, theoretical formulas and parameters involved. Presentation of exploited commercial simulation software.
- *Chapter 3*: step-by-step development of the automatic scripting code used to

create the complete antenna structures inside the simulation software environment.

- *Chapter 4*: presentation of numerical results obtained by full-wave simulations and optimizations supported by plots and figures. Improvements and possible approaches to new scenarios.
- *Chapter 5*: conclusions.

1 Metasurface antennas

1.1 Metasurface overview and general attributes

Metasurfaces are two-dimensional (2D) or planar versions of metamaterials with subwavelength thickness. They have unique abilities for blocking, absorbing, concentrating, dispersing, or guiding waves both on the surface at grazing incidence and in space at normal and oblique incidence [1].

A MTS can be macroscopically described by averaging the tangential fields. This leads to a characterization based on homogenized *isotropic or anisotropic boundary conditions* that can be described by a homogeneous equivalent impedance. This characteristic can be graphically sketched as in Figure 1 that shows how a *curved* wave propagation is supported starting from an impedance modulation.

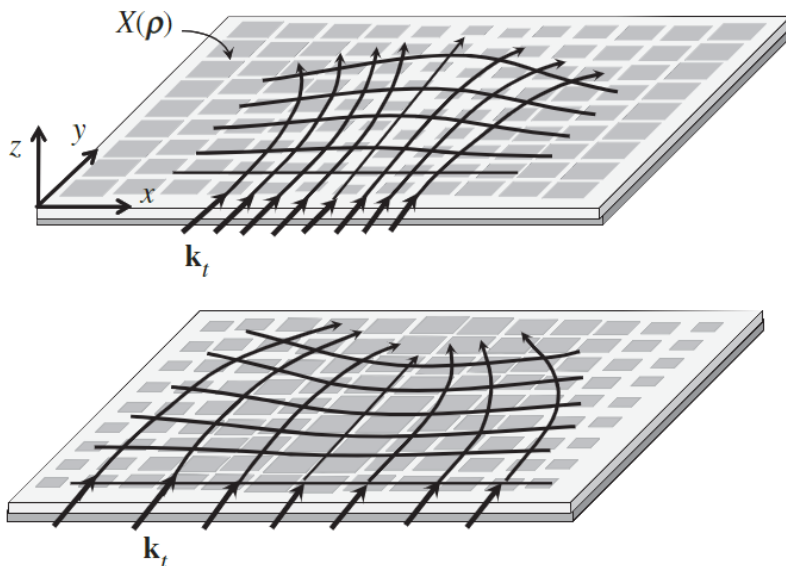
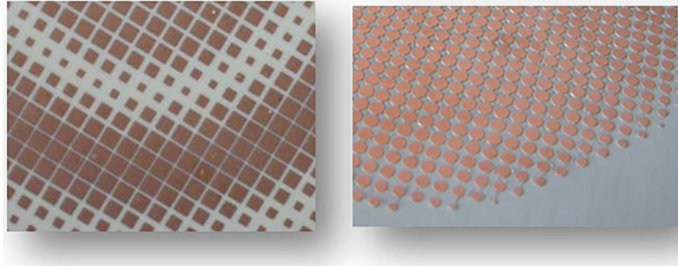


Figure 1: Curved wavefront supported by impedance modulation [2].

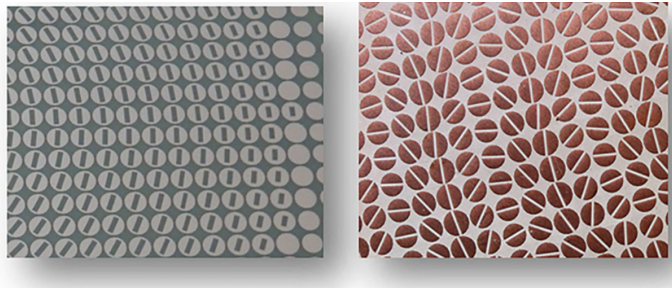
Considering its intrinsic features, a Metasurface can be exploited to control the propagation of *plane* and *surface* waves (SWs). This controlling operation can be obtained just by exploiting the equivalent impedance characteristic. More specifically, it is done by modulating the impedance value through a spatial modulation described by the local change of size, or orientation, of the texture elements that compose the MTS.

The implied *impedance boundary conditions (IBC)* lead to the definition of a certain

Surface Wave Tensor that will describe the propagation of the SW. Differently, when the shape of the elements is regular enough (Figure 2a), the impedance tensor becomes a scalar and therefore the average effect of the boundary conditions is isotropic with respect to the direction of propagation of the SW. When the element shape contains additional features, like slots, grooves, or cuts, the effect is anisotropic and the anisotropy can be easily controlled for elements with two orthogonal symmetry axes (Figure 2b) [2].



(a) Isotropic MTS: regular square and circular patches with variable sizes.



(b) Anisotropic MTS: circular patches with an internal slot or cuts. Presence of two symmetry axes.

Figure 2: Isotropic and anisotropic MTS examples.

Metasurfaces can be practically realized in two main ways. Using very thin host mediums or conducting screens (characterized by small holes), realizing *penetrable MTSs*. Otherwise, exploiting grounded dielectric slabs by printing small and periodic elements on their surface, defining *impenetrable MTSs*.

All the investigations developed in this work are performed on antennas designed by using Metasurfaces constituted by perfectly electric conducting elements printed on a dielectric substrate. A grounded dielectric is used to obtain a guided mode through the *supercritical reflections* that happen inside the slab. This imposes, at the interface between MTS and free space, an equivalent boundary condition defined by a *reactive impedance* $Z(\rho) = jX(\rho)$.

Therefore, it can be guessed that the above discussed spatial modulation of the printed elements leads to the variability of the reactance $X(\rho)$.

1.2 Metasurface antennas

Metasurface antennas exploit the interference between two or more waves to generate a different wave phenomenon. This is specifically obtained by properly designing the arrangements of electrically small *metallic-dielectric* inclusions in a regular planar lattice.

Assuming that a certain plane wave is propagating inside a regular lattice substrate, with elements printed on the surface, the propagation can be described by defining its *wavevectors* k_t . The value of $|k_t|$ at a certain point of the structure can be modulated by properly controlling the reactance value at that point. More precisely, the larger the value of reactance, the larger the local decrease of wavevector value. Such effect is directly related to a local phase velocity decreasing. What is macroscopically obtained is that the wavevector is forced to bend towards the region characterized by higher levels of impedance, as shown in Figure 1.

The surface wave propagation can be generally described by a field whose tangential electric components present a behavior described by:

$$E_t^{SW} \cong V_0(\rho)\hat{k}_t e^{-j\phi(\rho)} \quad (1)$$

where the local wavevector $k_t = \nabla_t\phi(\rho)$.

The described functioning is related most to regular elements, making an isotropic situation. A more complex situation is linked to elements that present more symmetry axes because, in that case, the local impedance is described by a *tensor impedance*.

The use of anisotropic impedance boundary conditions leads to obtaining an aperture field quite controllable through the interaction between the surface wave. In particular, it is ruled by a *leaky wave (LW)* effect. Such principle is related to the “energy leakage” and it can be intuitively associated with losses due to dissipative systems. In open systems, the oscillation energy can also be gradually lost in the form of radiation toward the remote boundaries of an open region.

These structures exploit the MTS lattice by using elements that, considering the operating frequency, are small in terms of wavelength (typically from $\lambda_0/5$ to $\lambda_0/10$). This approach is identified as *pixel-like*. In this way, the propagating surface wave sees the boundary condition defined by the interface impedance as a continuum.

1.2.1 State of the art

The attractive features discussed make these types of devices very interesting in the research context. Indeed, a quite large number of challenging designs have been proposed by several papers and articles in the literature.

Metasurface antennas, or in general Leaky-Wave antennas are characterized by the reduction of feeding complexity by using a single feeder. Moreover, they represent

a significant solution for low-profile and high-directivity applications.

Considering *Huygens MTSs*, which are described by surfaces with orthogonal electric and magnetic current that act as ideal sources (Huygens source), in [3] is proposed a solution to alter and control the propagation of electromagnetic field by maintaining the continuity of the tangential fields across a material boundary. It has to be emphasized that, this is not made by commonly using material interfaces, but by purposely engineering the boundary itself to obtain desired wave propagation effects. This will allow achieving a desired behavior by synthetizing a surface of currents, and so have a larger degree of freedom in radiating field control.

Moreover, other purposes can be taken into account as the *multi beam radiation*, and the achieving of an extended *relative bandwidth* (until 35%) linked to a gain value comparable to high gain antennas.

The trend of gain with respect to the relative bandwidth of different antenna systems is shown in the following figure.

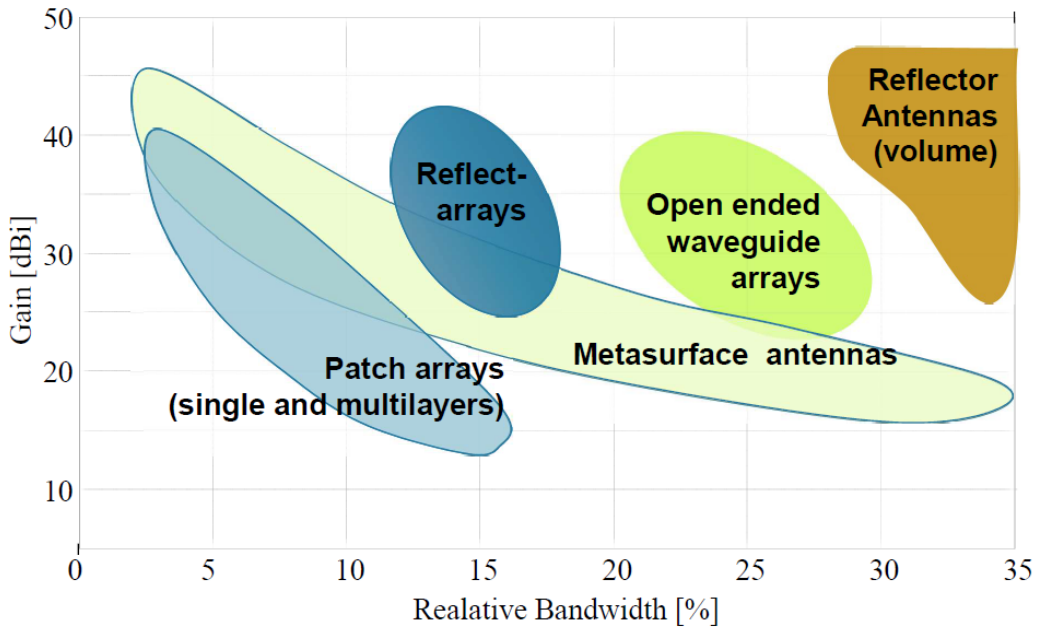


Figure 3: Gain over relative bandwidth trend for different antenna systems.

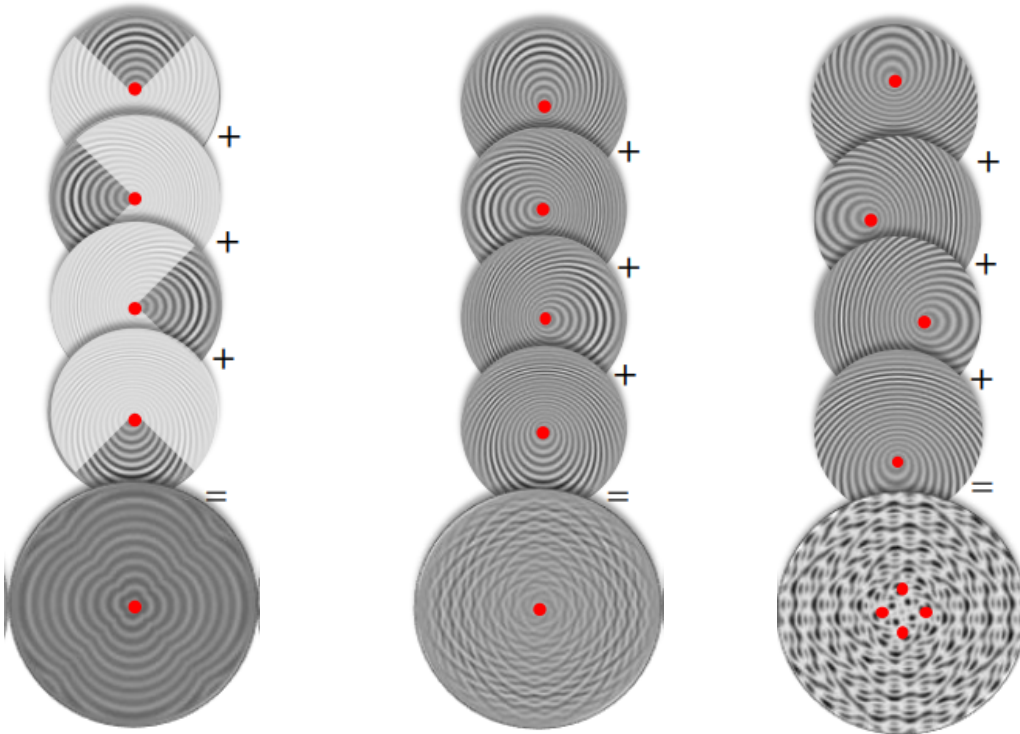
In [4] there are presented several new designs and prototypes of MTS antennas which possess high-efficiency (for broadside and squinted beams), shaped beam, broadband, dual-band, and dual-beam, respectively; these prototypes extend considerably the class of applications covered by this technology.

Regarding multi-beam approaches, recent works [5] [6] deal with isotropic surface impedances, which present poor performance in terms of aperture efficiency. Since this feature is a key parameter in many applications, *David González-Ovejero et al.* propose different possibilities for designing multibeam antennas using a single

Metasurface aperture described by an anisotropic impedance [7].

More specifically, *single-source* (with two possible implementations) and *multi-source* feeding schemes are proposed. What they have proven is that, regarding the single-fed MTS, dividing the aperture in N angular sectors (Figure 4a), poor beam efficiency is provided (about 18%). Differently, the aperture can be shared by all the modulations required to produce a beam in a desired direction (Figure 4b) and so the whole structure contributes to the radiation, leading to a largely improved efficiency (55%).

As opposed, multi-fed approach (Figure 4c) provide an independent control of the beams, defined by correctly exciting a source to activate a wanted beam. The produced beams are quasi-orthogonal, which offers a significant advantage for processing signals impinging from different directions.



(a) Single feeding solution with aperture sharing and partition in 4 angular sectors (b) Single feeding solution with superposition of modulated impedance patterns (c) Multi feeding solution with superposition of modulated impedance patterns

Figure 4: Different designs for multibeam purposes.

With the development of 5G communication systems, the use of MTS has been promoted as very useful within frequencies in the range of microwaves and millimeter waves. Particular attention to solutions of these types is given by the attractive features of low profile, low cost, and reduced power consumption, which can satisfy the needs of new generation mobile networks. By exploiting multi-beam features

of MTS antennas, in [8] authors proposed an antenna topology composed of quasi-optical beamformer used to feed an MTS radiating aperture in a very compact structure. The realized system leads to a high-gain and low-profile antenna whose structure is shown in Figure 5. The presented design could be an appealing solution for wireless backhaul at K band. Indeed, the MTS antenna solution provides in this case multi-beam radiation able to transport data between the internet and subnetworks using microwaves or radio waves.

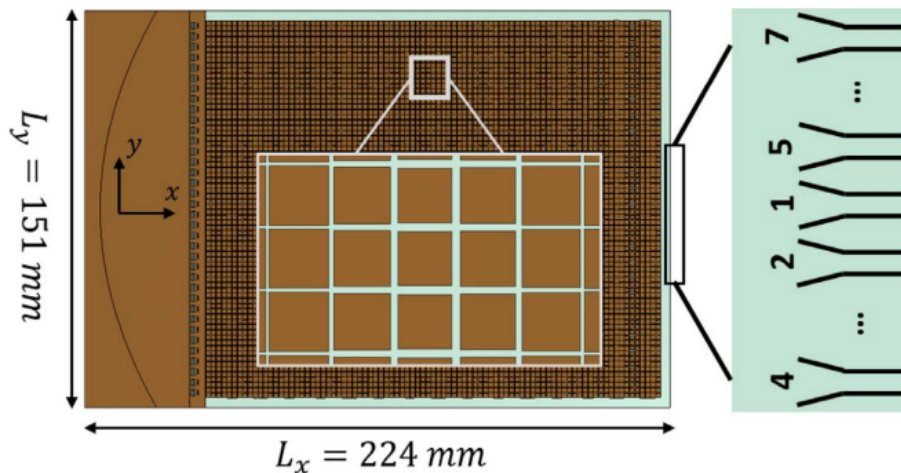


Figure 5: Top view of the MTS structure, emphasis on square patches modulation and ports disposition.

1.2.2 Current developments

The thesis aims at the development of new possible approaches to Metasurface Antennas design.

First of all, it must be said that this work adds no innovation in terms of technology for this field of interest. The main purpose is the development of an automatic code that allows to easy create a complete MTS antenna structure inside a simulation environment.

Considering that the devices to which this project is addressed are exploited for high-gain purposes, the number of subwavelength radiating elements that define the antenna structure is in the order of thousands. For this reason, the importance of the automatic generation of such very complex structures can be understood.

The aforementioned complexity of the complete antenna generation within the simulation environments led, in the structures proposed by the articles above mentioned, to a direct transition to the production stage of the antennas and, consequently, did not allow a preliminary optimization step of the designs.

Hence, the development of an automatic code for the structures generation leads properly to the execution of a preliminary optimization session and adds more degrees of freedom for the design.

Once the Metasurface antenna is obtained within the simulation environment, *full-wave* simulations can be performed to obtain the antenna performance and then to aim the optimization towards specific goals. These kinds of simulations are required because, considering the total dimension of the antenna, an electrically-large structure is implemented. Moreover, less idealized results can be achieved.

Regarding optimization, particular attention is paid to the increase of the antenna feeder performance in order to improve the efficiency related to this aspect of the design. Indeed, in order to maximize the propagation of the SW within the dielectric substrate, the feeder should be designed and optimized in such a way as to radiate as little as possible in the open field.

Furthermore, an investigation of the accuracy of the surface impedance reconstruction is performed using different types of the MTS lattice subdivisions.

In general, an overall optimization of antenna radiating features, such as directivity, gain, and reflection coefficients, is performed in order to improve performance for high-gain purposes.

More detailed discussions about optimization and full-wave simulation results are postponed to Section 4.

All the results and methodologies presented in this thesis are part of an internship program at *fondazione LINKS, Torino - Italy* whose components take an active part in the development of this project and are provided exploiting the *Academic License* of CST Microwave Studio supplied by *Politecnico di Torino*.

2 Numerical simulation

2.1 Equations and parameters involved

2.1.1 Maxwell's equations

Maxwell's equations are a set of coupled partial differential equations that provide a mathematical model for classical *EM* technologies. They describe electric and magnetic phenomena at the macroscopic level.

The general expression of the time-varying equations can be written as:

$$\begin{cases} \nabla \times \bar{\mathcal{E}} = \frac{-\delta\bar{\mathcal{B}}}{\delta t} - \bar{\mathcal{M}} \\ \nabla \times \bar{\mathcal{H}} = \frac{-\delta\bar{\mathcal{D}}}{\delta t} + \bar{\mathcal{J}} \\ \nabla \cdot \bar{\mathcal{D}} = \rho \\ \nabla \cdot \bar{\mathcal{B}} = 0 \end{cases} \quad (2)$$

where the implied quantities can be described as follow

- $\bar{\mathcal{E}}$ is the electric field [V/m].
- $\bar{\mathcal{H}}$ is the magnetic field [A/m].
- $\bar{\mathcal{D}}$ is the electric flux density [$Coul/m^2$].
- $\bar{\mathcal{B}}$ is the magnetic flux density [Wb/m^2].
- $\bar{\mathcal{M}}$ is the (fictitious) magnetic current density [V/m^2].
- $\bar{\mathcal{J}}$ is the electric current density [A/m^2].
- ρ is the electric charge density [$Coul/m^3$].

The sources of the electromagnetic field are the currents $\bar{\mathcal{M}}$ and $\bar{\mathcal{J}}$ and the electric charge density ρ . The magnetic current is a fictitious source in the sense that it is only a mathematical convenience: the real source of a magnetic current is always a loop of electric current.

Since electric current is really the flow of charge, it can be said that the electric charge density ρ is the ultimate source of the electromagnetic field [9].

In free space, the relationships between field intensities and flux densities are simply described by:

$$\bar{\mathcal{B}} = \mu_0 \bar{\mathcal{H}}^1 \quad (3)$$

¹Free space permeability $\mu_0 = 4\pi \times 10^{-7}$

$$\bar{\mathcal{D}} = \epsilon_0 \bar{\mathcal{E}}^2 \quad (4)$$

Assuming an $e^{j\omega t}$ time dependence, the Maxwell's equations can be described in phasors form

$$\begin{cases} \nabla \times \bar{E} = -j\omega \bar{B} - \bar{M} \\ \nabla \times \bar{H} = j\omega \bar{D} + \bar{J} \\ \nabla \cdot \bar{D} = \rho \\ \nabla \cdot \bar{B} = 0 \end{cases} \quad (5)$$

2.1.2 Helmholtz equation

Assuming a linear, source-free situation ($\bar{M} = 0, \bar{J} = 0$), the curl equations in (5) can be better written considering the definitions given in (3) and (4)

$$\nabla \times \bar{E} = -j\omega \mu \bar{H} \quad (6)$$

$$\nabla \times \bar{E} = j\omega \epsilon \bar{E} \quad (7)$$

hence, it can be noticed that there are two equations for the two unknowns (\bar{E}, \bar{H}). They can be either solved by defining the *Helmholtz equation (also known as wave equation)*

$$\begin{cases} \nabla^2 \bar{E} + \omega^2 \mu \epsilon \bar{E} = 0 \\ \nabla^2 \bar{H} + \omega^2 \mu \epsilon \bar{H} = 0 \end{cases} \quad (8)$$

The EM wave that is propagating, under the defined conditions, is therefore described by this rule.

2.1.3 Plane wave propagation

Plane waves are the simplest form of electromagnetic waves. They are characterized by a physical quantity, such as phase, whose value is constant, at any moment, over a plane perpendicular to the direction of propagation.

Like periodic waves, plane waves are defined by wavelength, frequency, and wave speed.

²Free space permittivity $\epsilon_0 = 8.854 \times 10^{-12}$

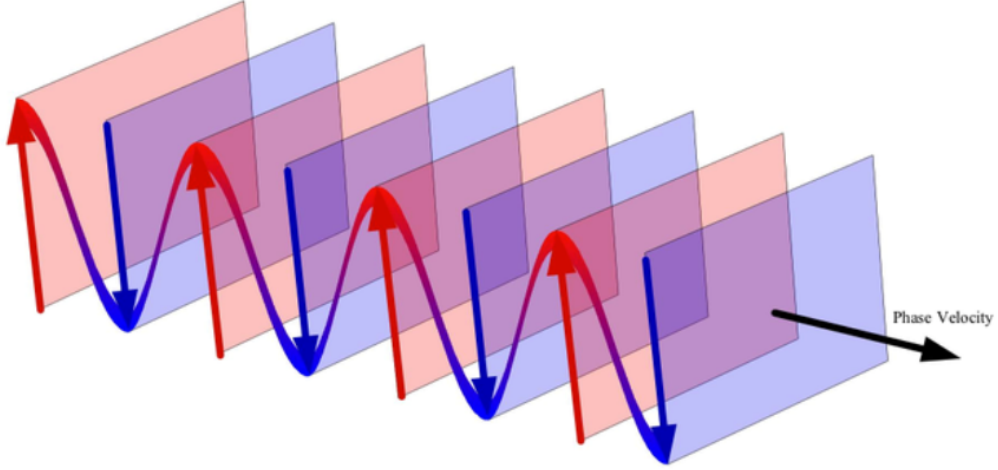


Figure 6: Generic traveling plane wave.

Defining a constant $k = \omega\sqrt{\mu\epsilon}$, identified as *wave number (or propagation constant)*, from the Helmholtz equation, a basic plane wave solution can be obtained assuming an electric field characterized by only an \hat{x} component and uniform in x, y directions ($\delta/\delta x = \delta/\delta y = 0$):

$$\frac{\delta^2 E_x}{\delta z^2} + k^2 E_x = 0 \quad (9)$$

that leads to two independent solutions

$$E_x(z) = E^+ e^{-jkz} + E^- e^{jkz} \quad (10)$$

The propagation of the electric field along x is therefore described by the superimposition of a forward and backward plane wave, with E^+, E^- identified as amplitude constants.

2.1.4 Wavelength

In physics, the wavelength is the spatial period of a periodic wave. It is the distance between consecutive corresponding points of the same phase on the wave.

The wavelength λ of a sinusoidal waveform traveling at constant speed v and frequency f is given by

$$\lambda = \frac{v}{f} \quad (11)$$

When free-space electromagnetic propagation is considered, the speed of the wave propagation corresponds to the speed of light $c = 3 \times 10^8 \text{ m/s}$. The expression of free-space wavelength is therefore

$$\lambda_0 = \frac{c}{f} \quad (12)$$

2.1.5 Far-Field conditions

Considering a generic transmitting antenna, two main regions can be defined around the device:

- space region close to the antenna, identified as *Near Field (NF)*. Non-radiative behavior is dominant.
- space region far enough from the antenna, identified as *Far Field (FF)*. Radiation behavior is dominant.

Considering the main transmission purposes of antenna systems, radiation conditions (far field conditions) are considered in almost all possible applications.

A space region far enough to be in the far field is identified as the *Fraunhofer region*:

$$r > 2D^2/\lambda \quad (13)$$

where D is the physical dimension of the considered antenna.

Assuming this condition as verified, the far field “layout” is characterized by the following relations between field components

$$E_r \ll E_\theta, E_\phi \quad H_r \ll H_\theta, H_\phi.$$

Considering a point of observation P , the spatial situation can be better understood by looking at Figure 7.

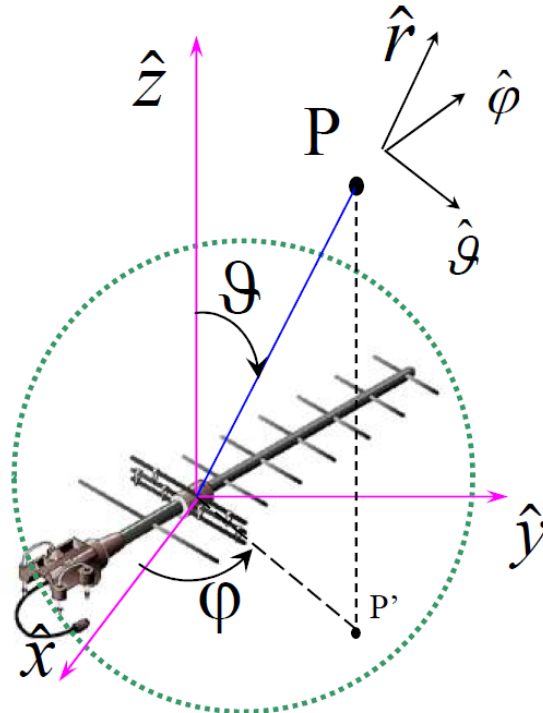


Figure 7: Transmitting antenna example.

Radiated EM field in FF region is always tangent to a sphere centered at the antenna center. It can be shown that the FF radiation in a lossless medium can be factored as:

$$\underline{E}(\underline{P}) = \frac{e^{-jk_0r}}{4\pi r} \underline{e}(\theta, \phi) \quad (14)$$

where the first term (ratio) is defined as the “*universal*” *spherical wave* while the second one is the *antenna specific* “*radiation vector*” (that will depend on the specific antenna characteristics).

2.1.6 Field polarization

When a field is propagating, the geometrical orientation of the oscillations is defined by its *polarization*.

This characteristic depends on the spatial orientation and the relative amplitude of in-phase and quadrature vectors of the field. It is described by a unit (complex) vector

$$\hat{p} = \frac{\underline{E}}{|\underline{E}|} = \frac{\underline{E}' + j\underline{E}''}{\sqrt{|\underline{E}|^2}} = \underline{p}' + j\underline{p}'' \quad (15)$$

The definition of polarization unit vector implies that it can be written:

$$\underline{E} = \hat{p}|\underline{E}|$$

The polarization of a propagating EM field is in principle defined as *elliptical*. This generic situation can lead to particular cases: *linear polarization*, *circular polarization*.

2.1.7 Antenna directivity

The directivity (IEEE Std 145TM-2013) is the normalized distribution function of field power density over angular directions. Following a non-standard definition, it can be also identified as the ratio of the radiation intensity in a given direction from the antenna to the radiation intensity averaged over all directions.

Being $S(r, \theta, \phi) = \frac{dP}{d\Sigma}$ the field power density, the standard directivity expression is:

$$d(\theta, \phi) = \frac{S(r, \theta, \phi)}{S_{average}(r)} \quad (16)$$

and assuming that the average is taken over a sphere with radius r

$$S_{average} = \frac{1}{4\pi r^2} \int \int_{sphere} S(r, \theta, \phi) d\Sigma = \frac{1}{4\pi r^2} P_{rad}^3$$

therefore the expression of directivity becomes (not IEEE std definition):

$$d(\theta, \phi) = \frac{\left(\frac{dP}{d\Sigma}\right)_{(r,\theta,\phi)}}{\frac{P_{rad}}{4\pi r^2}} \quad (17)$$

³Radiated power P_{rad} is different from the input power and depends on the energetic efficiency η of the antenna considering $P_{rad} = \eta P_{in}$)

2.1.8 Antenna gain

The *gain* of an antenna is defined as the parameter that relates the radiated field strength to the input power through the energetic efficiency of the antenna itself:

$$g(\theta, \phi) \equiv \eta d(\theta, \phi) = \eta \frac{\left(\frac{dP}{d\Sigma}\right)_{(r,\theta,\phi)}}{\frac{P_{rad}}{4\pi r^2}} \quad (18)$$

being $P_{rad} = \eta P_{in}$ the expression becomes

$$g(\theta, \phi) \equiv \eta d(\theta, \phi) = \frac{\left(\frac{dP}{d\Sigma}\right)_{(r,\theta,\phi)}}{\frac{P_{in}}{4\pi r^2}} \quad (19)$$

which shows the relation between the power density and the power accepted by the antenna.

2.1.9 Radiation pattern

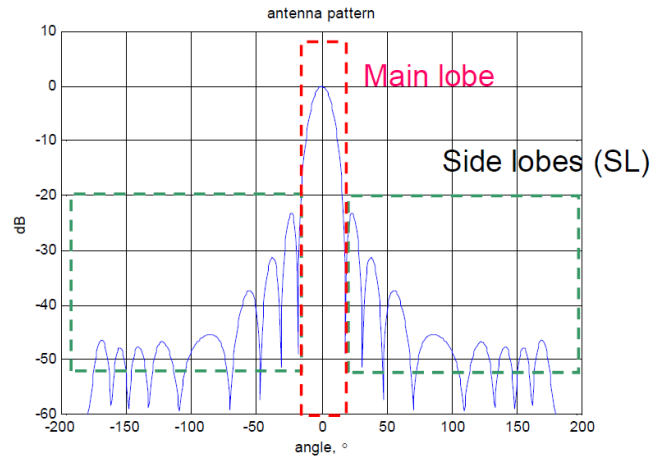
The antenna *radiation pattern* can be defined as a mathematical function of the FF radiation properties of the antenna. More specifically it refers to the angular dependence of the strength of waves radiated by an antenna.

The function $f(\theta, \phi)$ that rules the radiation pattern of an antenna is related to a normalization with respect to the *max gain* of the antenna

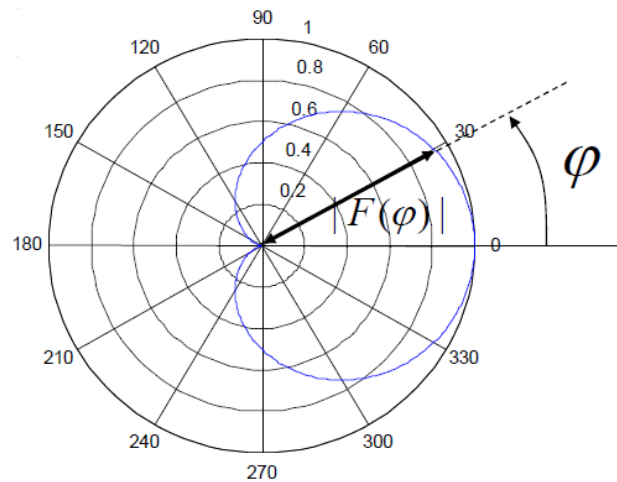
$$f(\theta, \phi) = \frac{g(\theta, \phi)}{\max g(\theta, \phi)} \leq 1 \quad (20)$$

A general example of an antenna pattern can be seen in Figure 8

Strictly speaking, it is characterized by: *main lobe*, *side lobes (SL)*, *first null beam width (FNBW)*, *half power beam width (HPBW)*, and *side lobes level (SLL)*. It can also be represented in polar form (Figure 8b) to give a better “spatial idea” of the radiation characteristics.



(a) Cartesian form.



(b) Polar form.

Figure 8: Radiation pattern examples. (a) shows an example of antenna radiation pattern in Cartesian form and (b) shows a polar representation (of a radiation pattern different from the previous one).

2.1.10 Link budget, Friis formula

An antenna-based communication system is described by two types of antennas: *transmitting antenna (TX)* and *receiving antenna (RX)*. The previously discussed features will therefore be related to the type of antenna that is considered. Indeed it is possible to define:

- P_{TX} : transmitted power, related to TX antenna.
- P_{RX} : received power, related to RX antenna.
- g_{TX} : gain of the TX antenna.

- g_{RX} : gain of the RX antenna.

It is quite intuitive that the signal received by the RX antenna corresponds to the transmitted signal after the propagation through a certain medium. However, the signal seen by the receiving antenna is not strictly equal to the transmitted one but it is quite modified by the features that define the specific link considered. The power budget that defines the ratio between received and transmitted power, is identified as *Link budget*.

$$\frac{P_{RX}}{P_{TX}} = \frac{1}{(4\pi r/\lambda)^2} g_{TX}(\theta, \phi) g_{RX}(\theta, \phi) \chi(\theta, \phi) \quad (21)$$

where $\chi(\theta, \phi)^4$ is the loss due to polarization mismatch between transmitting and receiving antenna (*polarization loss*).

Neglecting additional losses, from (21) is possible to obtain the *Fris Formula*, which properly defines the amount of the received power:

$$P_{RX} = \frac{P_{TX} g_{TX}(\theta, \phi) g_{RX}(\theta, \phi)}{(4\pi r)^2} \chi(\theta, \phi). \quad (22)$$

The amplitude of the received power will therefore be related to: power delivered by the TX antenna, antenna gains in link direction, polarization loss, and free space loss.

2.1.11 Scattering parameters

Scattering parameters are used to easily describe the electrical behavior of linear electrical circuits when high-frequency situations are considered. Indeed, for example at RF frequencies, it is not possible to describe a circuit by classically using its *Z-matrix* or *Y-matrix*. This issue is related to the fact that frequency of this magnitude cannot be correctly related to short-circuit or open-circuit conditions (necessary to define Z and Y parameters).

To obtain the *S-matrix*, the circuit under test will be terminated with *matched loads*. In this case, the electrical characteristics of the circuit are not defined by examining voltage and current waves but by considering *power waves*.

For a generic multi-port network, the ports are numbered from 1 to N, where N is the total number of ports. For port i , the associated S-parameter definition is in terms of incident and reflected power waves, a_i and b_i respectively:

$$a_i = \frac{1}{2} \frac{(V_i + Z_0 I_i)}{\sqrt{|\Re\{Z_0\}|}}$$

$$b_i = \frac{1}{2} \frac{(V_i - Z_0^* I_i)}{\sqrt{|\Re\{Z_0\}|}}$$

⁴Polarization loss given by $\chi(\theta, \phi) = |\hat{p}_{TX}(\theta, \phi) \cdot \hat{p}_{RX}(\theta, \phi)|^2$

where Z_0 is the nominal characteristic impedance of the circuit and Z_i , V_i and I_i are respectively the impedance, the complex amplitude of voltage, and the complex amplitude of current at port i .

The scattering matrix defines the relation between the components of a and b vectors:

$$\begin{pmatrix} b_1 \\ \vdots \\ b_n \end{pmatrix} = \begin{pmatrix} S_{11} & \dots & S_{1n} \\ \vdots & \ddots & \vdots \\ S_{n1} & \dots & S_{nn} \end{pmatrix} \begin{pmatrix} a_1 \\ \vdots \\ a_n \end{pmatrix}$$

2.1.12 Leaky-wave antennas

As briefly introduced in Section 1.2.1, all the interesting features related to array antennas are followed by a high complexity of the design.

From the late 1950s, different antenna systems, known as *Leaky-wave antennas*, became increasingly popular within the microwave communication environment [10]-[11]. This attention was linked to the possibility of designing high directivity antennas without the complexity limitation given by the need for complicated feeding networks and a high number of elements inherent to classical phased array designs. More precisely, the feeding system is based on the propagation of a leaky wave inside the antenna structure that is able to excite the radiating elements. Generally, this leads to the realization of an effective antenna aperture that is able to radiate energy.

The field above the aperture is characterized, using the Helmholtz equation, by a transverse (vertical) wavenumber

$$k_x = \pm \sqrt{k_o^2 - k_z^2} = \beta_x - j\alpha_x \quad (23)$$

so, properly described by the complex wavenumber $k_z = \beta - j\alpha$ where β and α are respectively the phase and the attenuation constants.

For small attenuation values, the radiation angle θ can be approximated as [12]:

$$\theta = \arccos\left(\frac{\beta}{k_0}\right) \quad (24)$$

The complex wavenumber of the leaky wave on the aperture directly determines the main features of its radiation pattern: direction of the main beam, beamwidth, and sidelobe level. The attenuation constant controls the angular width of the main beam in the far field, i.e., the antenna directivity. If the leaky waveguide is sufficiently long to avoid end reflections, the leakage rate directly determines the size of the effective antenna aperture: a large (small) implies a short (long) effective aperture, which corresponds - after a Fourier transformation - to a wide (narrow) beam in the far field [13].

For one-dimensional (1D) uniform leaky-wave antennas, the half-power beamwidth is linearly proportional to α/k_0 through the approximate formula [12]:

$$BW = 2csc(\theta) \frac{\alpha}{k_0} \quad (25)$$

2.1.13 Electromagnetic modeling

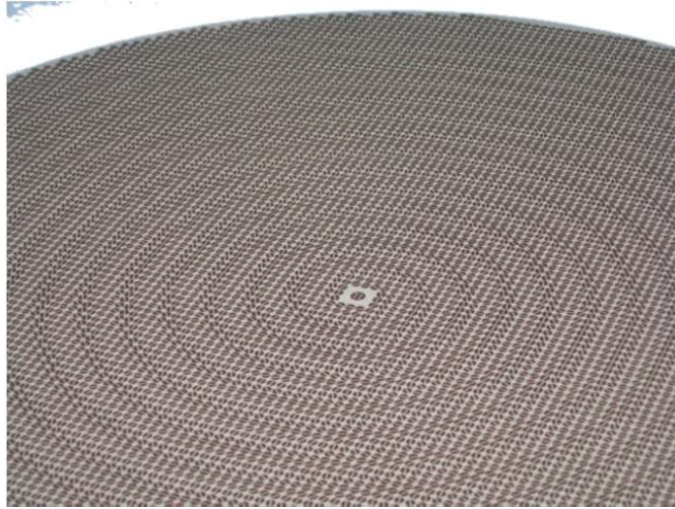
Once discussed the theoretical support to the study of interest, a preliminary introduction to the model of the involved antennas can be given.

The MTS can be fully described by Maxwell's equation using *appropriate* boundary conditions. For this reason, the interested investigation can be described as a “*Boundary Value Problem (BVP)*”. In this regard, the exploitation of the commercial simulation software is aimed at the numerical solution of actual BVP through full-wave simulations, hence without the introduction of other approximations (apart from the numerical solution which, of course, is an approximation itself).

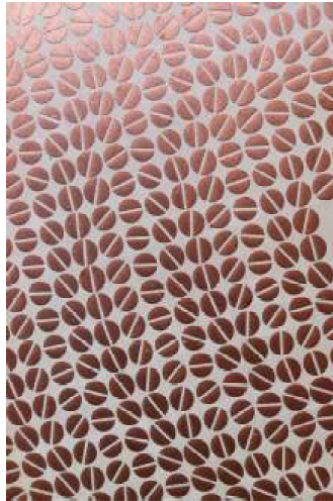
Many methods can be useful for numerically solving Maxwell's equation. In Section 2.2, some of them are briefly explained since exploited by the commercial simulation software used for this thesis work.

Considering the EM modeling of a general MTS, it can be defined as a “*Multiscale problem*” [14] which can realize a more complex situation for numerical solvers. This is related to the fact that, as explained, the total structure is realized by the interaction of many “elementary” structures whose are therefore related to different scale with respect to the wavelength. More in detail:

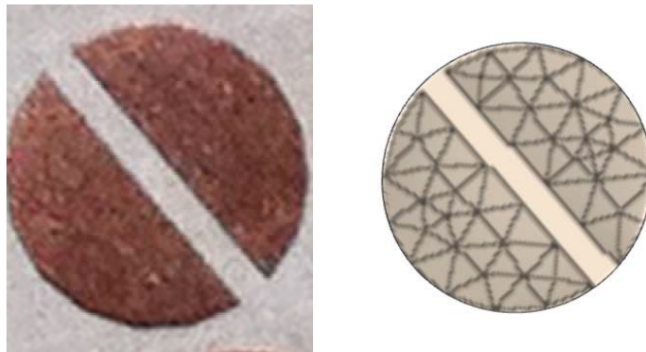
- considering the total dimension, the MTS antenna is related to a *macroscale*, $L \gg \lambda$ (Figure 9a);
- considering local lattice modulations, the MTS antenna is related to *mesoscale*, $L \simeq \lambda$, (Figure 9b);
- considering singular radiating elements, the MTS antenna is related to *microscale*, $L \ll \lambda$, (Figure 9c)



(a) Antenna total dimension.



(b) Local lattice.

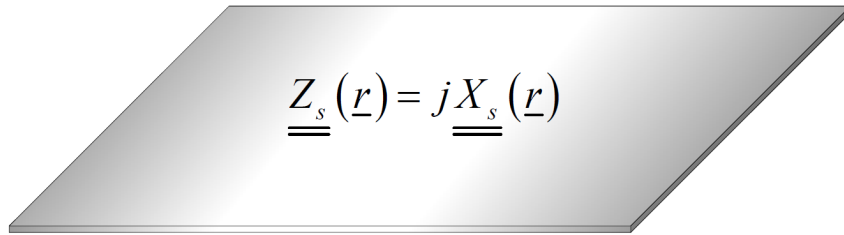


(c) Patches dimension.

Figure 9: Multiscale problem. (a) shows the *macroscale* related to antenna total dimensions; (b) shows *mesoscale* related to local lattice dimensions; (c) shows *microscale* related to patches and mesh dimensions.

The already discussed impedance modulation allows analyzing the overall MTS as a *surface impedance*. This leads to a reduction of the unknowns number of the numerical problem and a lattice easier to modify. In this way, the approach consists in design and analyze the reactance profile, and then to synthesize the designed profile. Figure 10 shows an example of the procedure.

➤ design/analyze the reactance profile



➤ synthesize the designed profile

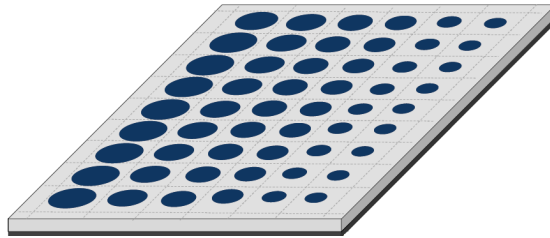


Figure 10: MTS modeling approach.

For the sake of completeness, some examples of MTS antenna structures are reported. In Figure 11 there are shown examples of antennas practically realized for specific purposes while, in Figure 12, there are shown some examples of structures that are implemented in CST environment to carry out the results this thesis is aimed to.

It must be said that, in this introduction step, just the “final” structures are shown. The step-by-step generation of the complete structures is postponed to section (Section 3).

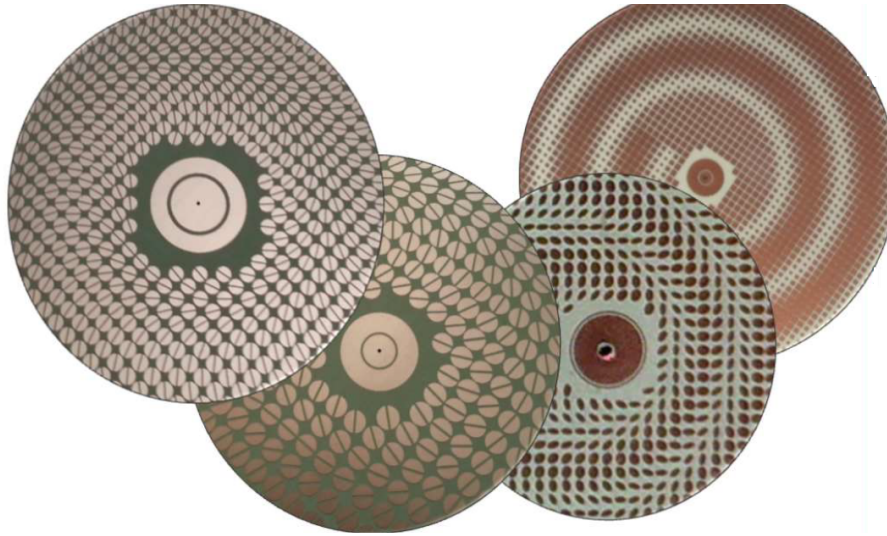
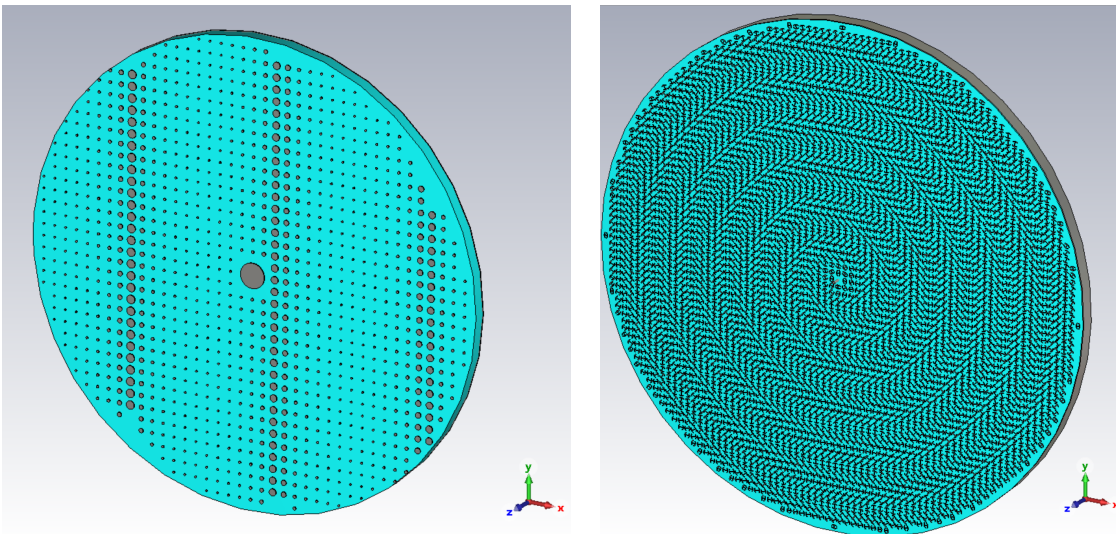


Figure 11: Examples of physically realized MTS antenna.



(a) CST MTS antenna example with circular patches.

(b) CST MTS antenna example with double anchors.

Figure 12: CST examples of MTS antennas. (a) shows a structure with variable-size circular patches as radiating elements; (b) shows a structure with double anchors shapes as radiating elements.

2.2 CST software

The results later on presented in this work are obtained by performing numerical simulations of the designed structures in *CST Microwave Studio*. This commer-

cial simulation software, developed by *Dassault Systèmes Simulia*, is highly used in telecommunications, defense, and aerospace environments. It can be defined as an electromagnetic design tool able to numerically solve Maxwell's equation giving specific solvers for EM and multiphysics problems.

2.2.1 CST environment

As well as other simulation software, CST offers a user-friendly interface by which is possible to build the geometric structure of interest, and then, properly set up the simulation solver. More specifically, CST is able to exploit different solver types for the numerical solution of the EM problem.

Two solvers are mainly related to the scope of this thesis, *Time Domain Solver (TD)* and *Frequency Domain Solver (FD)*.

2.2.2 Time Domain solver

Time domain solver calculates the development of fields through time at discrete locations and at discrete time samples. Consequently, a time domain solver is remarkably efficient for most high-frequency applications such as connectors, transmission lines, filters, antennas, etc.

TD solver can be based on the *Finite Integration Technique (FIT)*, just called *Transient* solver, or differently, on the *Transmission Line Method (TLM)* that refers to TLM solver. Both solvers work on hexahedral grids [15].

FIT technique for time domain solver is the only one used during this thesis work.

Strictly speaking, this numerical method is based on the discretization of the *integral form* of Maxwell's equations leading to a spatial discretization scheme that can be applied to various EM problems (from static field to high-frequency applications). The numerical solution of the equations is provided by reducing the calculation domain to a finite space that encloses the application problem. Hence, the considered finite domain is consequentially split into a large number of small elements by exploiting a mesh system.

The spatial discretization of Maxwell's equations is finally performed on two orthogonal grid systems where the degrees of freedom are introduced as integral values. Considering Faraday's Law (shown in Figure 13), the closed integral on the equation's left side can be rewritten as a sum of four grid voltages without introducing any supplementary errors. Consequently, the time derivative of the magnetic flux defined on the enclosed primary cell facet represents the right-hand side of the equation, as illustrated in the figure below. Repeating this procedure for all available cell facets summarizes the calculation rule in a matrix formulation, introducing the topological matrix as the discrete equivalent of the analytical curl operator [15]:

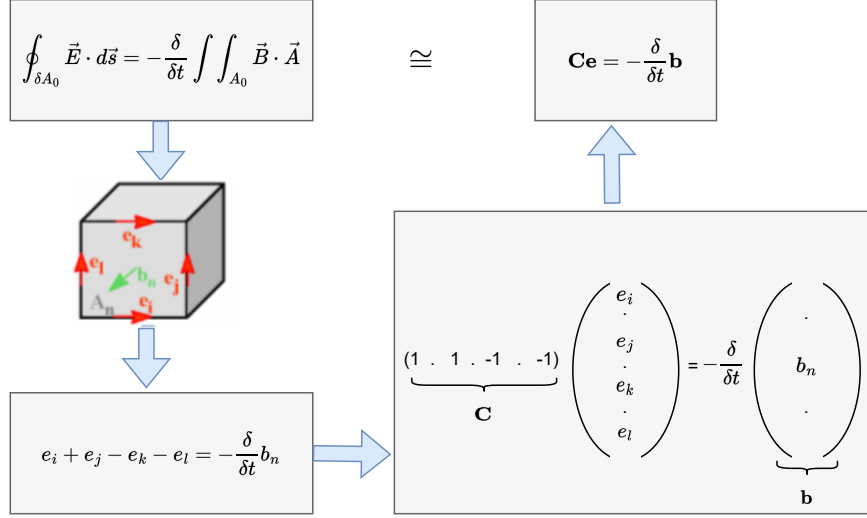


Figure 13: Finite domain discretization of Maxwell's equations.

2.2.3 Frequency Domain solver

The FD solver is able to provide Maxwell's equations solution in the frequency domain exploiting the *Finite Element Method (FEM)*. Applying a transformation from time to frequency domain, a time-harmonic dependence of the fields can be assumed. Considering this, fields are completely described by phasors of transient fields by properly multiplying the phasor for the time factor $e^{(j\omega t)}$ and taking the real part of the result:

$$\overline{E}(t) = \Re\{\overline{E}(\omega) \cdot e^{(j\omega t)}\} \quad (26)$$

However, the frequency domain solver uses special broadband frequency sweep techniques in order to derive the full broadband spectrum from a relatively small number of frequency samples.

General purpose broadband frequency sweep, particularly defined by tetrahedral mesh, offers the widest range of applications. It evaluates the solution for the underlying equation for a single frequency at a time, and for a number of adaptively chosen frequency samples. For each frequency sample, the linear equation system will be solved by an iterative solver or sparse direct solver.

As an alternative to the general purpose sweep, a *Fast reduced order model sweep* is available, which efficiently generates broadband results from very few equation system solver runs. A special model order reduction technique is used to reduce the size of the system [15].

For the discretization of the geometry, the hexahedral mesh as well as the tetrahedral mesh may be chosen.

2.2.4 Matlab-CST interface

Going into a more detailed description of the automatic implementation in the simulation environment, CST software may present a possible criticism related to the *manual* generation of the structures interested in simulating. To be more specific, the software presents the possibility to directly control the geometric modeling by using scripts based on *VBA* language.

What this thesis is referred to is the exploitation of a pre-defined library that is able to create a CST object which acts as an interface between Matlab and CST Microwave Studio in order to provide a translation between Matlab and VBA language. In this way, a more common programming language can be used, and therefore, the complexity of the written code lines is reduced by considering that the sets of VBA instructions are directly given by the library.

The mentioned interface was developed in 2018 by Henry Giddens, Antennas and Electromagnetics Group at Queen Mary University London [16].

This thesis project aimed at the exploitation of the Giddens library to properly generate a Matlab script organized into high-level and low-level functions. To be more specific, low-level functions will directly use VBA translating codes to implement, starting from Matlab, the automatic generation of geometric structures in CST environment. The generation of single objects will be controlled by properly using singularly the functions given by the library, while the generation of multiple objects will be done by the aimed generation of “*for*” loops. Geometry generation will be better described in Section 3.

Differently, at high level, the low order functions will be exploited to correctly generate the entire structure of an investigated MTS antenna.

Matlab-CST interface is not just used to create the antenna geometries. It is also used to correctly set software settings, and field monitors, to obtain the specific results to which the current investigation is directed.

3 Automatic code development for Metasurface antenna design

3.1 Possible approaches

As introduced, there were two main possibilities for the development of the automatic code. The first approach is based on the exploitation of the *macro scripting* that is directly given by CST software, based on VBA language.

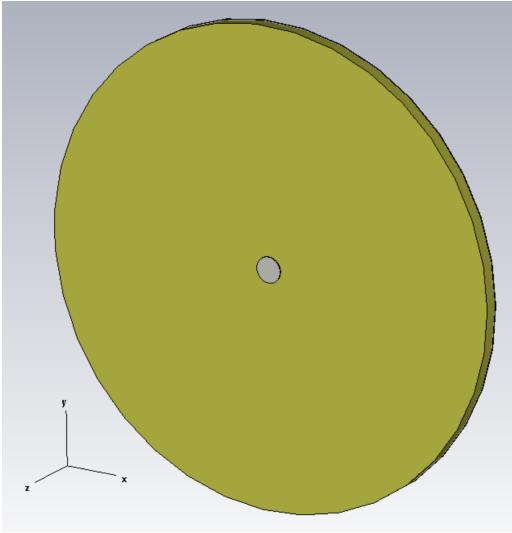
The second approach is, instead, based on the use of Matlab scripting for the implementation of CST instruction sets able to create the desired geometries within the simulation environment.

To obtain an automatic code based on a more common and friendly-user programming language, the Matlab-based code was chosen for the development of this thesis project.

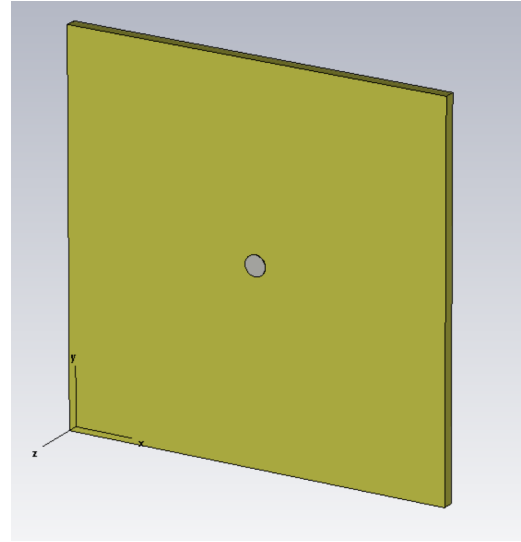
Advancing in the project, also VBA approaches were exploited, in particular, to generate and add some new functions to the Giddens interface library. This was necessary to carry out some specific tasks required by the considered type of antennas. Detailed descriptions of the implemented functions will be later on discussed in Section 3.3.

3.2 Automatic structure generation

To better understand the scripting code organization, an example of the MTS antenna structure is reported to show, broadly, the kind of geometries that the code must be able to generate.



(a) Circular antenna example.



(b) Square antenna example.

Figure 14: CST implementation of general MTS (not complete) structures. (a) shows a circular antenna geometry; (b) shows a square antenna geometry.

In Figure 14 two different grounded dielectric slabs that can be used as supporting structures for the Metasurface layer are reported; while, in Figure 15, is reported an example of a complete MTS antenna structure.

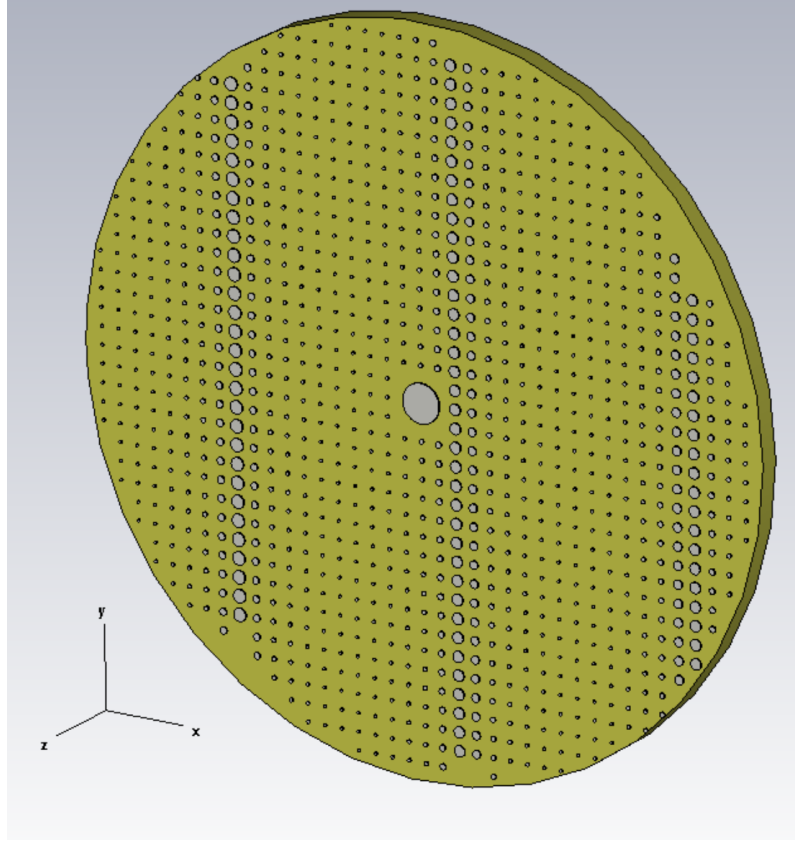


Figure 15: First example of MTS antenna complete structure with circular patches as radiating elements. CST implementation.

As can be seen, in the displayed case the radiating elements consist of circular patches made by PEC. The radius of each patch is chosen following the values stored in an example *HDF-5* file (more detailed discussion on this aspect is postponed to Section 3.5).

Regarding the spatial position of the patches, this is ruled by the partitioning of the considered dielectric slab (squared or circular) in a regular grid that identifies *unit cells* within the dielectric plane. The size of the unit cells is chosen, as already said, in a range between $(\lambda/6 - \lambda/10)$.

Intuitively, the maximum number of radiating elements that can be printed on the dielectric surface depends on the total dimension of the antenna and the size of the unit cells: $N_{elements} = Antenna\ Size / Unit\ Cell\ Size$.

In the following, the generation of the elements that compose the complete antenna structure is sketched in terms of pseudo-code, in order to introduce the reader to the detailed description of functions generation.

3.2.1 Dielectric substrate and ground plane generation

The examples of the grounded dielectric slabs shown in Figure 14 present two different antenna structures: a circular and a square antenna.

In the case of a circular antenna, a cylindrical geometry is created in CST environment and its generation is ruled by:

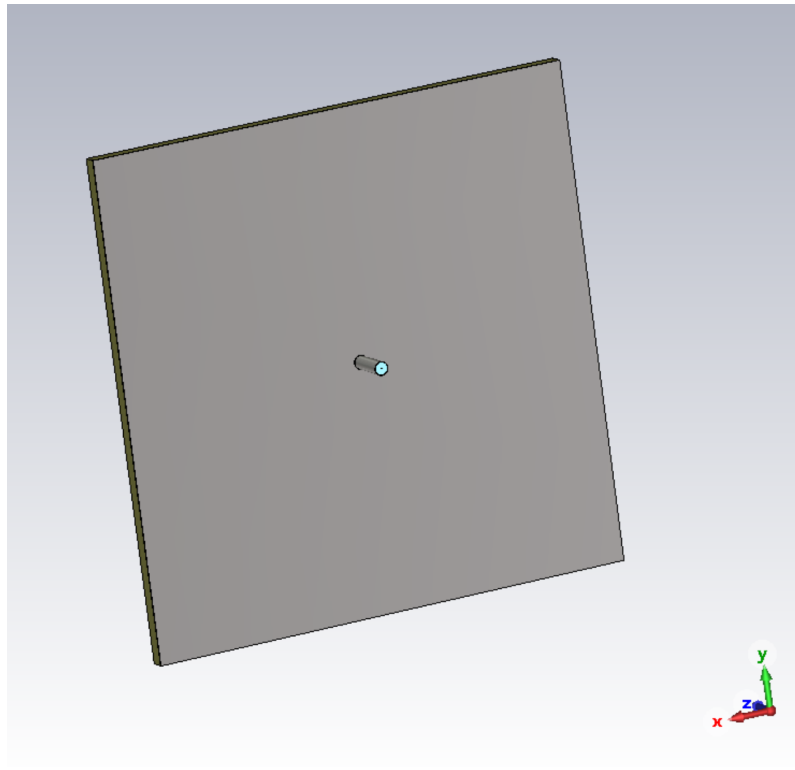
- radius of the cylinder that defines the total size of the antenna;
- thickness of the dielectric substrate.

While, for the square antenna, the generation of a brick is performed and it is ruled by:

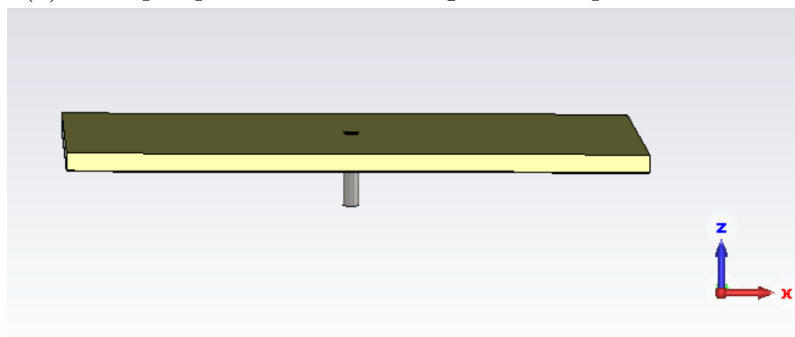
- values of x_{min} , x_{max} and y_{min} , y_{max} that define the extension of the brick in x and y directions, and therefore the total size of the antenna;
- thickness of the dielectric substrate.

In both cases, a ground plane is also designed. The shape of this conducting surface is, of course, chosen in relation to the geometry of the considered antenna. This part of the structure is controlled by the code exactly in the same way as the dielectric layer, the only difference compared to the substrate is that the GND plane is managed in such a way as to possibly have an infinitesimal thickness, contrary to the dielectric slab that is always defined as a finite element.

To better appreciate the presence of the GND plane, the following figures show back (Figure 16a, Figure 17a) and lateral (Figure 16b, Figure 17b) views of the two grounded dielectric slabs implemented in CST by exploiting the automatic code.

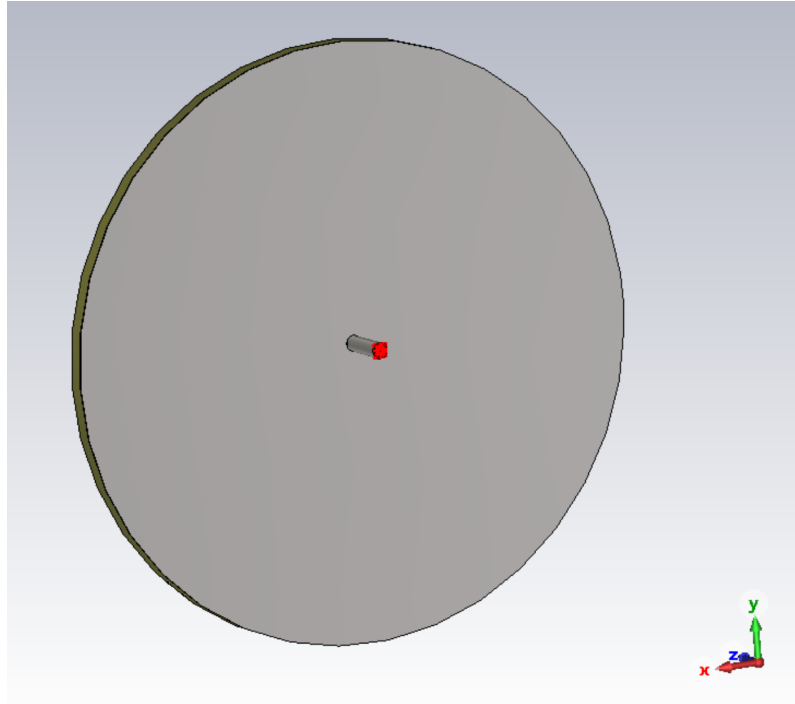


(a) Back perspective view of the grounded square dielectric.

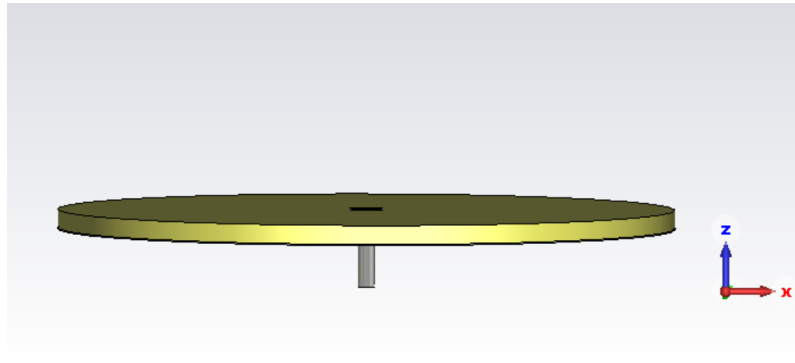


(b) Lateral view of the grounded square dielectric.

Figure 16: Detailed CST views of the square dielectric structure.



(a) Back perspective view of the grounded circular dielectric.



(b) Lateral view of the grounded square dielectric.

Figure 17: Detailed CST views of the circular dielectric structure.

3.2.2 Feeding element generation

As can be guessed by looking at Figure 16 and Figure 17, also a feeding element is designed in CST to add a discrete port and correctly insert a voltage signal inside the structure.

The considered feeding system, used in each of the designed antennas, is a coaxial cable whose dimensions are precisely chosen to implement a wanted value of impedance.

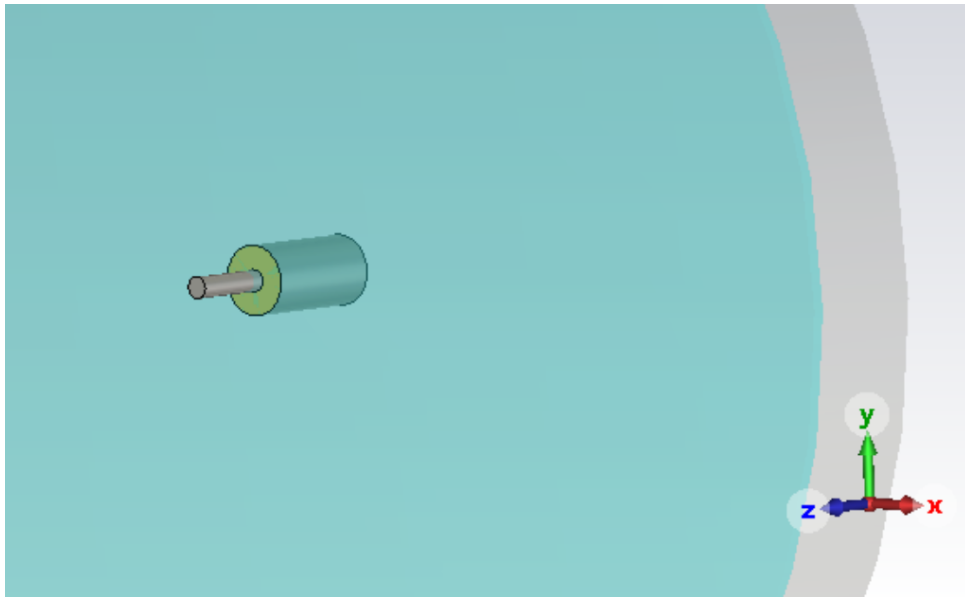
The designed cable has a 50Ω characteristic impedance by using:

- a 2.7 mm - diameter dielectric substrate with relative permittivity $\epsilon_r = 2.1$;
- a 0.85 mm - diameter inner conductor;
- an ideal coaxial coating with infinitesimal thickness.

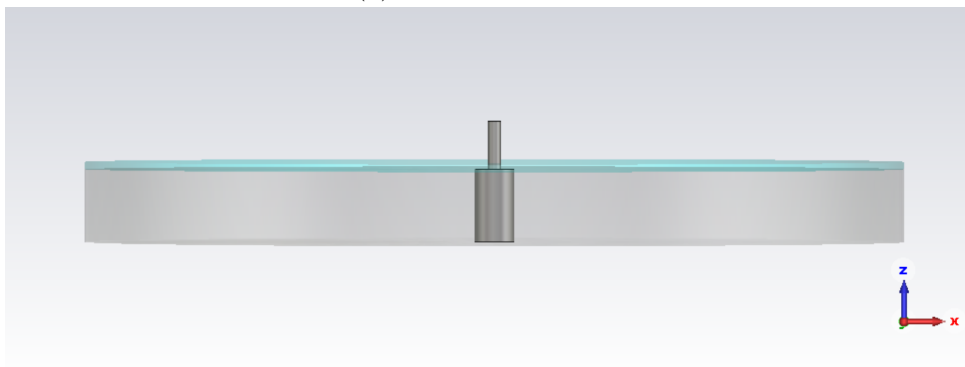
Figure 18 and Figure 19 report different perspective views of the designed coaxial cable.

From the lateral view (Figure 18b), it can be noticed that the extension of the inner conductor of the cable does not stop at the interface between dielectric and air, but it goes through the substrate to end with a protruding height.

This aspect leads to a better definition of the feeding system. In fact, this structure implements a *coaxially fed vertical monopole* that radiates the exciting surface wave. The described system is placed at the center of the structure so that, in this way, it is possible to feed the MTS antenna with a SW that can be always assumed to be cylindrical and azimuthally symmetric, as the one provided by a monopole.

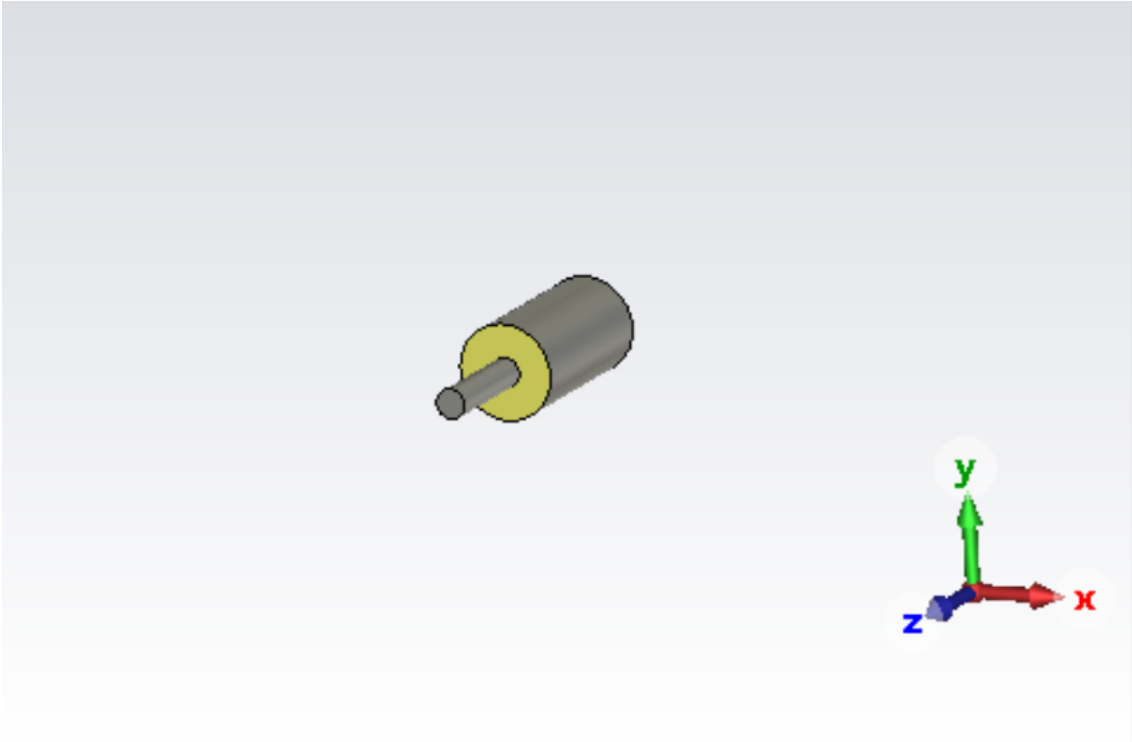


(a) Perspective view.

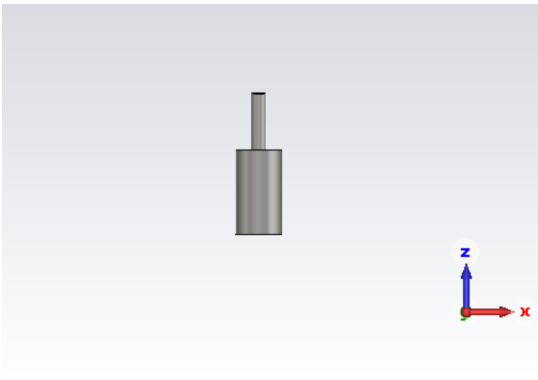


(b) Lateral view.

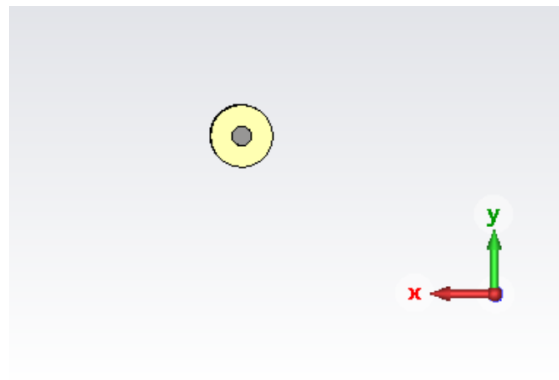
Figure 18: Detailed CST views of the coaxial feeding system.



(a) Perspective view.



(b) Lateral view.



(c) Back view.

Figure 19: Isolated CST views of the coaxial feeding system.

The discussion relative to the height value of the prominent monopole is postponed to section 3.5, dedicated to the optimization of the feeder.

3.2.3 Radiating elements generation

Finally, the last aspect of the antenna structure that needs to be presented is the radiative element (RE). There are some possible shapes that can be chosen. For the sake of completeness, the shapes that will be depicted in the following, do not

represent all the possible solutions that can be adopted to design an MTS antenna, but they are general enough to discuss the capability of this work.

Figure 20 shows and summarizes the features related to each RE shape.

	Coffee Bean	Grain of Rice	Double anchor
			
# parameters	2	3	3
Anisotropy Control			
Range of X_{pp}			
Bandwidth (group velocity)			
Sensitivity to tolerances			
Loss in the metal			

Figure 20: Radiating elements examples [4].

Taking into consideration the geometric form of the elements, it is possible to sketch up how the pseudo-code has to be organized to correctly control the implementation of the shapes.

Firstly, it must be said that two of the features that the code must be able to control are common to each kind of radiating element: the spatial position in terms of (x, y) coordinates within the dielectric substrate, and the rotation of the element with respect to the center of the unit cell to which it belongs.

Regarding the “*Coffee Bean*” elements, this profile is essentially made by a circular patch that is slotted in its center. The parameters that should be controlled (in addition to the 2 aforementioned common parameters) are:

- radius of the circular geometry (cylinder in CST);
- width of the central slot.

For the “*Grain of Rice*” shape, this profile is given simply by an ellipse without other features. Hence, the code must be able to control:

- minor radius of the ellipse (identified as a in the relative image in Figure 20),
- major radius of the ellipse (identified as b in the relative image in Figure 20).

Considering the “*Double Anchor*” shape, this turns out to be the trickiest structure to generate. That’s because it is not linked to a single geometric form but is realized

by the overlapping of several of them (more detailed information on the generation of double anchor profiles will be given in the dedicated Section 3.3.7).

In this case, the code must be able to specifically control:

- the radius of the external circle of the element (identified as b in the relative image in Figure 20);
- the radius of the internal (empty) circle of the element (identified as a in the relative image in Figure 20), that defines the thickness of the element;
- the generic angle α , took from the center of the shape, that defines the angular aperture between the extremities of the two anchors;
- the rectangular strip at the center of the element that links the two anchors.

At last, as shown previously in Figure 15, also circular patches can be used as radiating elements. In this case, the profile is simply implemented with a circle, so the unique parameter that has to be controlled (as well as the mentioned parameters common to each shape) is the radius of the circle itself.

3.2.4 VBA scripting examples

In this section, some examples of VBA scripting are reported in such a way as to validate the chosen approach by showing the order of complexity of the VBA instructions.

To do so, the automatic generation of the circular dielectric substrate is reported as a simple example in Figure 21.

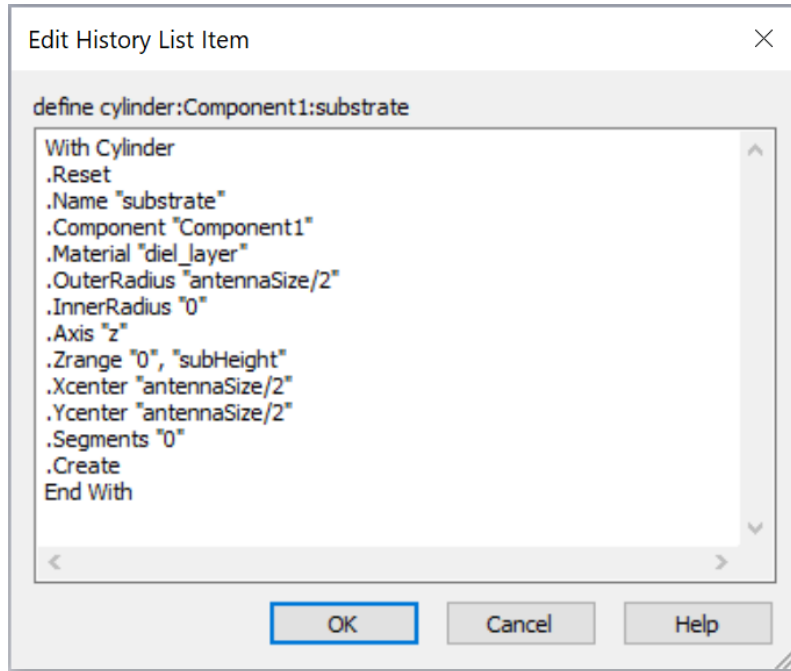


Figure 21: Automatic generation of a cylinder in VBA.

The cylinder used to create the slab is parametrized regarding values preliminary defined. For this example, the used parameters are:

- *antennaSize* is the total size of the antenna, i.e. the diameter of the circular slab, so the outer radius of the cylinder is equal to half of the value ($antennasize/2$);
- *subHeight* is the height of the considered substrate;
- *substrate* is the name given to the item inside the software environment;
- *diel_layer* is the material assigned to the substrate, whose dielectric constant and color were preliminarily defined.

What has to be underlined is the difference between the code lines shown in this VBA example, with respect to a more common object-oriented or procedural programming language. A more concrete comparison can be achieved by looking at the Matlab example shown in the next section.

3.2.5 Matlab scripting examples

The Matlab code written to generate the substrate cylinder is parametrized with respect to the same values introduced in the VBA example previously reported.

```

1  cst.addCylinder(" antennaSize/2", 0, 'z', " antennaSize/2", " antennaSize/2", ...
    {0 'subHeight'}, 'substrate', 'Component1', 'diel_layer');

```

As can be seen, recalling the dedicated function, just two code lines are enough to generate the wanted geometry. This is possible because all the complex controls that allow CST to understand what is written in Matlab are provided by the discussed interface.

To emphasize the complexity that the Matlab-CST interface has, the function that provides the Matlab implementation of the generic cylinder (named as “*addCylinder*”) is given below.

```

function addCylinder(obj,R1,R2,orientation ,X,Y,Z,name,component ,material)
2
    R1 = obj.checkParam(R1);
    R2 = obj.checkParam(R2);
    X = obj.checkParam(X);
    Y = obj.checkParam(Y);
    Z = obj.checkParam(Z);
8
    VBA = sprintf(['With Cylinder\n' ,...
10     '. Reset\n' ,...
        '. Name "%s"\n' ,...
12     '. Component "%s"\n' ,...
        '. Material "%s"\n' ,...
14     '. OuterRadius "%s"\n' ,...
        '. InnerRadius "%s"\n' ,...
16     '. Axis "%s"\n' ] ,...
        name,component ,material ,R1,R2,lower(orientation));
18
    switch lower(orientation)
20     case 'z'
        VBA2 = sprintf([VBA,...
22         '. Zrange "%s" , "%s"\n' ,...
            '. Xcenter "%s"\n' ,...
24         '. Ycenter "%s"\n' ,...
            '. Segments "0"\n' ,...
26         '. Create\n' ,...
            'End With' ] ,...
            Z(1),Z(2),X,Y);
30     case 'y'
        VBA2 = sprintf([VBA,...
32         '. Yrange "%s" , "%s"\n' ,...
            '. Xcenter "%s"\n' ,...
34         '. Zcenter "%s"\n' ,...
            '. Segments "0"\n' ,...
36         '. Create\n' ,...
            'End With' ] ,...
            Y(1),Y(2),X,Z);
38     case 'x'
        VBA2 = sprintf([VBA,...
40         '. Xrange "%s" , "%s"\n' ,...
            '. Ycenter "%s"\n' ,...
42         '. Zcenter "%s"\n' ,...
            '. Segments "0"\n' ,...
44         '. Create\n' ,...
            'End With' ] ,...
            X(1),X(2),Y,Z);
46
    end
48
    obj.update(['define cylinder:' ,component ,':' ,name] ,VBA2);
50
52 end

```

Strictly speaking, what is implemented by the interface is a macro function that takes as input the parameter defined by the user (as the geometry dimensions, the spatial position in x and y directions, the thickness of the structure, etc) and then, prints exactly the same VBA instructions shown in Figure 21 transmitting to them the input parameters. The Matlab object created is interpreted by CST through the VBA instruction printed by the code.

3.3 Creating Matlab functions

In this section, detailed descriptions of the functions written to generate the entire antenna structure are given.

Having introduced the kind of geometries that compose the antenna, it is possible to understand that the type of functions that needs to be written depends on the geometric form that describes the considered shape. A hierarchical approach is so defined.

Firstly, low-level functions (as the one previously reported) were created. Then, to generate a more simple and efficient code, a *function wrapping* is performed in order to create a high-level script that is able to exploit the lower order functions to generate the complete structure.

This aspect is particularly important because, following this procedure, a generic user has no need to understand how the Matlab-CST interface is structured and works. The user has only to define, in Matlab, the parameters that describe the specific system (operating frequency, type of dielectric, type of conductors, antenna's dimensions, etc), and after, to pass them as input to the generating functions. In this way, a very compact and user-friendly code is obtained.

To better appreciate the differences between high and low-level functions, both types are reported in the following. From now on, just circular substrates will be considered, while each radiating element shape previously discussed is used.

3.3.1 Circular substrate generation

The low-level function written to correctly generate this geometry corresponds to the one already shown in Section 3.2.5

```
2 cst.addCylinder(" antennaSize/2", 0, 'z', 0, 0, {0 'subHeight'}, ...  
  'substrate', 'Component1', 'diel_layer');
```

It can be noticed that a user who is totally unaware of how the Matlab-CST interface function works cannot correctly generate the structure. Indeed, in this case a generic user should know how to define:

- the total size of the antenna;
- the null value of the inner radius of the cylinder (being the circular substrate generation based on the definition of a cylinder);
- the orientation of the vertical extension of the antenna (z direction generically);
- the couple of (x, y) values with respect to which the antenna is centered;
- the height of the dielectric substrate;
- the component to which the item belongs;

- the name of the dielectric material that composes the substrate (if not in the CST material library it has to be preliminarily defined).

Table 1 summarizes the realized situation to better understand how the indicated parameters are organized in the example code shown before.

(1)	Antenna total size (radius)	“antennaSize/2”
(2)	Cylinder inner radius	0
(3)	Cylinder orientation	‘z’
(4)-(5)	(x, y) center	(0, 0)
(6)	Z extension vector (height of the substrate)	{0 ‘subHeight’}
(7)	Name of the generated item	‘substrate’
(8)	Name of the component to which the generated item belongs	‘Component1’
(9)	Name of the material that composes the item	‘diel_layer’

Table 1: Circular substrate low-level function input parameters.

It can be understood that the parameters which rule the execution of the low-level function are not just related to antenna specs (total size, dielectric characteristics), but some of them are just linked to the correct operation of the function itself. Hence, if a generic user is not aware of how to exactly define each parameter, some CST or Matlab error will occur.

Differently, using high-level functions, a generic user has just to know how a Matlab function works. In this case, the user should simply recall the function and understand which parameters the function requires as inputs. Once given the input parameters, the function returns in CST an object defined by the specified values. The wrapped function that generates the circular substrate is named “*CreateCircularSubstrate.m*”

```
function CreateCircularSubstrate(antennaSize, eps_r, mu_r, subHeight)
```

It should be quite intuitive that in this case, the parameters that the user has to give as inputs are just related to the specific antenna that he wants to create, there are no “technical” parameters related to the correct execution of the function itself.

(1)	Antenna total size (diameter)
(2)	Relative permittivity of the dielectric substrate
(3)	Relative permeability of the dielectric substrate
(4)	Height of the dielectric substrate

Table 2: Circular substrate high-level function input parameters.

Of course, what is contained inside the high-level function is properly a wrapping of the low-level one.

```

1     function CreateCircularSubstrate(antennaSize, eps_r, mu_r, subHeight)
3 tmp= evalin('caller', 'CST');
5 tmp.addNormalMaterial('diel_layer', eps_r, mu_r, [0 1 1]);
   tmp.addParameter('antennaSize', antennaSize);
7 tmp.addParameter('subHeight', subHeight);
9 tmp.addCylinder(" antennaSize/2", 0, 'z', 0, 0, ...
   ...
11     {0 'subHeight'}, 'substrate', 'Component1', 'diel_layer');
13
   end

```

3.3.2 Circular GND plane generation

As previously stated, the generation of the GND plane has no differences (apart from dimensions and spatial position) from the substrate generation. In this case, the parameters that the user should define as input are the total antenna size and the thickness that the conductor should have. In each considered case, a PEC plane is used for simplicity and it extends along negative values of 'z' direction.

```

   function CreateCircularGNDPlane(antennaSize, thickness)
2
   tmp= evalin('caller', 'CST');
4
   tmp.addParameter('antennaSize', antennaSize);
6 tmp.addParameter('thickness', thickness);
8 tmp.addCylinder(" antennaSize/2", 0, 'z', 0, 0, {"-thickness", 0}, 'GND', 'Component2', 'PEC');

```

3.3.3 Coax cable feeder generation

Regarding the generation of the feeder, the generating function presents, as input parameters, the values of relative permittivity and permeability of the coax cable dielectric. This is related to the preliminary evaluation of the correct dimensions of the cable that implements a 50Ω characteristic impedance.

The dimensions introduced in Section 3.2.2 are so carried over inside the high-level function to create the wanted feeder.

```

function CreateOptimizedCoax50(eps_r_coax, mu_r_coax, coax_coating_radius,
   coax_dielectric_inner_radius, coax_dielectric_outer_radius, coax_wire_outer_radius)
2
   tmp= evalin('caller', 'CST');
4
   tmp.addNormalMaterial('diel_coax', eps_r_coax, mu_r_coax, [0.8 0.8 0.3]);
6
   tmp.addParameter('coax_coating_radius', coax_coating_radius);
8 tmp.addParameter('coax_dielectric_outer_radius', coax_dielectric_outer_radius);
   tmp.addParameter('coax_dielectric_inner_radius', coax_dielectric_inner_radius);
10 tmp.addParameter('coax_wire_outer_radius', coax_wire_outer_radius);
12 %creating the coax cable input feeding
   %coating
14 tmp.addCylinder('coax_coating_radius', 'coax_coating_radius', 'z', 0, 0, {"-thickness", 0}, 'Coax
   Coating', 'Component2', 'PEC');
   %dielectric
16 tmp.addCylinder(" coax_dielectric_inner_radius", " coax_dielectric_outer_radius", 'z', 0, 0, ...
   {"-thickness", 0}, 'Coax Dielectric', 'Component1', 'diel_coax');
18 %pin

```

```

20 tmp.addCylinder(" coax_wire_outer_radius", 0, 'z', 0, 0, ["-thickness", "subHeight+2.8078"], ...
    'Coax Wire', 'Component1', 'PEC');
22 %defining the boolean operation to correctly insert the coax calbe through the substrate
tmp.insertObject('Component2:GND', 'Component1:Coax Dielectric');
24 tmp.insertObject('Component2:GND', 'Component2:Coax Coating');
    %adding waveguide port
26 tmp.addWaveguidePort('zmin', {"-coax_coating_radius"} ("coax_coating_radius"), ...
    {"-coax_coating_radius"} ("coax_coating_radius"), "-thickness");

```

It can also be observed that the function is able to add a *discete waveguide port* to correctly feed the system with a traveling wave. Being the added port named as *port 1*, its reflection coefficient will be indicated as S_{11} .

Moreover, specific *boolean operation* is performed in order to correctly *insert* the coax cable within the dielectric substrate and GND plane.

3.3.4 Circular patches generation

Once implemented the Metasurface's supporting structure, the Matlab functions written to generate the wanted MTS lattice can be reported. Being the less complex shape, the circular patches generating function is firstly shown.

```

    function CreateCircularPatches(xCoordinate, yCoordinate, radius, antennaSize)
2
4 tmp= evalin('caller', 'CST');
    lambda_CST= evalin('caller', 'lambda_CST');
6 antenna_geometry= evalin('caller', 'antenna_geometry');
    x_grid= xCoordinate;
8 y_grid= yCoordinate;
    antennaRadius= antennaSize/2;
10
12 ii=0;
    for i = 1:length(x_grid)
14         ii = ii+1;
16         Xblock = x_grid(i);
            Yblock = y_grid(i);
18         %creating the name at each iteration
            name = ['CircularPatch', num2str(ii)];
20         %creating the single patch for the current iteration
            r=radius(i);
22         tmp.addCylinder(r, 0, 'z', Xblock, Yblock, {'subHeight', 'subHeight'}, name, 'Component1', '
            PEC');
24         %control on the position of the i-th block, if its position exceeds the substrate limits it
            must be deleted
            if (Xblock+r>antennaSize || (Yblock+r>antennaSize)) || ((Xblock-r)<0 || (Yblock-r)<0) || ...
26                 (abs(Xblock-antennaSize/2)<lambda_CST/10 && abs(Yblock-antennaSize/2)<lambda_CST/10) ...
                    || ((Xblock-antennaRadius)^2+(Yblock-antennaRadius)^2>=(antennaRadius-1)^2 &&
                antenna_geometry=='Circular') ...
28                 || ((Xblock-antennaRadius)^2+(Yblock-antennaRadius)^2>=(antennaRadius-1)^2 &&
                    antenna_geometry=='Circular')
                name_complete= ['Component1:', name];
30         %deleting function
            tmp.deleteObject('solid', name_complete);
32     end
end

```

Looking at the code lines, a more complex situation can be noticed for the generation of the radiating elements. Being the function related to the generation of multiple objects, the implementation is managed by the exploitation of a loop whose length is defined by the number of elements stored in the vector that contains the (x, y) spatial coordinates (externally defined by the user).

Considering a generic user that wants to generate N circular patches, it has to give

as input parameters N (x , y) couples, N radius values (variable or not), and the antenna total size. More specifically, the total structure dimension (*antennaSize*) is given as input in order to correctly implement an “*if*” statement able to control if the n -th element is generated outside of the dielectric substrate and, eventually, to delete it or issue a warning.

3.3.5 Elliptical patches generation

The same consideration described for circular patches can be extended to the generation of the grain of rice REs, since this shape can be practically realized by implementing an elliptic form.

What the user has to manage and give as inputs are the major and minor radii of the ellipse.

```

1  function CreateGrainOfRice(xCoordinate, yCoordinate, major_radius, minor_radius,
      rotation_angle_vector, antennaSize)
3
4  tmp= evalin('caller', 'CST');
5  lambda_CST= evalin('caller', 'lambda_CST');
6  antenna_geometry= evalin('caller', 'antenna_geometry');
7  x_grid= xCoordinate;
8  y_grid= yCoordinate;
9  antennaRadius= antennaSize/2;
11
12  ii=0;
13  for i = 1:length(x_grid)
14      ii = ii+1;
15
16      Xblock = x_grid(i);
17      Yblock = y_grid(i);
18      rotation_angle=rotation_angle_vector(i);
19
20      %creating the name at each iteration
21      name = ['GrainOfRice', num2str(ii)];
22      %creating the single patch for the current iteration
23      r=radius(i);
24      tmp.addECylinder(major_radius, minor_radius, 'z', Xblock(1), Yblock(1), {'subHeight', "
      subHeight"}, name, 'Component1', 'PEC');
25      %rotating the element
26      tmp.rotateObject_z(name-complete, rotation_angle);
27
28      %control on the position of the i-th block, if its position exceeds the substrate limits it
      must be deleted
29      if (Xblock+r>antennaSize || (Yblock+r>antennaSize)) || ((Xblock-r)<0 || (Yblock-r)<0) || ...
      (abs(Xblock-antennaSize/2)<lambda_CST/10 && abs(Yblock-antennaSize/2)<lambda_CST/10) ...
31      || ((Xblock-antennaRadius)^2+(Yblock-antennaRadius)^2>=(antennaRadius-1)^2 &&
      antenna_geometry=='Circular') ...
      || ((Xblock+antennaRadius)^2+(Yblock-antennaRadius)^2>=(antennaRadius+1)^2 &&
      antenna_geometry=='Circular')
33      %in order to correctly delete a specific solid the component's belonging must be specified
      name-complete= ['Component1:', name];
35      %deleting function
      tmp.deleteObject('solid', name-complete);
37
38  end
39 end

```

The same considerations done for the previously presented shape can be extended to coffee bean elements. In this case, also a rotation input parameter is added in order to correctly implement a wanted rotation of the element with respect to the center of the unit cell to which it belongs.

3.3.6 Coffee bean generation

Hereinafter, the anisotropic shapes generation is discussed. At first, the coffee bean generation is reported because it just amounts to the creation of a slot inside the circular patches shape already described.

```
1     function CreateCoffeeBean(xCoordinate, yCoordinate, radius, slot_width, rotation_angle_vector
   , antennaSize)
3 tmp= evalin('caller', 'CST');
   lambda_CST= evalin('caller', 'lambda_CST');
5
   slotWidth= slot_width;
7 x_grid= xCoordinate;
   y_grid= yCoordinate;
9
11 ii=0;
   for i = 1:length(x_grid)
13     ii = ii+1;
15
       Xblock = x_grid(i);
       Yblock = y_grid(i);
17     rotation_angle= rotation_angle_vector(i);
19
       %creating the name at each iteration
       name = ['CoffeeBean', num2str(ii)];
21     nameSlot= ['Slot', num2str(ii)];
       %creating the single element for the current iteration
23     r_bean=radius(i);
       tmp.addCylinder(r_bean, 0, 'z', Xblock(1), Yblock(1), {'subHeight', "subHeight+thickness"},
           name, 'Component1', 'PEC');
25     tmp.addBrick([Xblock(1)-slotWidth*r_bean, Xblock(1)+slotWidth*r_bean], ...
           [Yblock(1)-r_bean-0.1, Yblock(1)+r_bean+0.1], {'subHeight', "subHeight+thickness"}, ...
27     nameSlot, 'Component2', 'FR4');
29
       name_complete= ['Component1:', name];
       name_slot_complete= ['Component2:', nameSlot];
31     tmp.subtractObject(name_complete, name_slot_complete);
33
       %rotate the coffee beean according to user's angle
       tmp.rotateObject_z(name_complete, rotation_angle);
35
       %control on the position of the i-th block, if its position exceeds the substrate limits it
       must be deleted
37     if (Xblock(1)+r_bean>antennaSize || (Yblock(1)+r_bean>antennaSize)) || ...
           ((Xblock(1)-r_bean)<0 || (Yblock(1)-r_bean)<0)) || ...
39     (abs(Xblock(1)-antennaSize/2)<lambda_CST/10 && abs(Yblock(1)-antennaSize/2)<lambda_CST/10)
       name_complete= ['Component1:', name];
41     %deleting function
       tmp.deleteObject('solid', name_complete);
43
   end
45 end
```

The CST step-by-step implementation of the coffee bean shape is shown in Figure 22.

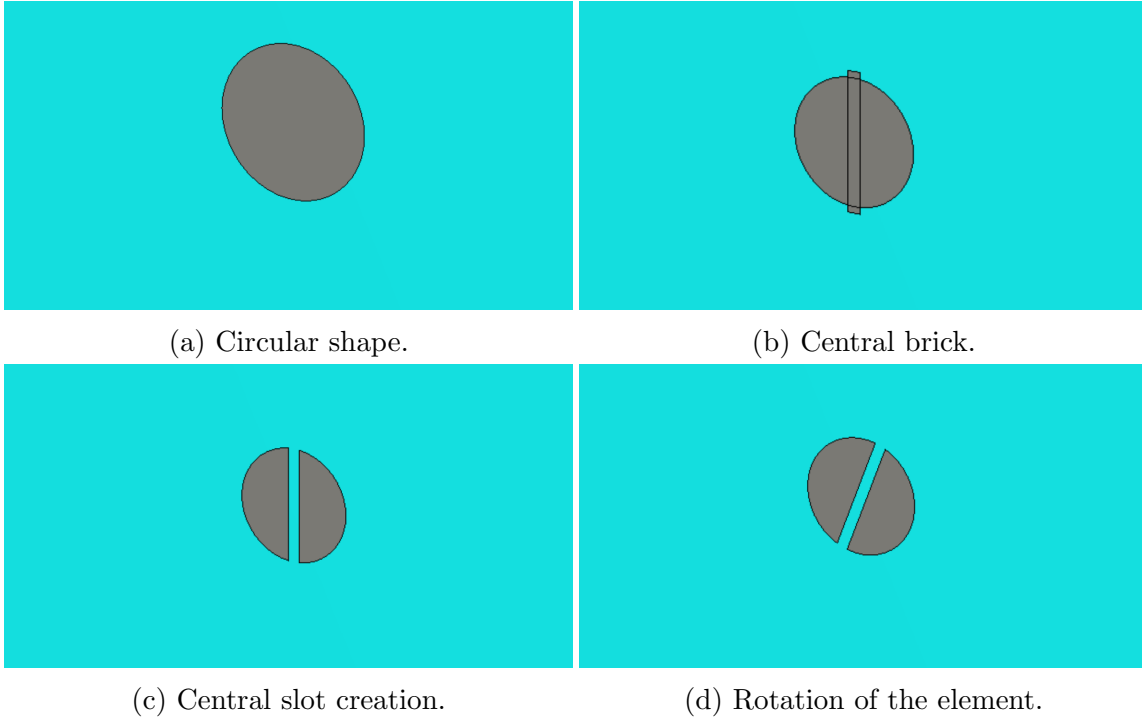


Figure 22: Coffee bean shape, step-by-step CST implementation.

3.3.7 Double anchors generation

At last, the trickiest shapes generation is reported. As stated before, the complexity of this function is related to the fact that in order to create the double anchor profile, more geometric forms must be combined.

```

1  function CreateDoubleAnchors(xCoordinate, yCoordinate, rotation_angle_vector, ...
    major_radius, minor_radius, alpha, thickness, antennaSize)
3
4  tmp= evalin('caller', 'CST');
5  subHeight=evalin('caller', 'subHeight');
6  lambda_CST= evalin('caller', 'lambda_CST');
7  antenna_geometry= evalin('caller', 'antenna_geometry');
8
9  x_grid= xCoordinate;
10 y_grid= yCoordinate;
11 antennaRadius= antennaSize/2;
12 alpha_deg= deg2rad(alpha);
13 tmp.AddParameter('major_radius', major_radius);
14 tmp.AddParameter('minor_radius', minor_radius);
15 tmp.AddParameter('double_anchors.thickness', thickness);
16
17 ii=0;
18 for i = 1:length(x_grid)
19     ii = ii+1;
20
21     Xblock = x_grid(i);
22     Yblock = y_grid(i);
23     rotation_angle= rotation_angle_vector(i);
24
25     %triangles points (considering generic rect triangle)
26     X_origin= Xblock;
27     Y_origin= Yblock;
28     Xl= X_origin;
29     Yl= Y_origin+major_radius;

```

```

X2= X1-(major_radius*tan(alpha_deg)); %alpha is the angle between the origin of the
double anchor and the aperture
31 Y2= Y1;
X3= X_origin;
33 Y3= Y_origin;
points_vector= [X_origin , Y_origin , X1, Y1, X2, Y2, X3, Y3];
35
37
%creating the name at each iteration
39 name = ['DoubleAnchor', num2str(ii)];
name_deleting_ellipse = ['DeletingEllipse', num2str(ii)];
41 name_curvePolygons= ['Polygon', num2str(ii)];
name_slot= ['Slot', num2str(ii)];
43 name_slot2= ['Slot2_', num2str(ii)];
45
%creating the single patch for the current iteration
tmp.addECylinder("major_radius", "minor_radius", 'z', Xblock(1), Yblock(1), {'subHeight',
"subHeight"}, name, 'Component1', 'PEC');
47 tmp.addECylinder("major_radius-0.1", "minor_radius-0.1", 'z', Xblock(1), Yblock(1), {'
subHeight', "subHeight"}, name_deleting_ellipse, 'Component2', 'PEC');
49
%creating full name to correctly delete solids
name_complete= ['Component1:', name];
51 name_deleting_ellipse_complete= ['Component2:', name_deleting_ellipse];
name_deleting_triangles_complete= ['Component2:', name_curvePolygons];
53 name_slot_complete= ['Component2:', name_slot];
name_slot2_complete= ['Component2:', name_slot2];
55
%to avoid PEC residue issue due to rounding error between matlab
%and CST parameter values
57 tmp.addBrick({Xblock(1)-0.01, Xblock(1)+0.01}, {Yblock(1)-minor_radius, Yblock(1)+
minor_radius}, {subHeight, subHeight}, name_slot2, 'Component2', 'PEC');
59 tmp.subtractObject(name_complete, name_slot2_complete);
61
%to create triangles
tmp.addPolygonBlock3Dtriangles(points_vector, subHeight, name_curvePolygons);
63 tmp.addCoverCurve('PEC', 'Component2', name_curvePolygons);
tmp.MirrorObject(name_deleting_triangles_complete, X_origin, Y_origin, subHeight, 1, 0, 0);
65 tmp.MirrorObject(name_deleting_triangles_complete, X_origin, Y_origin, subHeight, 0, 1, 0);
67
%deleting the solids to create correct shapes
tmp.subtractObject(name_complete, name_deleting_ellipse_complete);
69 tmp.subtractObject(name_complete, name_deleting_triangles_complete);
71
%adding the final slot to complete the double anchor geometry
tmp.addBrick({Xblock(1)-major_radius+0.05, Xblock(1)+major_radius-0.05}, {Yblock(1)-
thickness, Yblock(1)+thickness}, {subHeight, subHeight}, name_slot, 'Component2', 'PEC');
73 tmp.addObjects(name_complete, name_slot_complete);
75
%rotate i-th anchors by arbitrary rotation angle
tmp.rotateObject.z(name_complete, rotation_angle);
77
%control on the position of the i-th block, if its position exceeds the substrate limits
it must be deleted
79 if (Xblock(1)+major_radius>antennaSize || (Yblock(1)+major_radius>antennaSize)) || ...
((Xblock(1)-major_radius)<0 || (Yblock(1)-major_radius)<0) || ...
(Yblock(1)+major_radius>Yblock(2)) || ((Xblock(1)-antennaRadius)^2+(Yblock(1)-
81 antennaRadius)^2>=(antennaRadius-1)^2-1 && ...
antenna_geometry=="Circular") || ((Xblock(1)-antennaRadius)^2+(Yblock(1)-antennaRadius
^2)>=(antennaRadius-1)^2-1 && antenna_geometry=="Circular")
83 % name_complete= ['Component1:', name];
%deleting function
85 tmp.deleteObject('solid', name_complete);
end
87
end

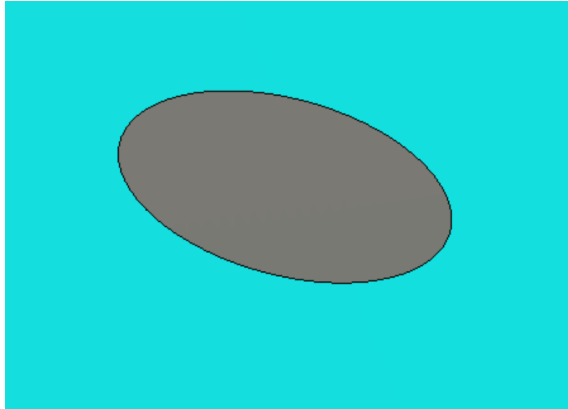
```

To be more specific, the required combination of geometric shapes to correctly implement the double anchor is:

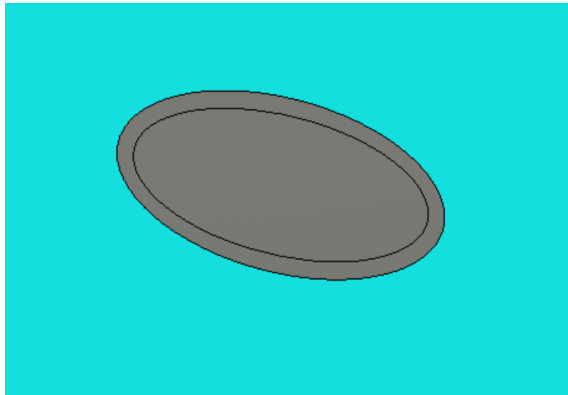
- generation of an external ellipse with radius r ;
- generation of an internal ellipse with radius r_1 whose value is assigned such as that the difference between the two radii is equal to the thickness of the double anchor, $r - r_1 = thickness$;
- generation of a triangle whose vertex is placed at the center of the radiating element, whose angle is defined by the user;

- mirroring of the generated triangle on the opposite side of the cell;
- deletion of the extra geometries;
- generation of the central brick that links the two anchors;
- rotation of the element by a user-defined value of the angle α with respect to the center of the belonging unitary cell.

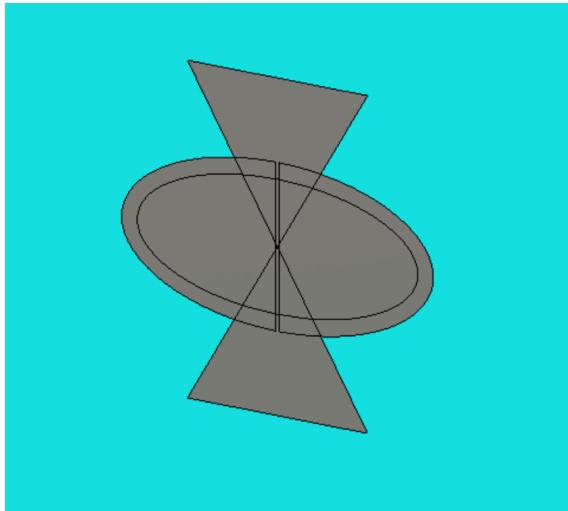
The discussed step-by-step implementation is graphically reported in Figure 23.



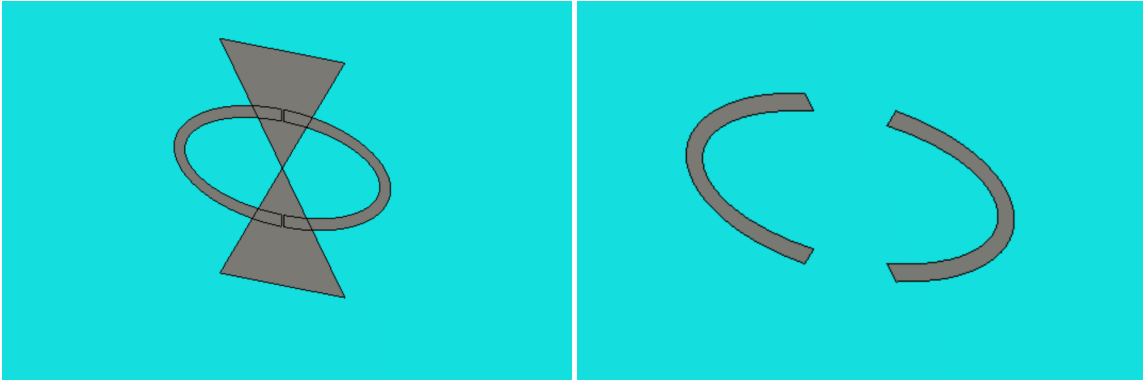
(a) Generation of the major external ellipse.



(b) Generation of the minor internal ellipse.

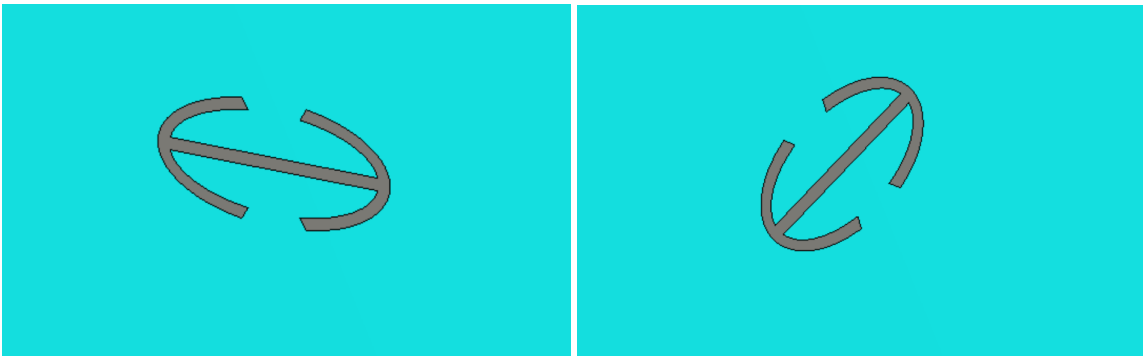


(c) Generation of the triangles to create the aperture in the shape.



(d) Deleting the inner ellipse.

(e) Deliting the triangle shapes.



(f) Complete double anchor shape.

(g) Rotation of the complete element.

Figure 23: Double anchor shape, step-by-step CST implementation.

3.4 VBA functions

In this section, the contributions related to VBA scripting are shown. In order to carry out different tasks during the development of the automatic code, there was a need for the implementation of new functions for the Matlab-CST interface.

Firstly, a new function able to provide the correct rotation of the generated object is written and added to the Giddens library. More precisely, a function linked to this purpose was already provided by the interface code, but it does not work well with shapes that need to be rotated with respect to one single direction. For this reason, considering that the MTS elements lie on the (X, Y) plane, a rotation with respect to Z direction is implemented.

The written code is shown in the following.

```

2     function rotateObject_z(obj,name_complete, z_rotation_angle)
3         VBA = sprintf(['With Transform\n', ...
4             '.Reset\n', ...
5             '.Name "%s"\n', ...
6             '.Origin "CommonCenter"\n', ...
7             '.Center "0", "0", "0"\n', ...
8             '.Angle "0", "0", "%f"\n', ...
9             '.MultipleObjects "False"\n', ...

```

```

10     '.GroupObjects "False"\n',...
12     '.Repetitions "1"\n',...
12     '.MultipleSelection "False"\n',...
12     '.Transform "Shape", "Rotate"\n',...
14     'End_With'] ,...
14     name_complete, z_rotation_angle);
16
16     obj.update(['transform: rotate ',name_complete],VBA);
18
18     end

```

Once written, the function is exploited in each high-level code that requires to rotate an element. The rotation is ruled by taking as input the value of the rotation angle. Furthermore, in order to correctly implement the double anchor shapes described in Section 3.3.7, it was necessary to implement *four* new functions for the Matlab-CST interface.

Having described the double anchors generation as ruled by the combination of ellipses and triangular shapes, and knowing that triangles are not directly provided by CST, the need for a function that generates triangular profile can be understood. The functioning of this code is based on the creation of a *polygon block* from the definition of 3 couples of (x, y) coordinates which, of course, depends on the n -th double anchor considered (the values of the coordinates are managed by the high-level function that creates the double anchors).

An example of the generic triangular curve that the function is able to provide is shown in Figure 24.

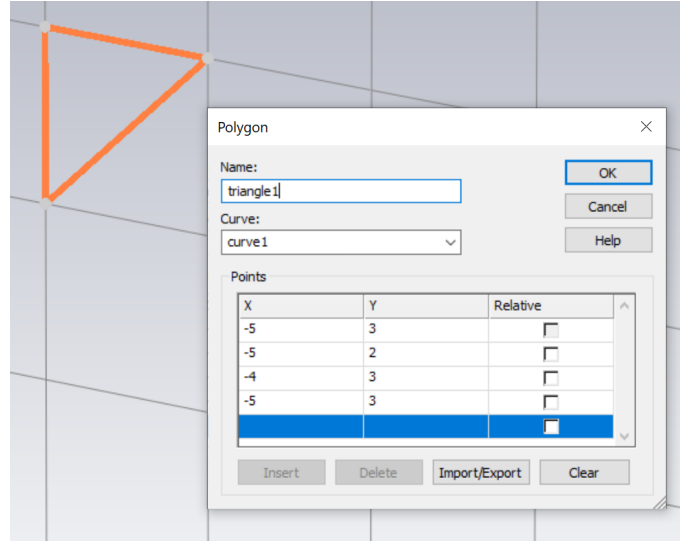


Figure 24: Generic triangular polygon generation.

At this point, there is the need to transform the polygon curve in a CST item in order to subtract it from the elliptical shapes. To do so, a *cover curve* function is implemented to transform the curved polygon into a manageable item.

```

2     function addCoverCurve(obj, material, component, name, varargin)
2         name_curve_complete=['curve1:',evalin('caller', 'name_curvePolygons')];

```

```

4
6
8     VBA = sprintf(['With CoverCurve\n' ,...
10     '. Reset\n' ,...
12     '. Name "%s"\n' ,...
14     '. Component "%s"\n' ,...
16     '. Material "%s"\n' ,...
18     '. Curve "%s"\n' ,...
20     '. DeleteCurve "True"\n' ,...
     '. Create\n' ,...
     'End With ' ] ,...
     name , component , material , name_curve_complete);

     obj.update(['define coverprofile: ' , component , ':' , name] , VBA);
end

```

The triangle item created by the function execution can be seen in Figure 25. In this case a PEC material is used because the shape will be related to a conducting element.

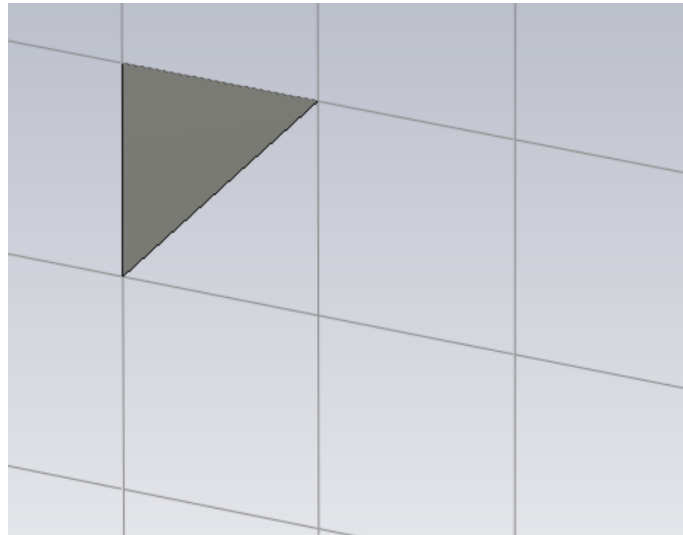


Figure 25: Generic triangular polygon generation.

Once obtained the triangular shape, a *mirroring function* is written in order to generate the specific structure that has to be subtracted from the elliptical shape to correctly create the double anchor.

```

function MirrorObject(obj , name , x , y , z , x_mirroring , y_mirroring , z_mirroring , varargin)
2
3     p = inputParser;
4     p.addParameter('repetitions' , 1);
5     p.addParameter('material' , '');
6     p.addParameter('destination' , '');
7     p.parse(varargin{:});
8
9     x = obj.checkParam(x);
10    y = obj.checkParam(y);
11    z = obj.checkParam(z);
12
13    VBA = sprintf(['With Transform\n' ,...
14    '. Reset\n' ,...
15    '. Name "%s"\n' ,...
16    '. Origin "Free"\n' ,...
17    '. Center "%f" , "%f" , "%f"\n' ,...
18    '. PlaneNormal "%f" , "%f" , "%f"\n' ,...

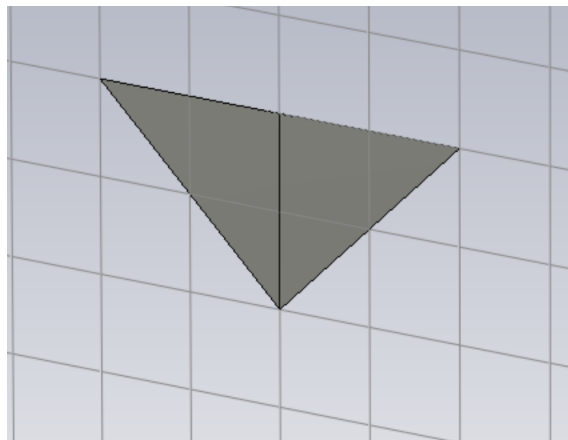
```

```

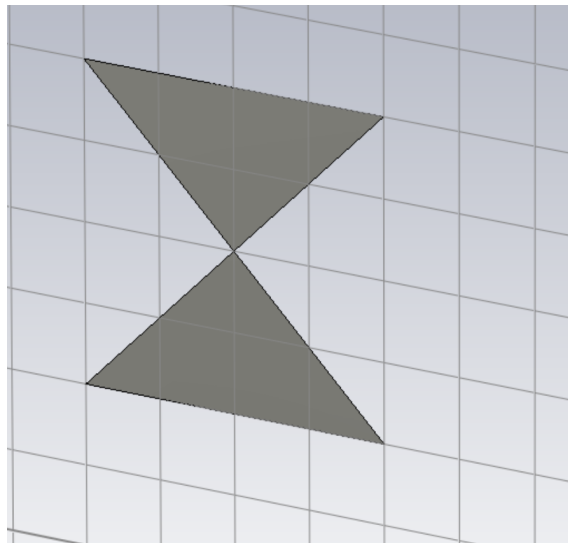
20     '. MultipleObjects "True"\n', ...
    '. GroupObjects "True"\n', ...
    '. Repetitions "%d"\n', ...
22     '. MultipleSelection "False"\n', ...
    '. Destination "%s"\n', ...
24     '. Material "%s"\n', ...
    '. Transform "Shape", "Mirror"\n', ...
26     'End With' ], ...
    name, x, y, z, x_mirroring, y_mirroring, z_mirroring, p.Results.repetitions, p.Results.
28     destination, p.Results.material);
30     obj.update(['transform: mirror ', name], VBA);
    end

```

In particular, this function is exploited twice to obtain the final profile shown in Figure 26b.



(a) Shape obtained after the first mirroring.



(b) Shape obtain after the second mirroring.
This is the geometric form that will be used to correctly create double anchors.

Figure 26: Geometric form obtained by exploiting mirroring function.

At last, also a VBA function that implements the *boolean add* operation is written to correctly “sum” two different items in CST.

```

1     function addObject(obj, object1, object2)
2         %add objects into each other
3         VBA = sprintf('Solid.Add "%s", "%s"', object1, object2);
4         obj.update(sprintf('boolean add shapes:%s,%s', object1, object2), VBA);
5     end

```

3.5 Parameters extraction

As shown in each reported function, the generation of a considered shape starts from the definition of input parameters that rule the dimensions of the element. The automatic code is organized in such a way as to read the values from an external file where they are stored in. In this way, it could be possible for a user to choose a pre-defined file that contains specific size values that properly design a MTS antenna with specific features and performance. More detailed information regarding this aspect are postponed to Section 4.5 where future improvements are presented.

The reading operation from a storing file is organized in such a way that Matlab variables are created starting from what is contained inside the file. It is quite obvious that, at the actual level of the development of the automatic code, the user must be aware of the exact organization of the storage file in order to pass the values to the corresponding variables.

An example of the reading from an external file for a MTS antenna with circular patches implementation is reported below. In this case, data are stored in a *.csv* file. Each row of the file contains the parameters of the *n-th* circular patches:

- *column 1*: *x* coordinate of the element;
- *column 2*: *y* coordinate of the element;
- *column 3*: patch radius value.

The shown file organization leads to an extraction example:

```

1     store_param= readmatrix('filename.csv');
2     for i=1:length(store_param)
3         x_grid(i)= store_param(i,1);
4         y_grid(i)=store_param(i,2);
5         patch_radius(i)= store_param(i,3);
6     end

```

3.6 Feeder optimization

Starting from the structures generation, it is possible to focus on the optimization of antenna features. Firstly, what is discussed is the performance related to the feeding

system.

Considering the single-feeder approach for the MTS antennas, the performance related to this element can be linked to different type of efficiencies [17]:

- the *feed efficiency* ε_{feed} defines the amount of power delivered to the SW with respect to the input power;
- the *tapering efficiency* ε_{tap} defines the deviation from a uniform illumination;
- the *conversion efficiency* defines the performance of the system in terms of conversion from the SW power into a radiated leaky-wave power;
- the *ohmic efficiency* ε_{Ω} defines the amount of losses due to the structure.

The overall efficiency of MTS antennas involves several wave and phenomena. Considering a generic MTS antenna, the situation can be figured out by looking at Figure 27.

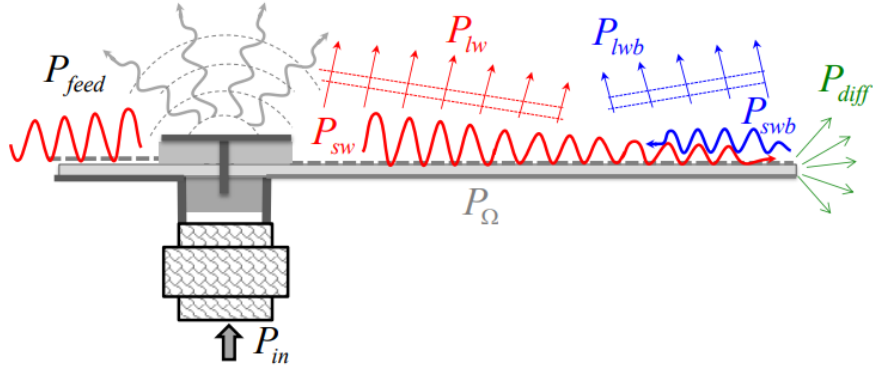


Figure 27: Power contributes of a generic MTS antenna. Taken from [17].

Where:

- P_{in} is the input power;
- P_{feed} is space wave power radiated by the feeder;
- P_{sw} is the SW power;
- P_{lw} is the power converted from the SW to the LW;
- P_{diff} is the power diffracted at the substrate edge;
- P_{swb} is the backward SW power (considering edge reflections);
- P_{lwb} is the LW power related to the reflected SW;
- P_{Ω} is the power dissipated by ohmic losses.

Strictly speaking, when a traveling wave is launched through the feeding system, the total amount of power is not delivered to the realized SW but it is, in part,

directly radiated in free space by the feeder itself. This feature is related to the feeder efficiency since $\varepsilon_{feed} = P_{SW}/P_{in}$.

The presence of the MTS on the dielectric surface realizes the conversion from the surface wave power into a leaky-wave power, whose radiation features are controlled by the defined modulation of the MTS lattice as already described. The capability of the system to transform the surface wave power P_{SW} into leaky-wave power P_{lw} is quantified by $\varepsilon_{conversion} = P_{lw}/P_{SW}$.

The amount of power decreasing related to metal and substrate losses can be, for simplicity neglected. At last, the tapering efficiency ε_{tap} depends on the amplitude tapering on the surface hence, the latter parameter is controlled by the modulation index of the surface impedance

The overall efficiency of the MTS antenna can be at this point described as:

$$\varepsilon_{TOT} = \varepsilon_{tap}\varepsilon_{conv}\varepsilon_{feed} \quad (27)$$

Taking into account that the modulation of the surface impedance is ruled by the metamaterial lattice and that the sizing and spatial parameters of the unitary elements are externally provided, it can be guessed that, at this level, the overall efficiency of the antenna cannot be improved by working on ε_{tap} and ε_{conv} . For this reason, the performance improvements to which this work is dedicated are related to the feeder, working on ε_{feed} .

Considering the definition of the feeder efficiency previously given, the first optimization session defined on CST is properly aimed to the reduction of the power radiated in free space directly from the feeder, in order to maximize the amount of power delivered as SW.

Certainly, being the surface wave power linked to the input wave, important considerations are also given to the optimization in terms of reflection waves working on impedance matching.

Usually, the monopole passes through the center of an annular patch loaded with an annular slot. This allows an impedance matching, as well as the maximization of the SW power launched on the MTS [4]. What is implemented in CST is exactly the described design of the feeder with annular patch.

In the following two examples of the considered design are reported. More precisely, Figure 28 shows a practical realization of an MTS antenna, while Figure 29 shows a CST implementation realized by exploiting the automatic code.

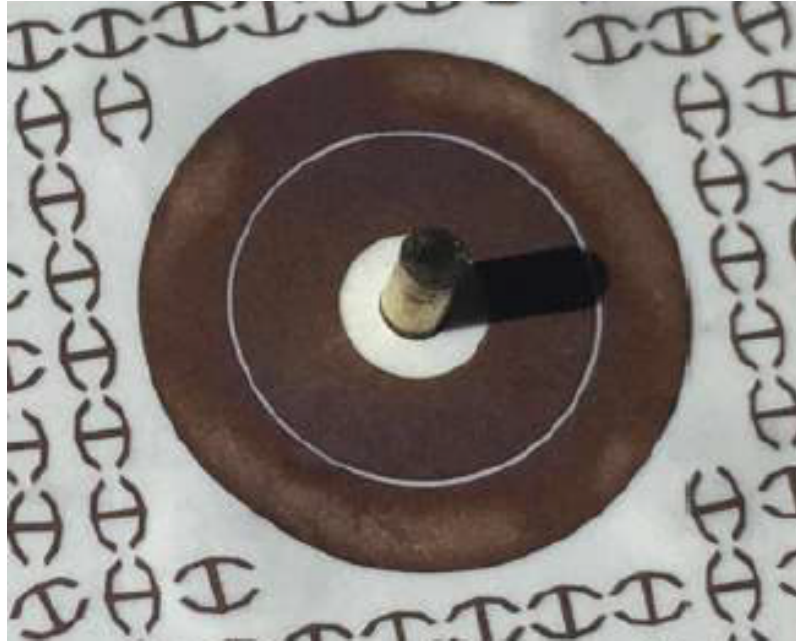


Figure 28: Zoomed view of the feeding annular termination of a practical MTS antenna. Taken from [4].

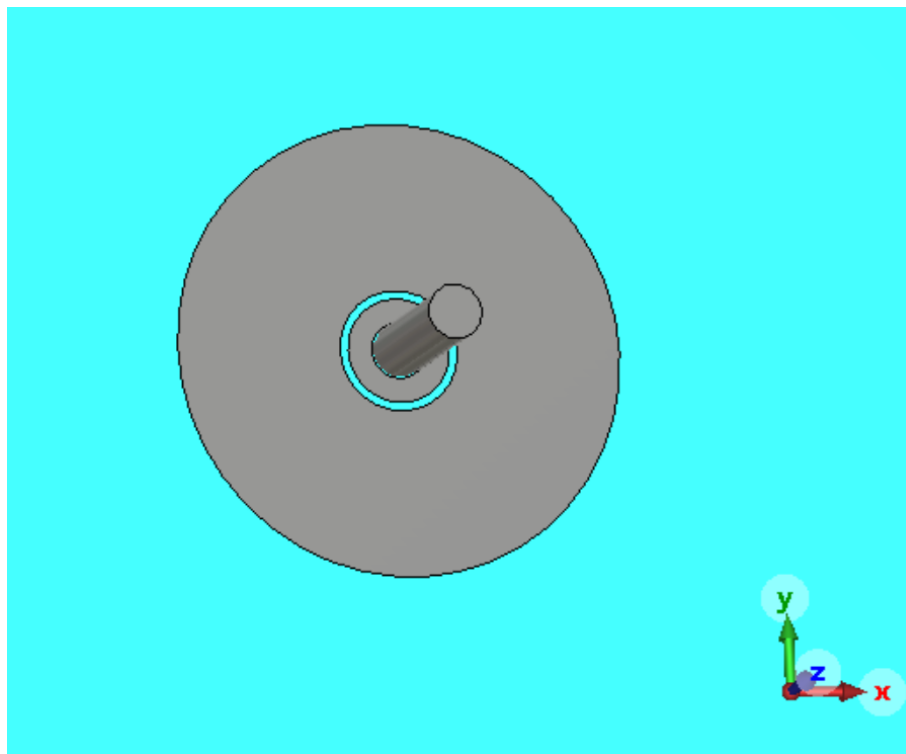


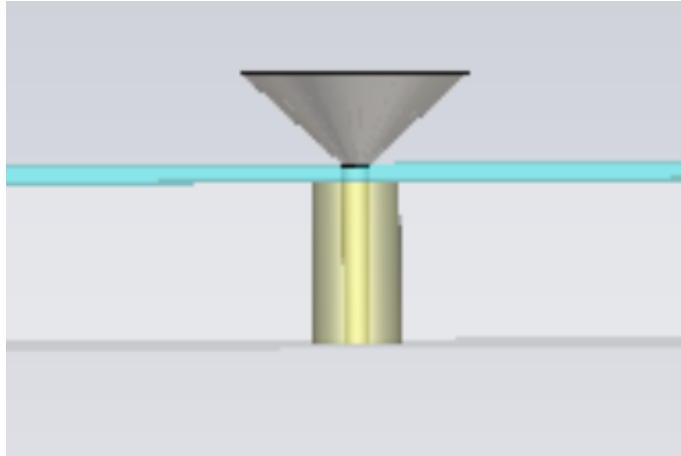
Figure 29: Zoomed view of the feeding annular termination of a MTS antenna implemented in CST environment.

The annular patches radii and the gap defined in this implementation are provided by literature [18]. It is important to say that the MTS antenna considered by the authors is quite different, in terms of substrate characteristics, total antenna dimensions, and operating frequency, from the structures considered in this thesis. For this reason, input impedance and reflection coefficient trends, which are obtained by simulating the structure, are rather far from optimal.

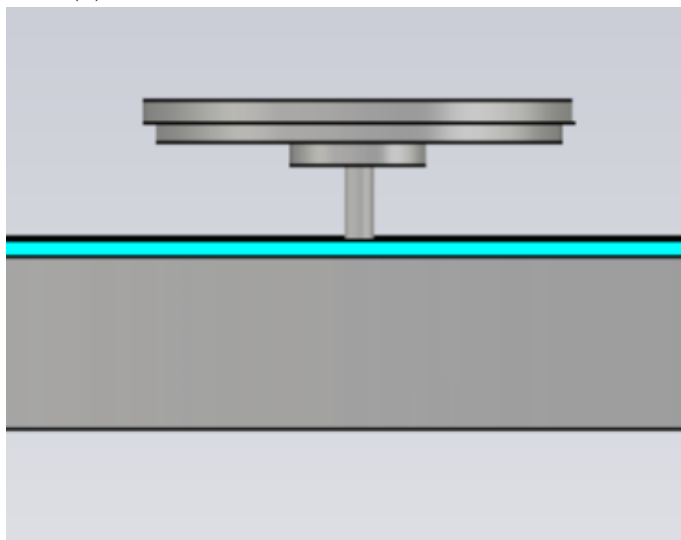
Further details regarding numerical and optimization results are postponed to Section 4.

To explore other possibilities, some “intuitive” feeding structures are designed starting from the wanted shape of the propagating wave that is generally searched for the enhancement of the SW power. Their CST implementation is realized through the exploitation of dedicated functions of the automatic code.

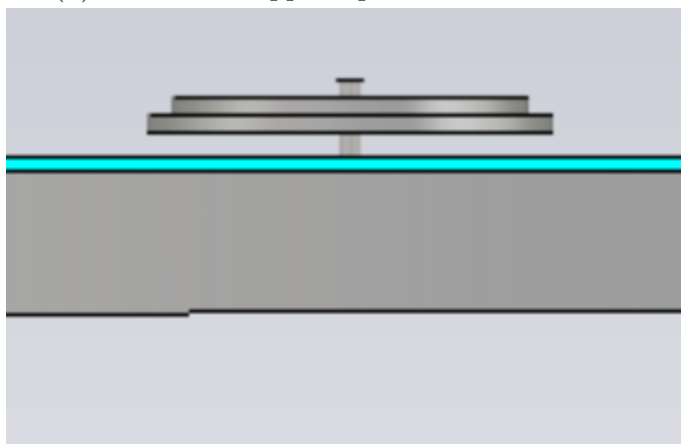
Figure 30a shows the “*horn-like*” feeder design, Figure 30b shows a “stepped hat” termination whose rings radius is increasing toward positive direction of Z coordinate, and at last Figure 30c shows the same design solution but with radii increasing that goes toward the negative direction of Z .



(a) Intuitive “horn-like” feeder termination.



(b) Intuitive “stepped up” feeder termination.



(c) Intuitive “stepped down” feeder termination.

Figure 30: Intuitive feeder termination structures.

As can be seen by looking at the reported structure, some design criticalities are achieved considering the tough realization complexity of horn-like structures considering the interested order of magnitude and the “multi-layer” approach. Results related to optimized structures are reported in Section 4.2.

3.7 Impedance reconstruction comparisons

As extensively described, the MTS antenna radiating features are strictly related to the macroscopic behavior of the Metasurface itself. Some methods are proposed in the literature in order to obtain an efficient mathematical treatment of the Metasurface exploiting the modelization of its IBC.

In [19] a solution is presented for the macroscopic modelization of the MTSs unit cells by partitioning the surface into small, electrically isolated cells which leads to a regularization effect on the impedance profile. The approach is in contrast with the “*continuous current*” designs [20] where no partitioning of the MTS domain is considered. Two particular types of cells are considered and investigated for surface impedance reconstruction:

- *square shape cells* (Figure 31a);
- *hexagonal shape cells* (Figure 31b).

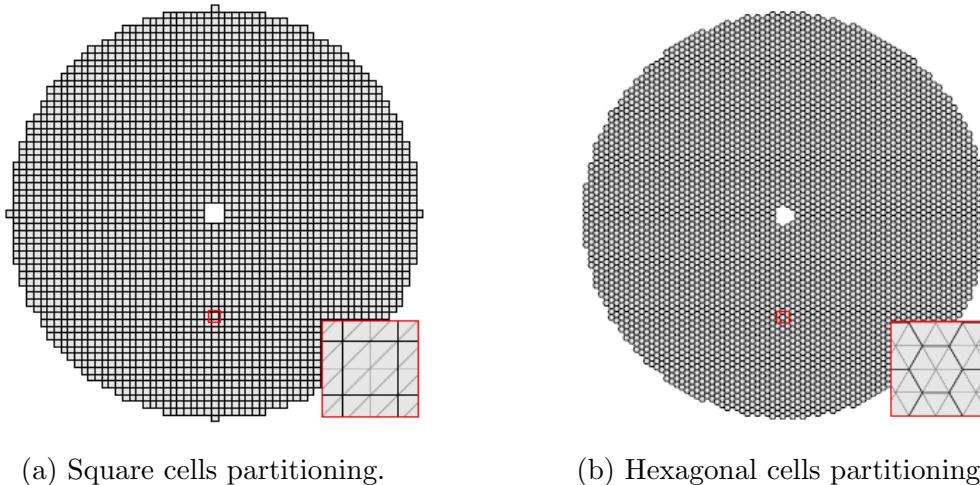


Figure 31: Partitioning of the MTS domain.

By applying the discussed subdivision to circular MTS antenna designs, complete structures are realized and radiation performance are obtained.

More in detail, considering the mentioned partitioning of the Metasurfaces, it can be guessed that different cell types imply different spatial coordinates that identify their own center. Therefore, being the position of the n -th radiating element related to the center of the n -th cell, different cell types provide different lattices for the

radiating element. At last, the complete structure of the MTS antenna depends on the chosen cell type.

Regarding this aspect, the automatic code developed by this thesis work constitutes great support considering the easy generation of different antenna structures in simulation environment.

Once generated the different structures, the simulations are performed in order to obtain FF radiation patterns and to compare them with the results of continuous current based designs.

3.8 MTS and feeder simulations

Once described the structure generation, the attention can be finally aimed toward the simulation of the entire antennas to obtain performance results.

The environmental variables that rule the CST simulations are also controlled by the automatic code. This aspect is managed by the implementation of two specific functions.

One deals with the definition of the *file name* that the user wants to give to the considered CST project, the definition of the solver type (frequency domain or time domain based solver), and the setup of the frequency range of the specific design. The written code is reported in the following.

```
1 function CST= BuildCSTModel(fileName , solverType , f_min , f_max)
3
4 %opening the application and creating a new project
5 CST = CST_MicrowaveStudio('C:\ generic file destination', fileName);
6 %defining the solver type
7 CST.setSolver(solverType); %setting the solver type
8 %setting boundary conditions
9 CST.setBoundaryCondition('xmin','open add space','xmax','open add space','ymin','open add space'
10 ,...
11 'ymax','open add space','zmin','open add space','zmax','open add space');
12 CST.addParameter('f_min', f_min);
13 CST.addParameter('f_max', f_max);
14 %setting the freq
15 CST.setFreq(f_min , f_max);
```

By looking at the code lines, it can be guessed that, at the current level of development, the managing of boundary conditions is not provided and controllable by the code but it is a priori set. Indeed, each antenna, designed for the purposes of this thesis, is simulated by considering *open boundary conditions* to mainly observe FF results.

Furthermore, to set up the FF monitor, another specific function is provided. Its functioning requires the user's inclusion of certain operating frequency values. Moreover, it implements a control statement dedicated to the check of the number of frequency values indicated. If multiple frequencies are inserted by the user, a correspondent number of FF monitors are set in CST environment.

```
function SetupFarfield(frequency)
2 tmp= evalin(" caller", "CST");
4 tmp.addFieldMonitor('farfield', frequency);
6 if length(frequency)>1
   for i=1:length(frequency)
8     tmp.addFieldMonitor('farfield', frequency(i));
   end
10 end
```

4 Numerical results

4.1 Automatic modelling of MTS antenna

In this chapter, the complete structures of the designed antenna and their relative simulation performance are reported. In order to correctly introduce the discussion of the obtained results, it is strictly important to remark that the main purpose of this thesis is not aimed at the thorough optimization of MTS antenna designs, but at the derivation of a method that allows obtaining the synthesized MTS structure in a simulation environment.

For this reason, at the current development level, it is not possible (or convenient) to directly perform the optimization of the MTS exploiting the automatic code itself. Therefore, the data related to the implementation of a desired surface impedance distribution have to be considered as an external study and optimization.

By performing the full-wave simulations and so by approaching less ideal conditions, it is possible to obtain concrete validations of what would be studied with preliminary analytical or numerical methods. Hence, it is possible to define the presented solution as a “*co-optimization*” method for the *design of MTS antennas*.

To emphasize the ease of generation of a complete MTS antenna structure, it is reported in the following an example of the automatic code able to generate a circular MTS antenna with circular patches radiating element, whose sizes and spatial positionings of the n -th cell are extracted from an external *.csv* file.

```
%% SECTION 1: defining user's antenna parameters
2 tic
  clc
4
% reading from csv file
6 store_param= readmatrix("impedance_profile.csv");
  for i=1:length(store_param)
8     x_grid(i)= store_param(i,1);
     y_grid(i)=store_param(i,2);
10    patch_radius(i)= store_param(i,3);
12 end
14
f0=23;      %GHz
16 lambda_CST=3e8/(f0*1e9)*1e3;      %lambda in mm
  antennaSize = 6*lambda_CST+1.15; %antenna's diameter in mm
18 antennaRadius= antennaSize/2; %antenna's radius
  unitCellSize= lambda_CST/10;      %(lambda/10)
20 nPix= antennaSize/unitCellSize;
22 %dielectric parameters
  eps_r= 6.5;      %relative permittivity
24 mu_r= 1;      %relative permeability
  subHeight= 0.508; %substrate thickness [mm]
26
  eps_r_coax= 2.1; %coax relative permittivity
28 mu_r_coax= 1; %coax relative permeability
30 thickness= 5; %ideal gnd plane thickness
  f_min= 20;
32 f_max= 26;
```

```

34 %% SECTION2: generating the CST Model
35 close all
36 antenna_geometry= 'Circular';
37
38 CST= BuildCSTModel('MetaSurfaceCircularAntenna_CircularPatches_MarcelloEX', 'frequency', f_min ,
39 f_max);
40
41 %%creating the substrate
42 CreateCircularSubstrate(antennaSize, eps_r, mu_r, subHeight);
43 %%creating gnd plane
44 CreateCircularGNDPlane(antennaSize, thickness);
45 %%creating the coax cable input feeding input: impedance value
46 CreateOptimizedCoax(eps_r_coax, mu_r_coax);
47
48 %%create circular patches
49 CreateCircularPatches2(x_grid, y_grid, patch_radius, antennaSize);
50
51 %%setting the field monitor for obtaining the far-field behavior on CST
52 SetupFarfield(f0);
53
54 %%save the project with the specified name
55 CST.save;
56
57 %% Run the simulation
58 CST.runSimulation
59 toc

```

Looking at the reported Matlab code it is possible to see how the first section is linked to the definition of the specific system parameters that the user wants to give to the antenna, then in the second section, the defined values are used as input for the specific functions able to generate the structures that compose the complete antenna.

4.2 Feeder design and optimization

Optimization results related to feeder design are now discussed. Firstly, an optimization session is performed starting from the feeder structure with annular termination shown in Section 3.6. The enhancement is particularly aimed at the improvement of the bandwidth behavior of the structure by trying to minimize the reflection coefficient (S_{11}). Being the considered antennas designed for operating at 23 GHz , a frequency range from 20 GHz to 26 GHz is considered.

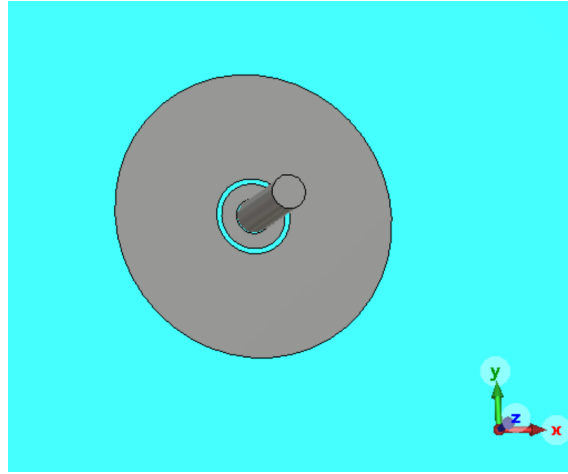
The swept parameters and their relative sweep ranges are reported in Table 3.

Parameter	Sweep range
Height of the protruding feeding monopole	[3 - 10] mm
Internal annular patch	[1 - 3] mm
External annular patch	[0.5 - 6] mm
Gap width between central monopole and internal patch	[0.1 - 1] mm
Gap width between internal and external patch	[0.01 - 0.5] mm

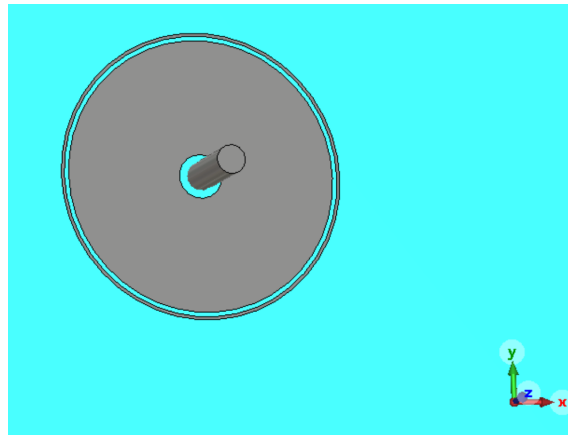
Table 3: Setup of swept parameters and their relative sweep range to optimize the feeder design.

Differences between the obtained feeder designs can be noticed in Figure 32, while

Figure 33 shows a perspective view of the complete simulated structure. Lastly, the optimized performance comparisons are reported in Figure 34.



(a) CST implementation of the feeder, non-optimized design.



(b) CST implementation of the feeder, optimized design.

Figure 32: CST designs of the feeding design before and after the optimization.

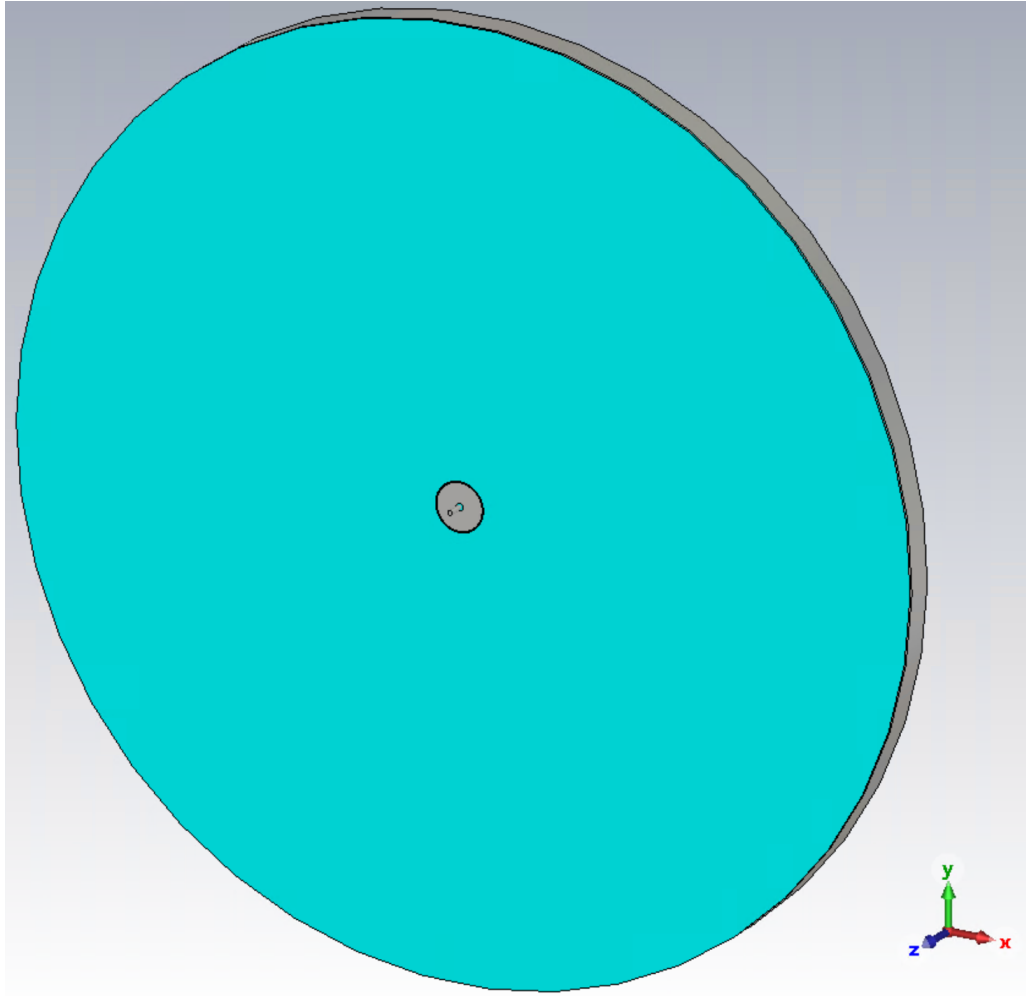
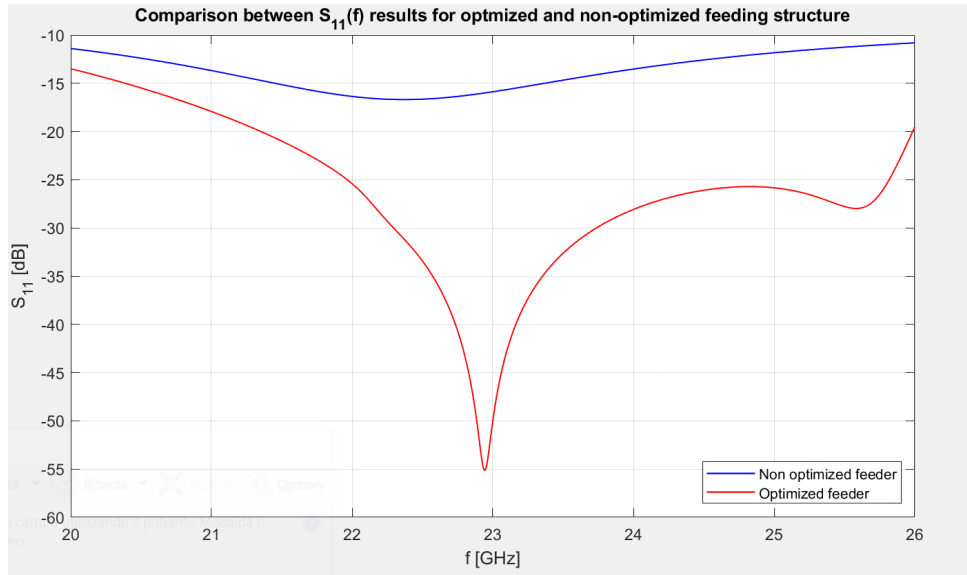
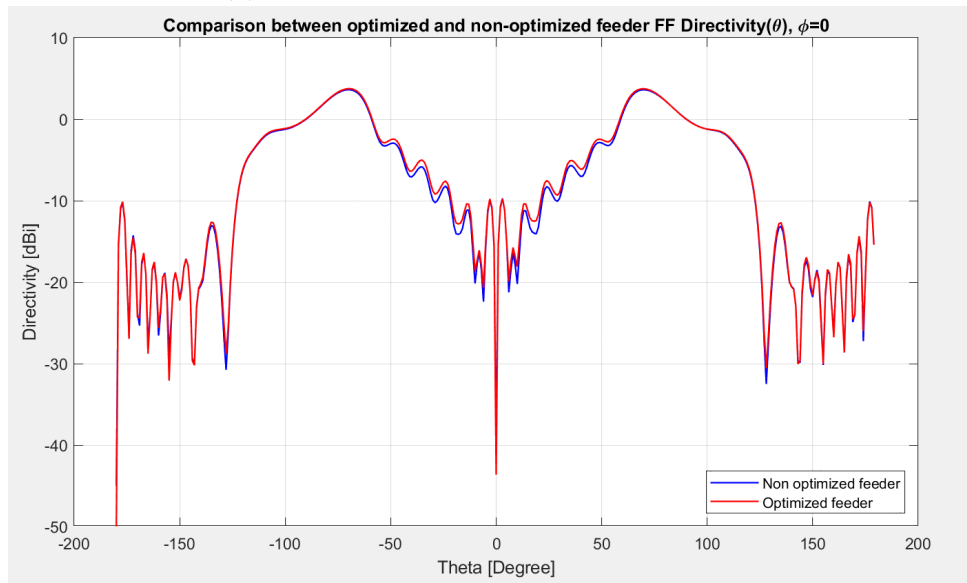


Figure 33: CST implementation of the complete structure simulated for the feeder optimization. Just the dielectric slab is considered at this level.



(a) Comparison between S_{11} performance.



(b) Comparison between FF Directivity(θ) in the plane cut $\phi = 0^\circ$.

Figure 34: Performance comparisons between optimized and non-optimized feeder. Blue curves report the non-optimized feeder trends, red curves report the optimized feeder trends.

The reported graphs show how, in terms of reflection features (Figure 34a), the performances are highly improved by obtaining a minimum value of $\simeq 55 \text{ dB}$ at the corresponding working frequency. A relatively “good” bandwidth behavior is also reached considering a possible operating range of $\simeq 6 \text{ GHz}$.

Different considerations can be done for the reported FF Directivity cuts (Figure 34b). In this case, it can be seen that there are no significant differences between

the two designs. Both trends show quite low values of Directivity, and the presence of a central hole, as quite expected considering the given symmetry of the structure. The achievement of a significant improvement in terms of input reflections, linked to a minimum increase of the free space radiated power, leads to obtaining a highly improved design of the feeder structure.

At this point, also the optimization of the other feeding structures (introduced in Section 3.6) is performed. In Figure 35 are shown the obtained S_{11} trends over the interested frequency range. Comparing the given results, it can be achieved that the discussed “annular patches” feeding structure results as the best within the optimized designs.

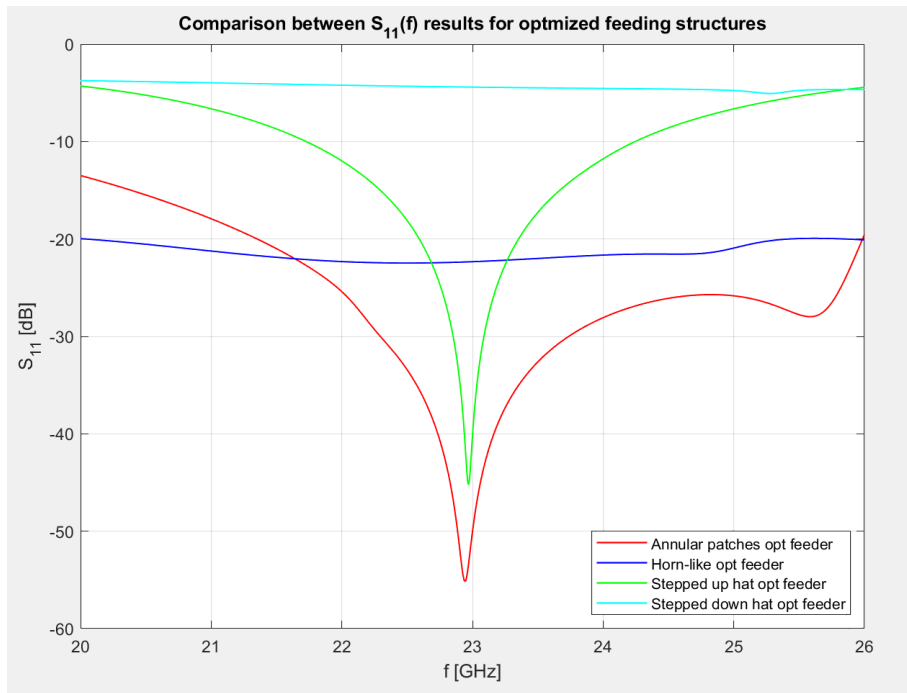


Figure 35: S_{11} comparison between optimized feeder structures.

Figure 36 shows a comparison between the trend of antenna’s input impedance in two different cases: the blue curve reports the value that the impedance assumes in a structure realized only with the grounded dielectric slab and the feeder, while the red curve shows the impedance value when a complete MTS antenna structure (with a random distribution of the Metasurface) is considered.

It can be stated that no significant differences between the two values are obtained and therefore the optimized reflection results, obtained considering no MTS, can be extended to the complete antenna structures since the same impedance matching is required.

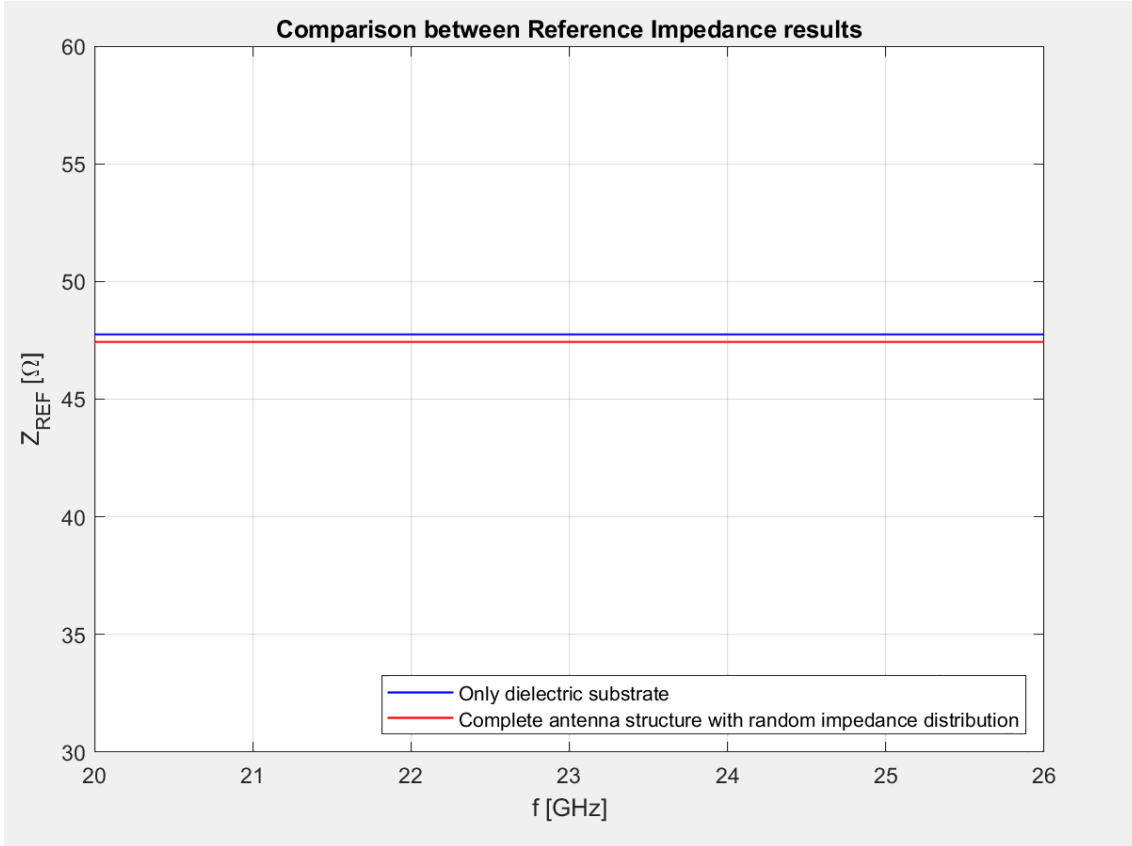


Figure 36: Comparison of input impedance values between the only substrate and complete MTS structure. The blue curve reports the reference impedance value for a structure made only by a dielectric substrate, red curve reports the reference impedance value for a complete MTS antenna structure with a random Metasurface distribution.

4.3 Feed efficiency optimization

The just discussed optimization of the feeding structure is aimed at the enhancement of the power related to the surface wave that is propagating through the dielectric substrate. As discussed in Section 3.6, the *feed efficiency* quantifies the capability of the system to convert the input power to a certain amount of SW power. However, CST software is not able to directly measure the power that is propagating within a surface and so, this quantity can not be directly optimized by defining it as a goal for the optimizer (as done for S_{11}). To solve this issue, a calculation method is developed and tested.

The solution consists of the definition of four waveguide ports that are placed through the dielectric substrate in such a way as to surround the feeding structure and to measure the power outgoing the ports themselves. This outgoing power is defined, in CST, as *power accepted per port*.

In order to obtain a quite fast simulation, the size of the lateral simulation domain is reduced to a square with 6λ sides structure, also, the boundary conditions are adjusted to allow considering the dielectric substrate as infinitely extended and minimize the reflections between the bounding box and the structure. In Figure 37 the CST implementation of the discussed method is shown.

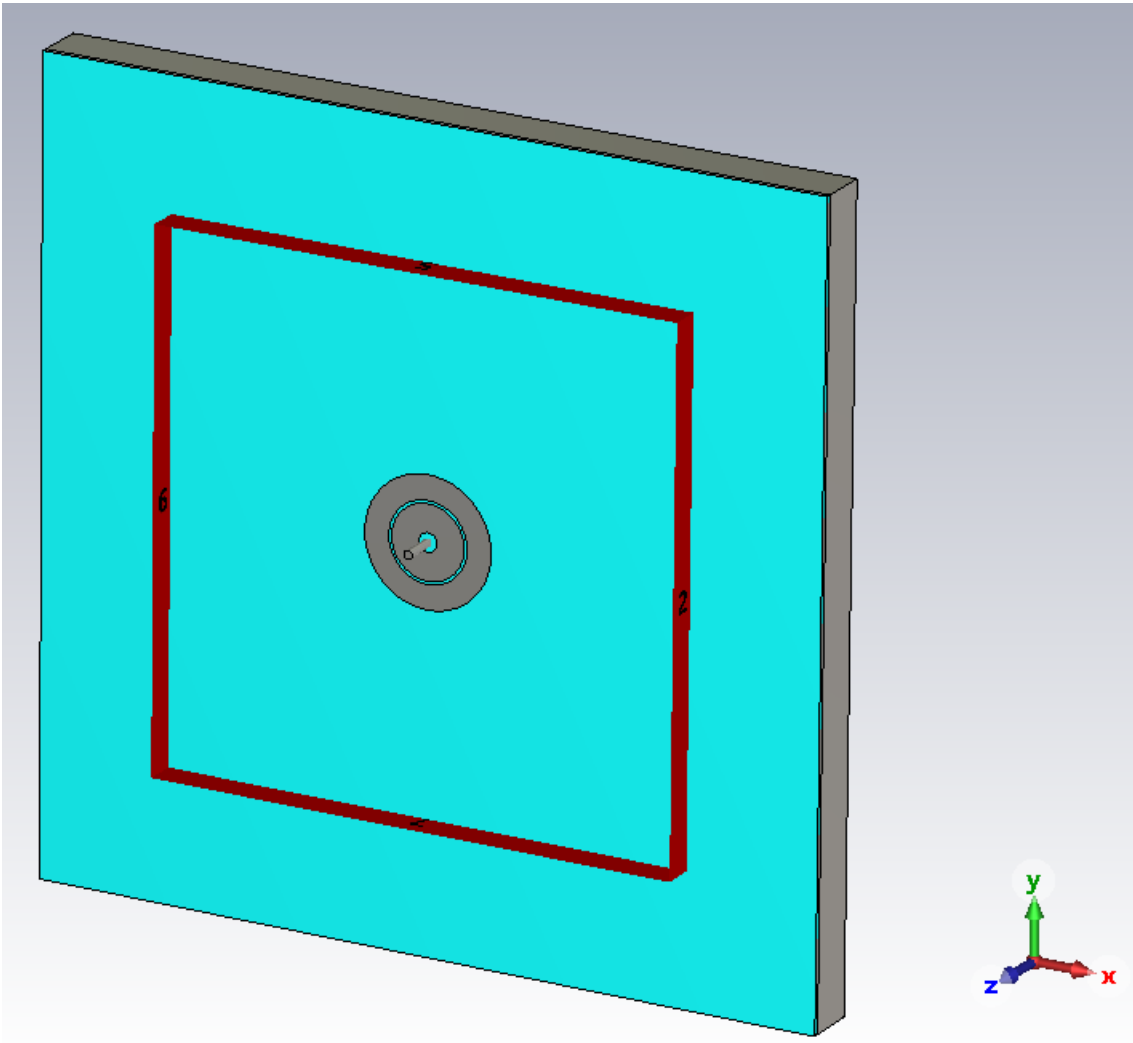


Figure 37: CST 3D perspective view of the model used for feed efficiency optimization. Red elements are the waveguide ports implemented to measure the surface wave power propagating through the dielectric substrate.

It can be noticed that the exploited waveguide ports go through the substrate for its entire thickness and stop at the interface with the GND plane (since no power should be propagating within the conductor plane). On the contrary, the ports are partly extended in the air in order to correctly include the surface wave components that are partly radiated in free space.

Through the exploitation of the presented method, the feed efficiency of the consid-

ered structure can be obtained considering the ratio between the value of the power that flows through the surrounding ports and the power delivered by the feeding port. In Figure 38 the comparison between the two mentioned power trends is reported. At the operating frequency of 23 GHz, the feed efficiency can be computed as:

$$\varepsilon_{feed} = \frac{P_{sw}|_{23}}{P_{in}|_{23}} = \frac{0.22}{0.49} \simeq 45\%$$

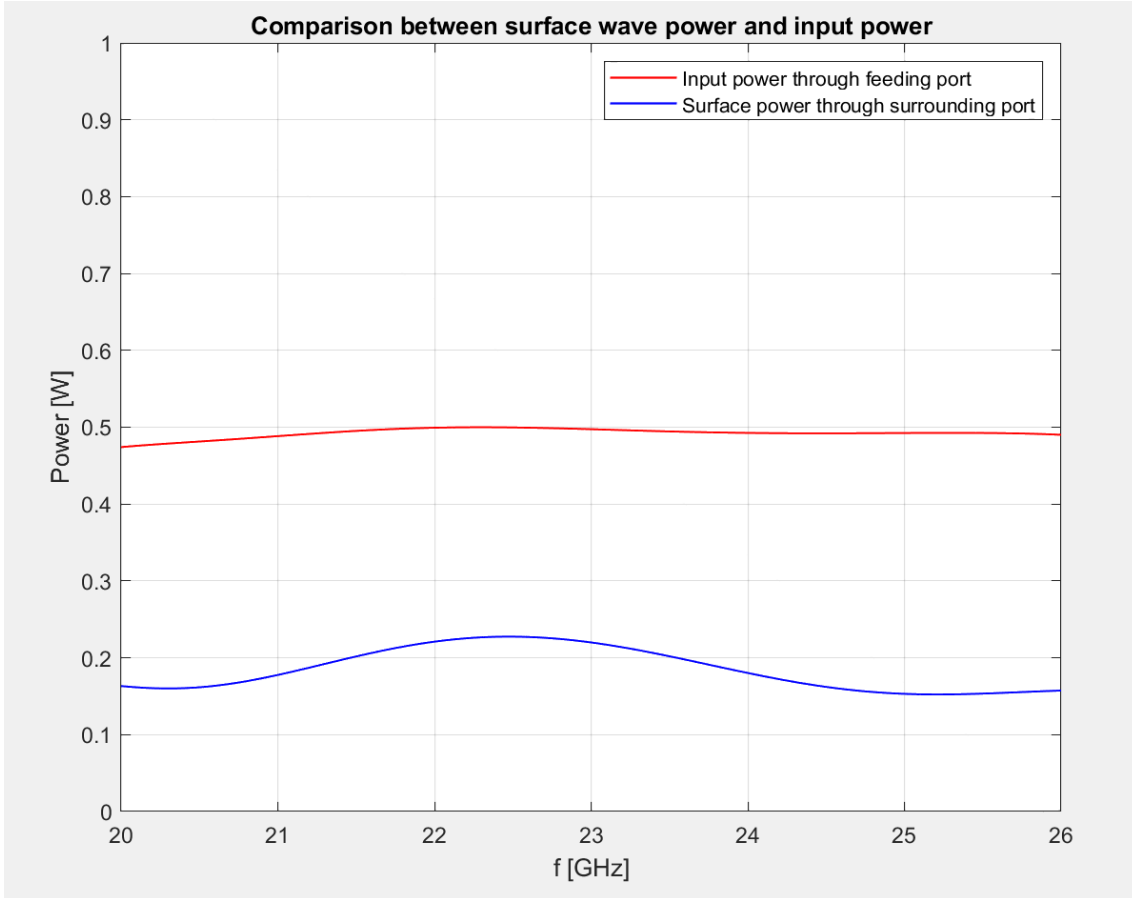


Figure 38: Comparison between SW and input power trends. Red curve shows the input power, blue curve shows the SW power.

Where, P_{sw} is the amount of power measured with the waveguide ports placed within the substrate, while P_{in} is the amount of power that is propagated by the feeder, accounting for reflections.

However, it must be said that no concrete optimized results are obtained. This can possibly be related to wrong considerations adopted for the definition of the ports introduced within the dielectric substrate and the relative powers that flow through them. Hence, it is important to highlight that this SW measuring method is surely not conclusive. Accurate further evaluation and developments are necessary to validate the presented investigation.

4.4 Simulation results and performance of complete MTS structure

In this section, the simulation results of a complete MTS antenna are reported and discussed. The presented antenna is obtained by generating each structure by exploiting the automatic code.

The design is realized considering an operating frequency of 23 GHz and using a circular geometry. The implemented structure is composed of a *Megtron-7* laminate dielectric substrate which presents:

- dielectric constant $\epsilon_r = 3.34$;
- dielectric height $h = 0.508$ mm;
- diameter $d = 12\lambda \simeq 156$ mm;
- ideal ground plane.

The MTS is printed on the surface of the dielectric slab realizing unit cells with $\lambda/6$ dimensions. Double anchor shapes are exploited as radiating elements.

In order to neglect losses and introduce a slight simplification, each conductor element is considered lossless, infinitely thin, and made by PEC.

In Figure 39 is shown the CST implementation of the mentioned MTS antenna. Inside the pane, it can be noticed a zoomed view of the implemented radiating elements and the design of the used feeder. More precisely, in this case, it is not used the optimized annular feeder termination discussed in Section 4.2, but just a monopole feeder with an optimized height is used to radiate a TM_0 cylindrical SW. This is due to the impedance distribution which, being related to a study prior to the optimization presented in this paper, does not consider any annular patches around the central feeder.

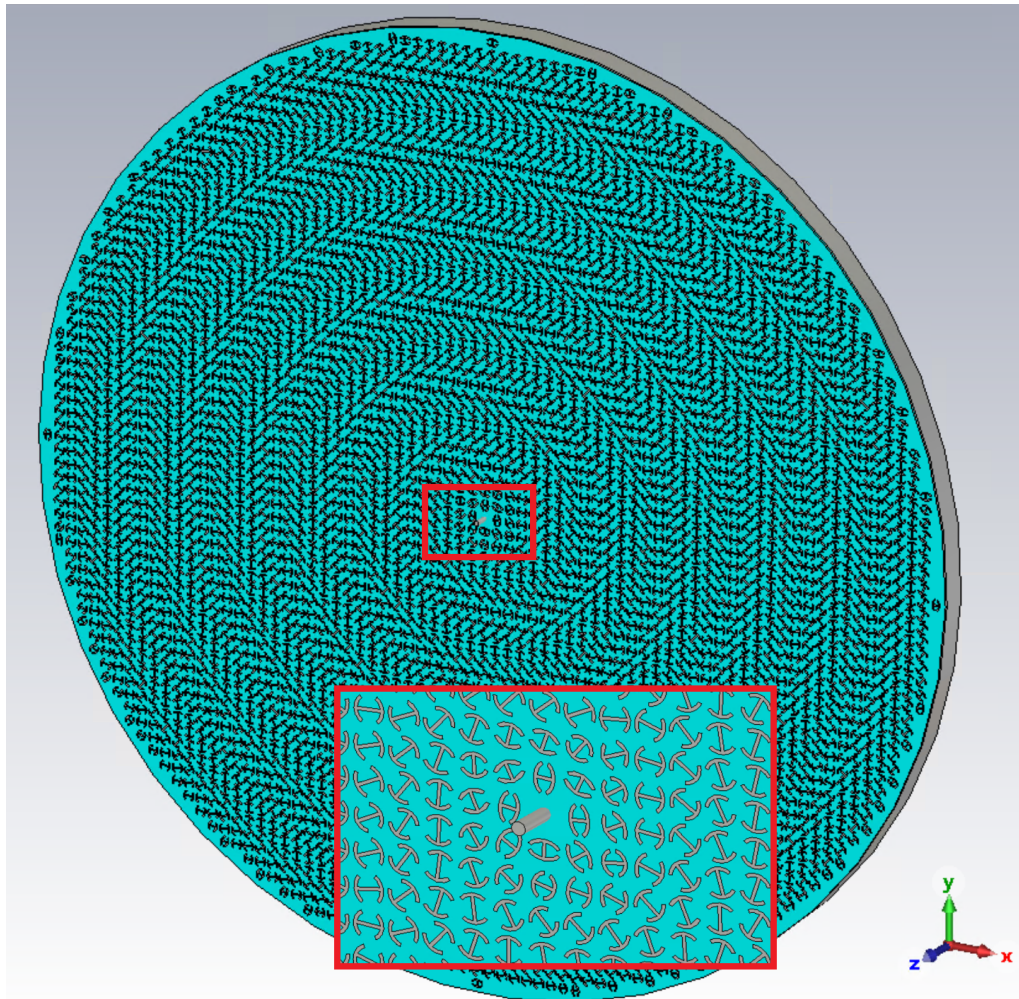
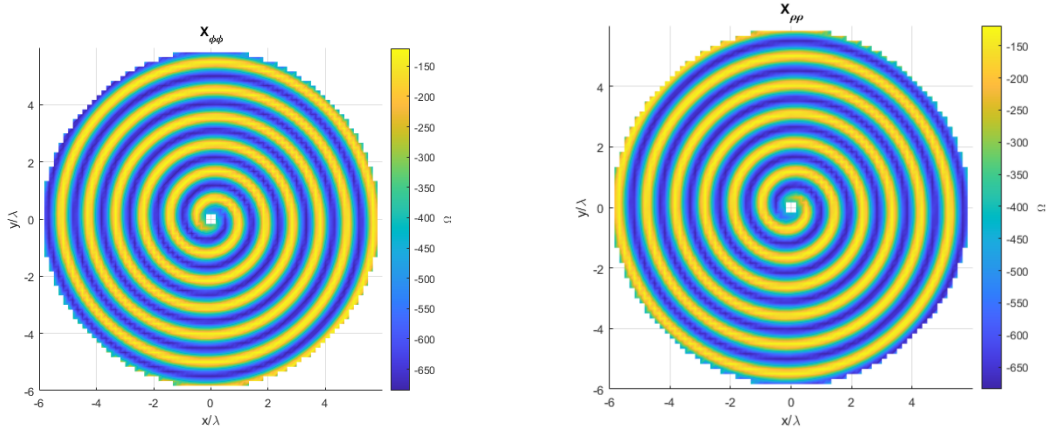


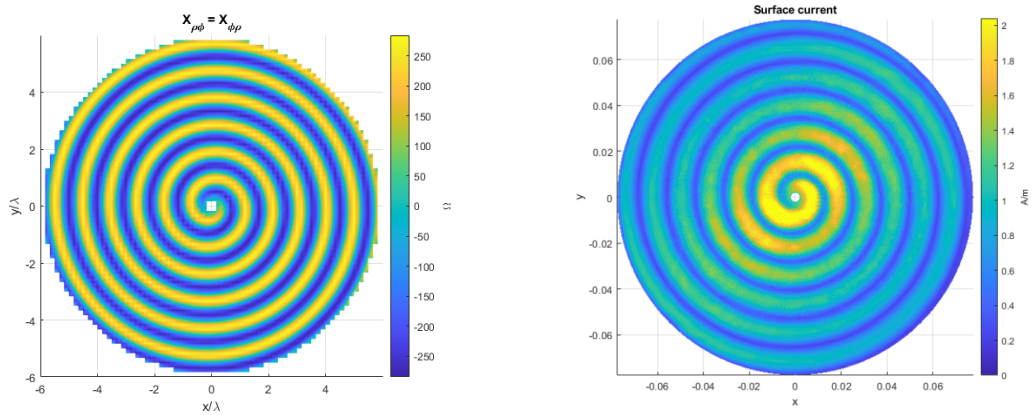
Figure 39: CST implementation of the complete MTS antenna with double anchors elements. The pane shows the zoomed view of radiating elements and the feeding system exploited for the considered design.

The reported structure is designed by using 4050 double anchors and the orientation of each element is ruled by specific polar rotations in such a way as to reconstruct the desired current density and surface impedance distribution. Tensorial components for reactance and optimized current are shown in Figure 40.



(a) Reactance distribution within the dielectric substrate for $\phi\phi$ component.

(b) Reactance distribution within the dielectric substrate for $\rho\rho$ component.



(c) Reactance distribution within the dielectric substrate for $\rho\phi$ component.

(d) Optimized current density within the dielectric substrate.

Figure 40: Reactance and optimized current distributions for the complete double anchors MTS antenna. Patterns are exploited to synthesized the MTS lattice.

Considering the large number of cells and their very small dimensions, the use of tetrahedral meshing exploited by frequency domain solver is not allowed because it would require the use of a machine with extremely high computational power. Therefore, for the simulation of the presented design, the time domain solver with hexahedral mesh is exploited. Taking into account the non-ideal precision of hexahedral meshing of the *Transient Solver* method (compared to *FEM* based solvers), a rather high level of mesh accuracy is chosen in order to compensate for the use of a solver type that is not exactly suitable for the purpose of interest. Once ran the time domain simulation, *26 million meshcells* are created by the solver to model the antenna structure.

Firstly *3D graphs* of FF Directivity are reported in Figure 41 and Figure 42 to better appreciate how the designed antenna is able to radiate in free space. As can be seen,

the pattern is described by a quasi-ideal pencil beam radiation

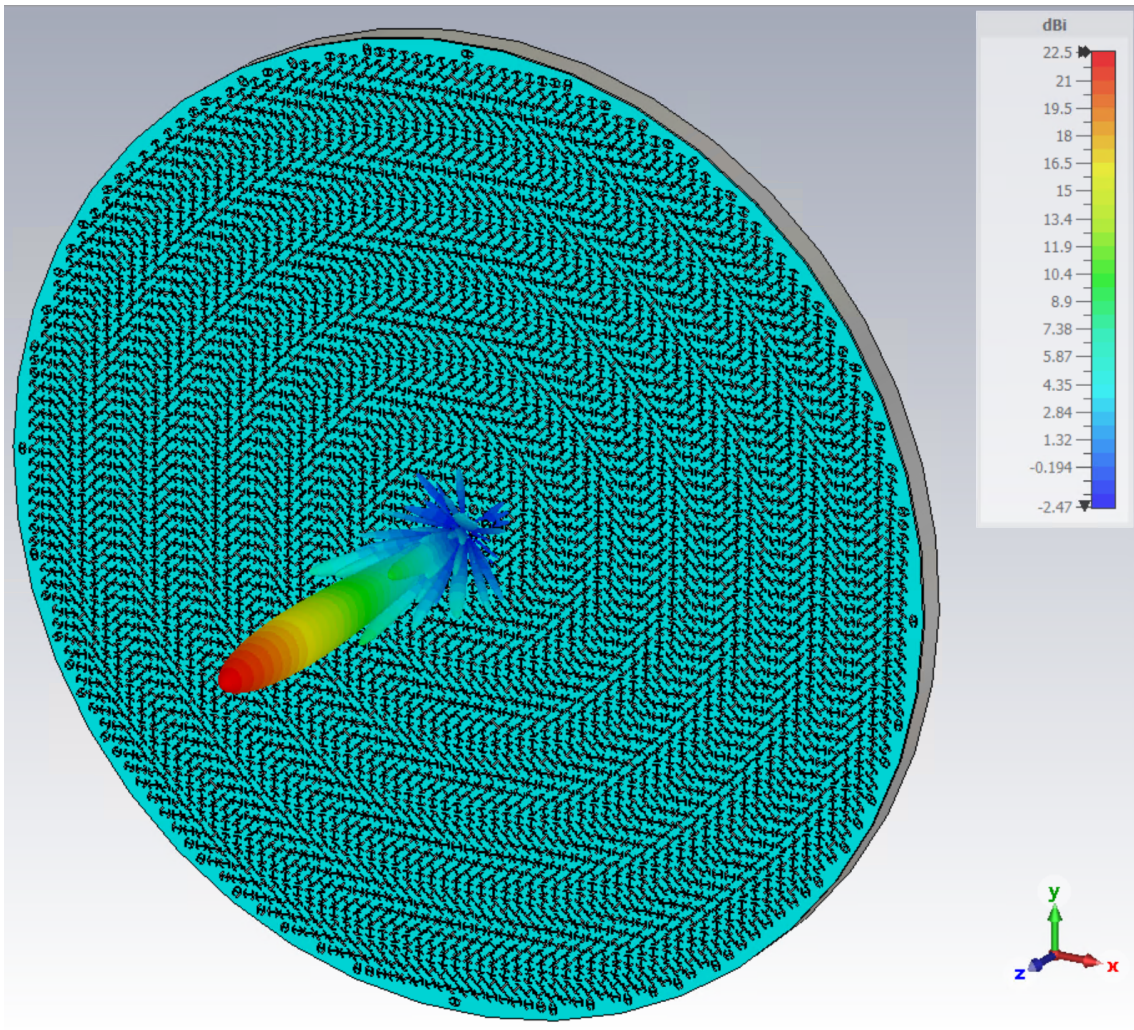


Figure 41: Perspective CST view of the FF radiation of the complete MTS antenna structure with double anchor elements.

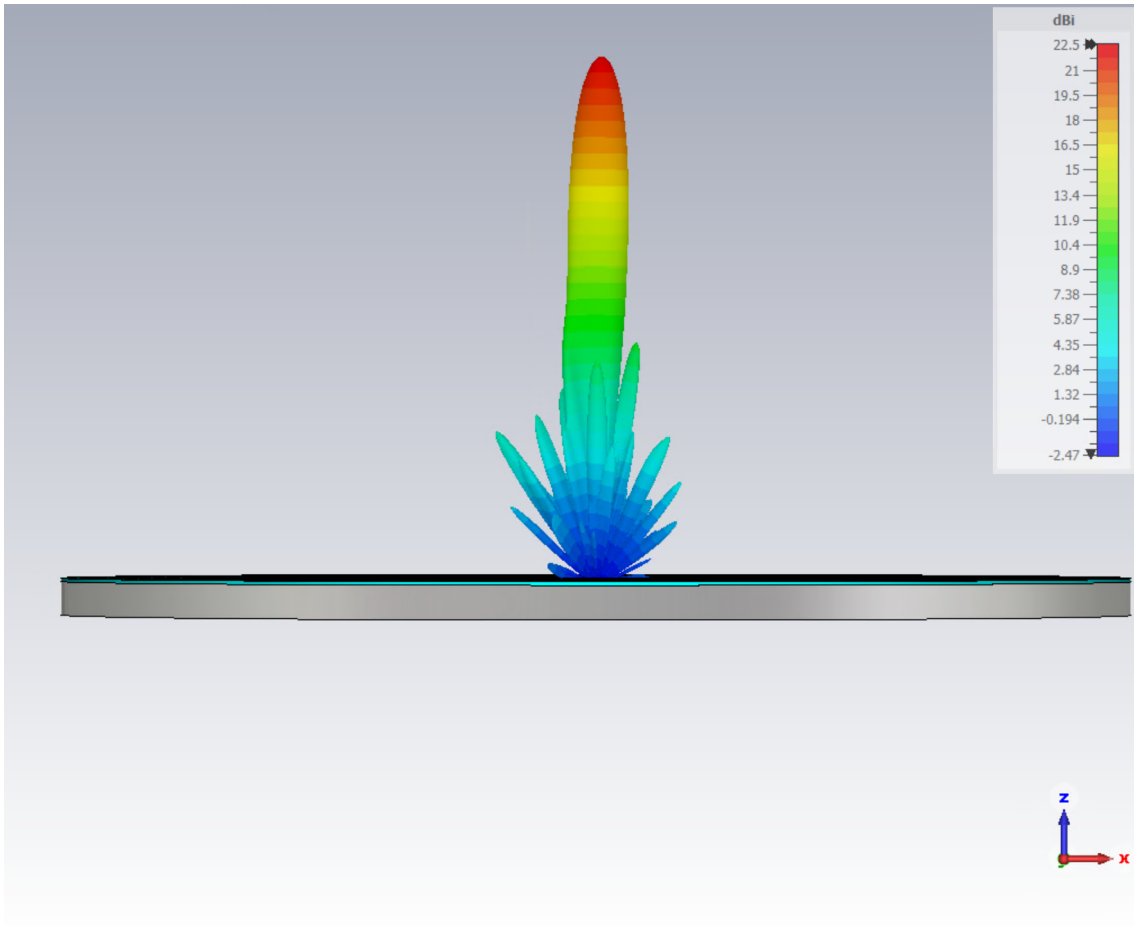
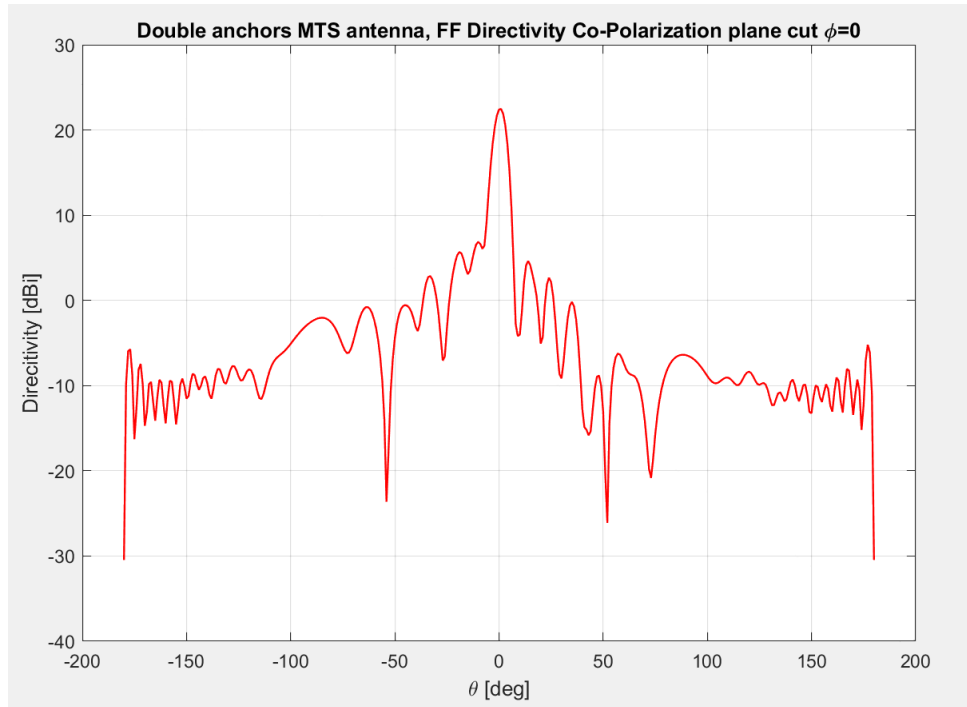
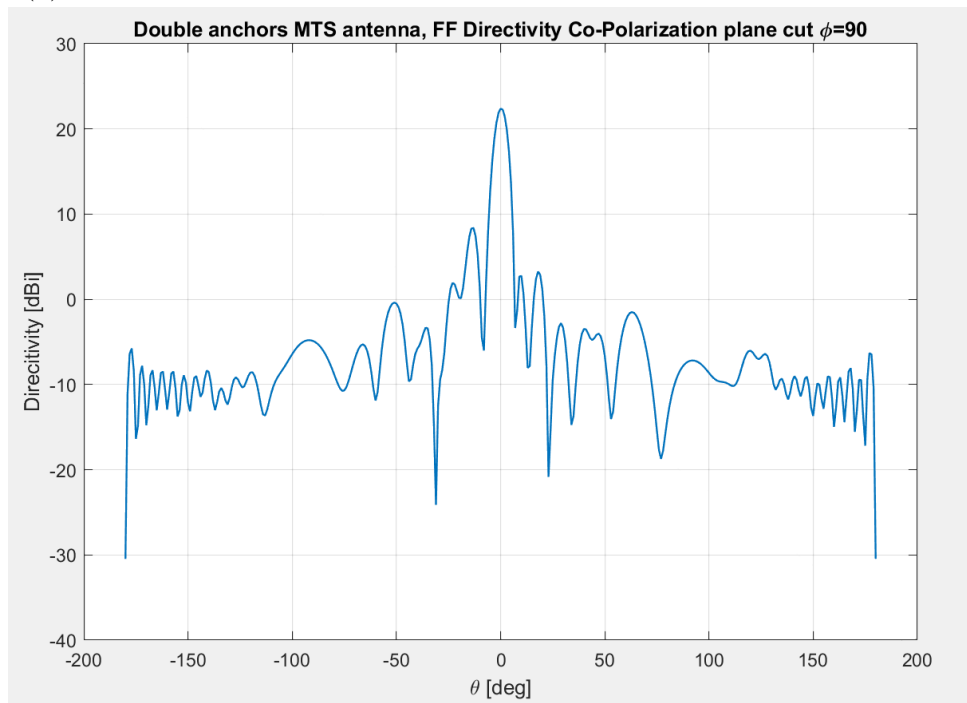


Figure 42: Lateral CST view of the FF radiation of the complete MTS antenna structure with double anchor elements.

In order to better discuss about the directivity results obtained by simulating the antenna, *1D Co-Polarization* patterns for both plane cuts $\phi = 0$ and $\phi = 90$ are reported in Figure 43.



(a) Co-Polarization component of FF Directivity in the plane cut $\phi = 0^\circ$.



(b) Co-Polarization component of FF Directivity in the plane cut $\phi = 90^\circ$.

Figure 43: Simulation results, FF Directivity Co-Polarization components of the designed MTS antenna for different plane cuts.

In both graphs it can be observed that the implemented MTS structure does not

present any kind of symmetry since for negative and positive values of θ no symmetric pattern is obtained. Also, no largely good values of max directivity are achieved, since the main lobe shows a magnitude of 22.4 dBi . However, as previously stated, the pattern shows quite good behavior in terms of beam width since a 6° HPBW is achieved. Also an acceptable *Side Lobe Level* is shown considering a maximum magnitude, related to the first side lobe, that is 15 dB lower than the main lobe.

At last, also an acceptable result for the reflection coefficient is obtained since a $S_{11} = -21 \text{ dB}$ is measured at the given operating frequency.

4.4.1 Impedance reconstruction results

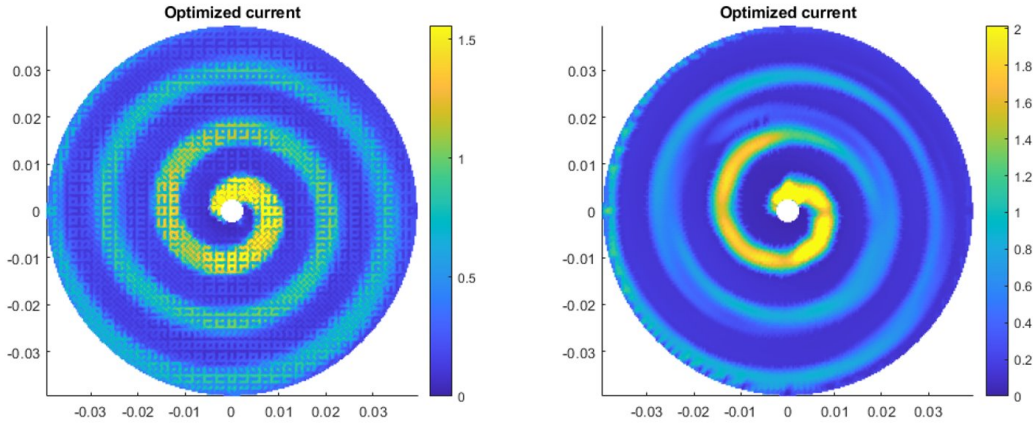
The method described in Section 3.7 is exploited to design a circular Metasurface antenna. For both square and hexagonal cells, two different cases are examined: *isolated cells*, where each unit cell is electrically neutral with respect to adjacent ones, and *continuous cells*, described by a continuous surface current within nearby cells.

The considered operating frequency is 23 GHz which describes a wavelength value of $\lambda = 13.04 \text{ mm}$.

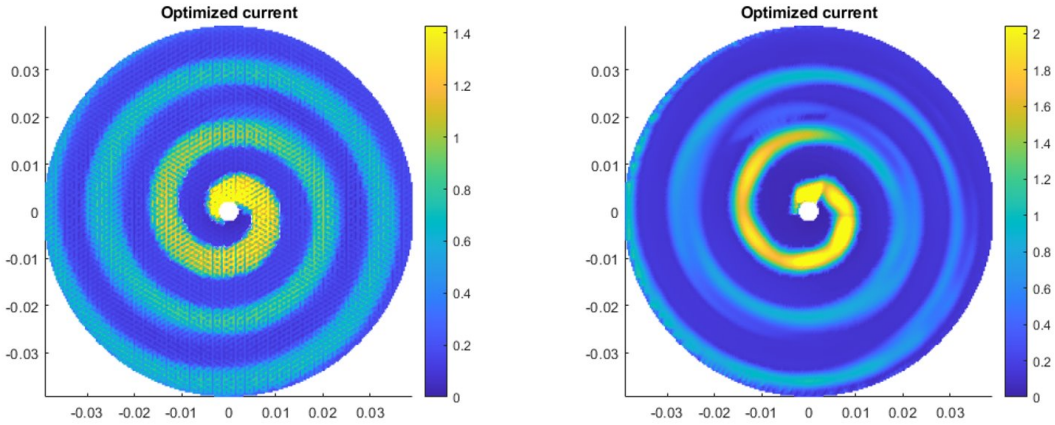
A laminate dielectric substrate with *high dielectric constant* is considered to design the circular antenna structure. This is particularly described by:

- $\epsilon_r = 6.5$;
- $\mu_r = 1$;
- substrate height $h = 0.508 \text{ mm}$;
- substrate diameter $d = 6\lambda \simeq 78 \text{ mm}$.

Figure 44 highlights the differences between the optimized current density distribution within the dielectric substrate when continuous and isolated cells are considered.



(a) Current density profile considering square isolated cells partitioning. (b) Current density profile considering square continuous cells.

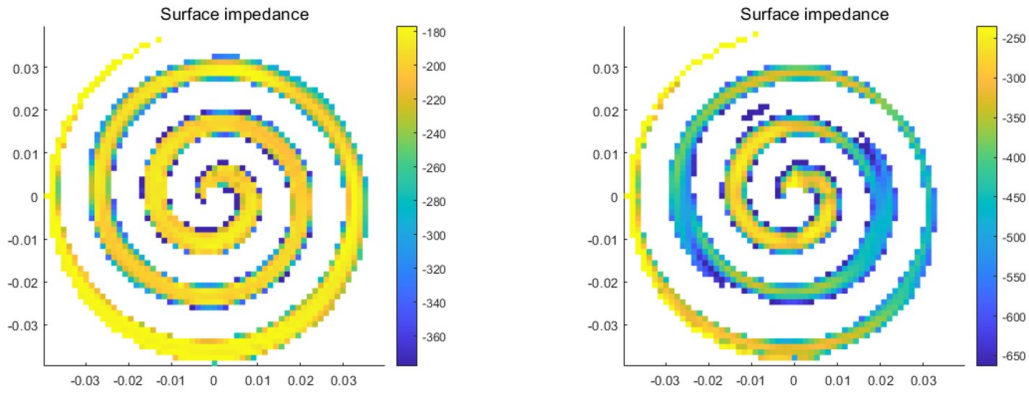


(c) Current density profile considering hexagonal isolated cells partitioning. (d) Current density profile considering hexagonal continuous cells.

Figure 44: Current density distributions for isolated and continuous MTS cells partitioning.

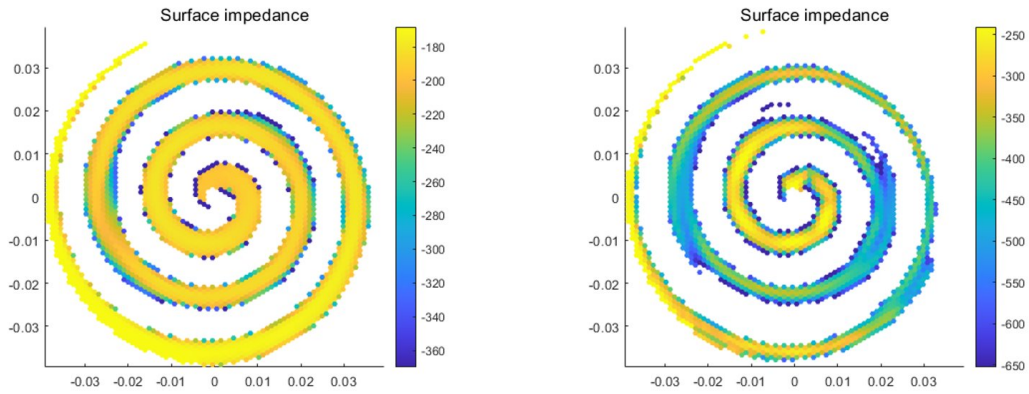
From the shown current densities, four different surface impedance distributions are obtained by exploiting the synthesis algorithm for IBC modeling. Results are reported in Figure 45.

Particular attention must be paid to the reactance profile that rules the MTS partitioning. Indeed, exploiting this solution, a surface granularity is introduced which is related to a reduction of accuracy due to decreasing the effective degrees of freedom.



(a) Surface reactance profile synthesized considering square isolated cells partitioning.

(b) Surface reactance profile synthesized considering square continuous cells partitioning.

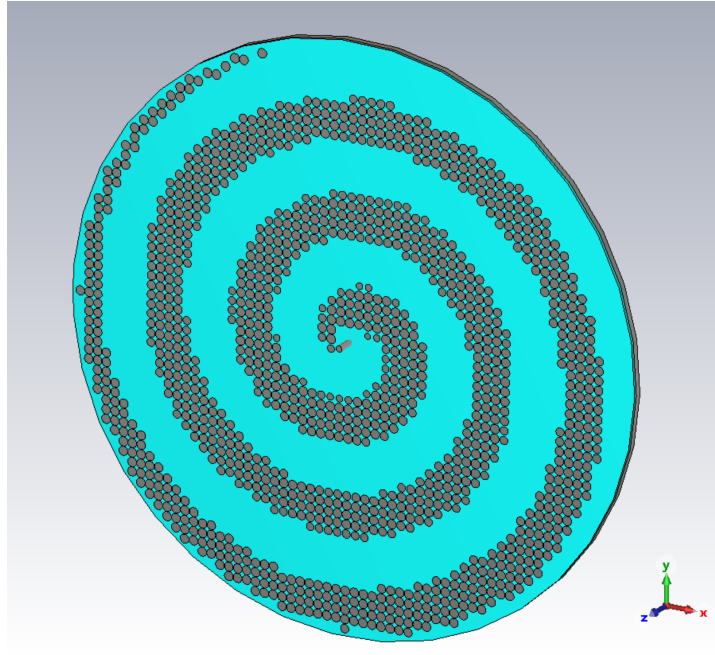


(c) Surface reactance profile synthesized considering hexagonal isolated cells partitioning.

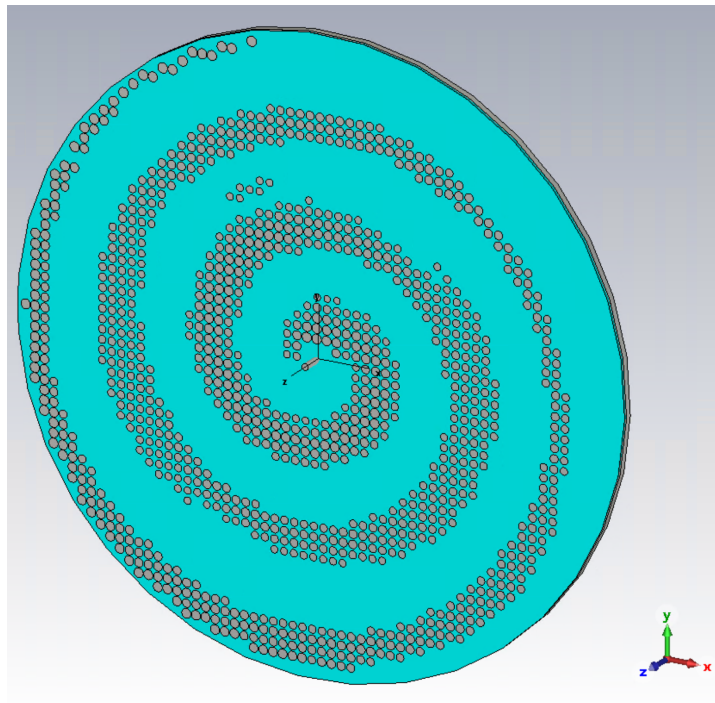
(d) Surface reactance profile synthesized considering hexagonal continuous cells partitioning.

Figure 45: Current density and synthesized reactance profiles for square and hexagonal MTS partitioning.

The structure designed in CST shown in Figure 46 is obtained by implementing an MTS lattice partitioning ruled by square isolated and continuous cells.



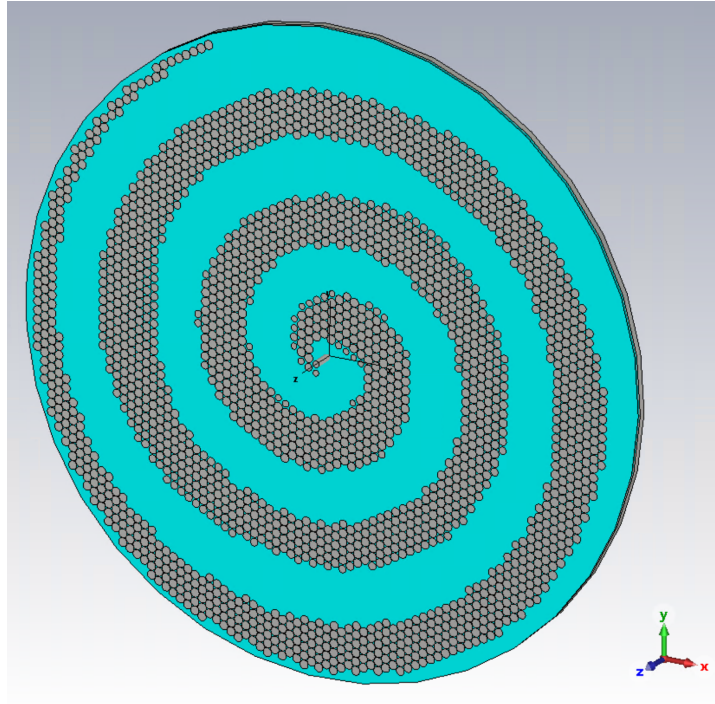
(a) Square isolated cells case.



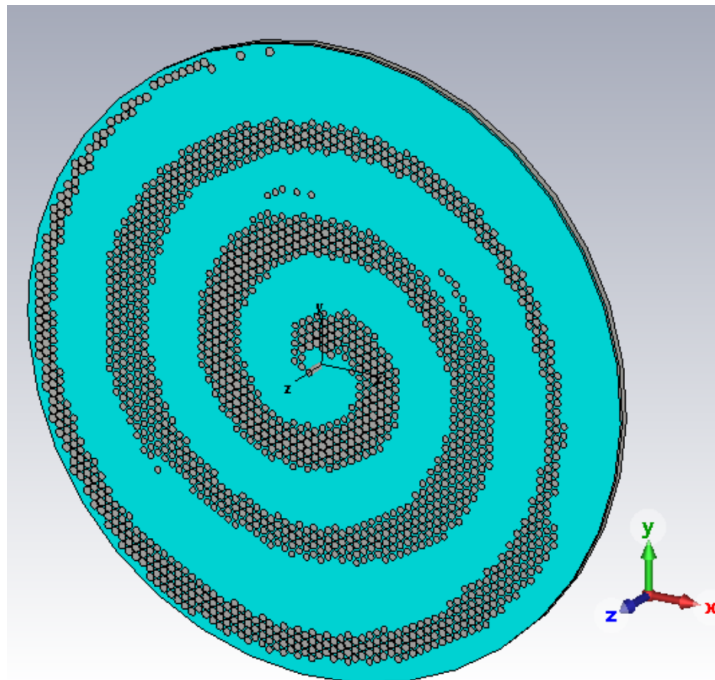
(b) Square continuous cells case.

Figure 46: CST view of MTS circular antenna with circular patches designed exploiting square cells.

In the same way, Figure 47 shows the complete MTS antenna designed using hexagonal cells for both isolated and continuous cases.



(a) Hexagonal isolated case.



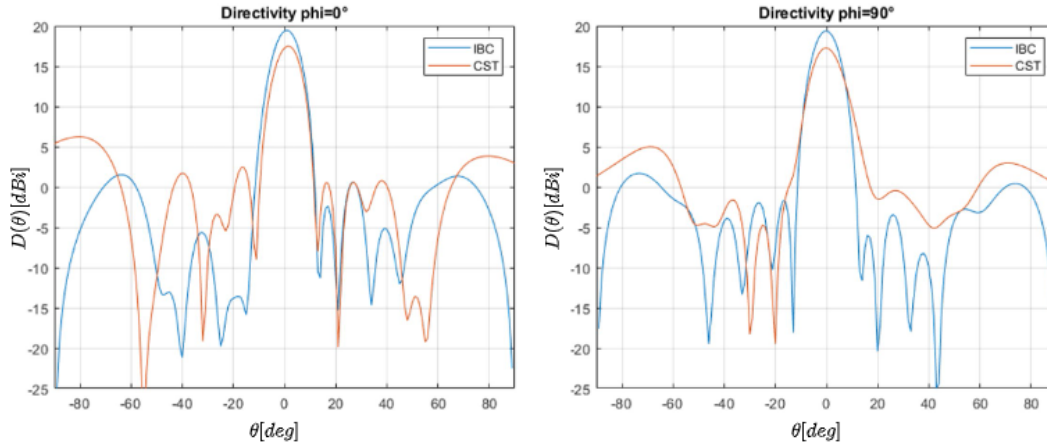
(b) Hexagonal continuous case.

Figure 47: CST view of MTS circular antenna with circular patches designed exploiting hexagonal cells.

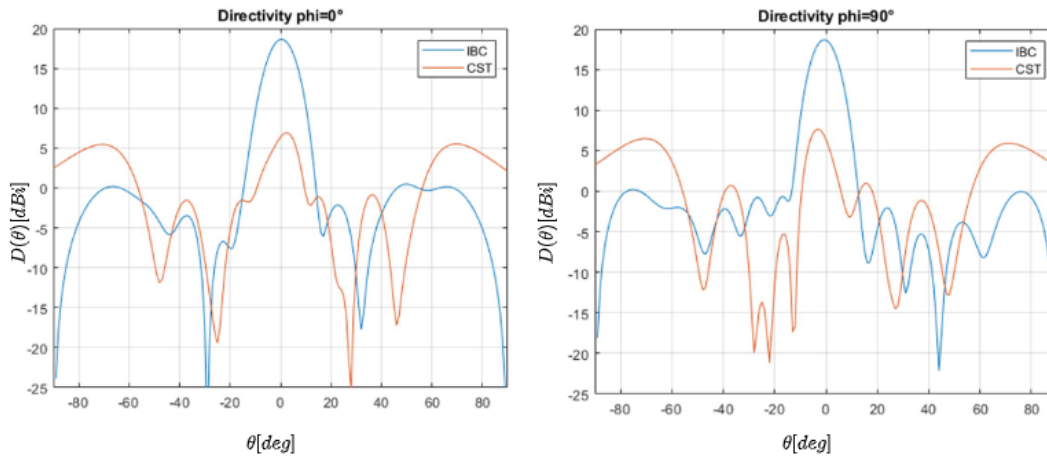
The synthesized radiation profiles that come out from the current method solver

(by solving IBC) are compared with the simulation results obtained through the full-wave simulation of the designed MTS antenna. The FF directivity comparison is reported in the following figures where Co-Polarization trends in the plane cut $\phi = 0^\circ$ and $\phi = 90^\circ$ are shown.

Figure 48 and Figure 49 show the results for isolated and continuous cells comparisons.

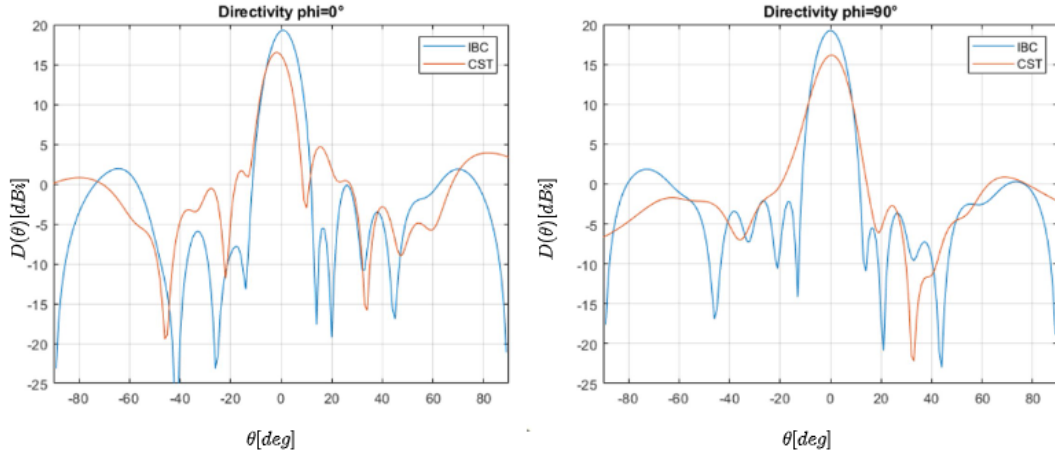


(a) Square isolated case.

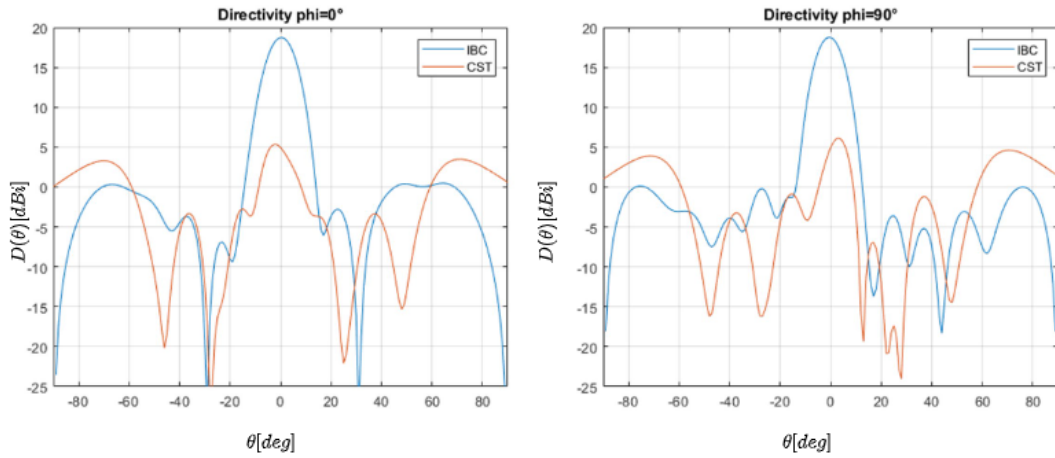


(b) Square continuous case.

Figure 48: Comparisons of FF Directivity plane cut $\phi = 0^\circ$ and $\phi = 90^\circ$ for square isolated and continuous MTS partitioning.



(a) Hexagonal isolated case.

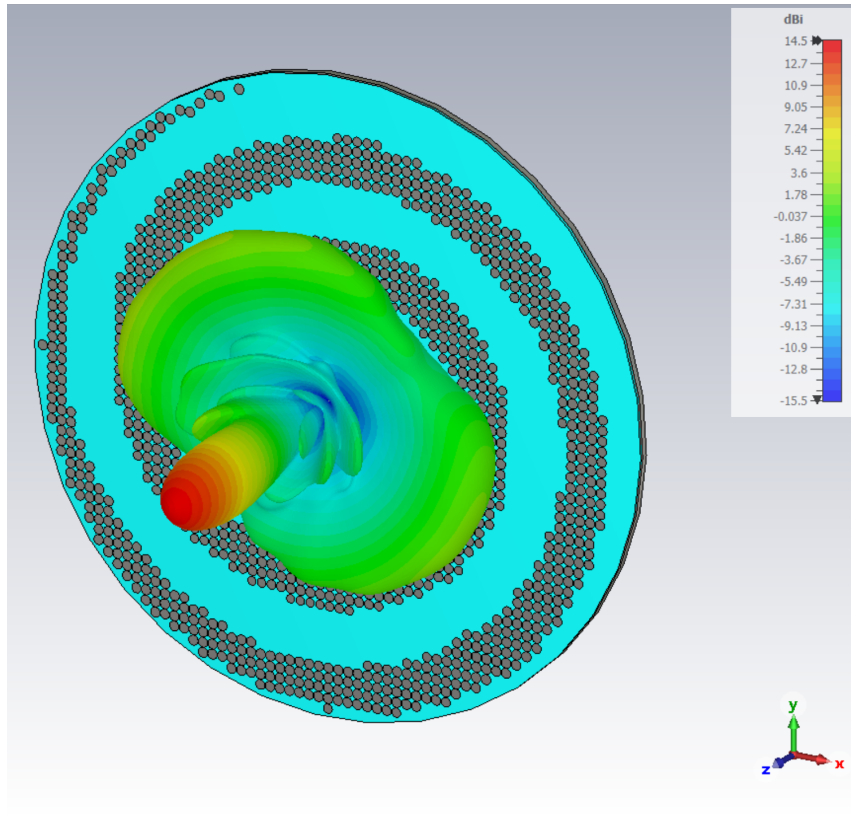


(b) Hexagonal continuous case.

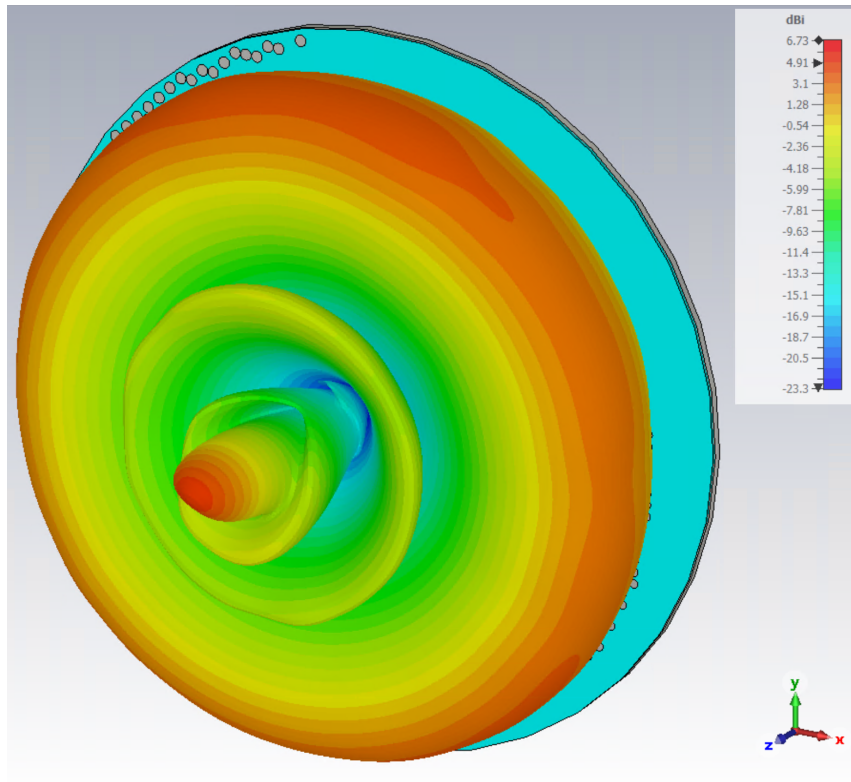
Figure 49: Comparisons of FF Directivity plane cut $\phi = 0^\circ$ and $\phi = 90^\circ$ for hexagonal isolated and continuous MTS partitioning.

What can be achieved by looking at the reported graphs is that, both for square and hexagonal cells, the Directivity trends obtained through full-wave simulation are quite congruent with the synthesized IBC results just in the case of isolated cells (Figure 49a, Figure 48a). Instead, for continuous cells distribution the simulation results are quite far from the synthesized ones.

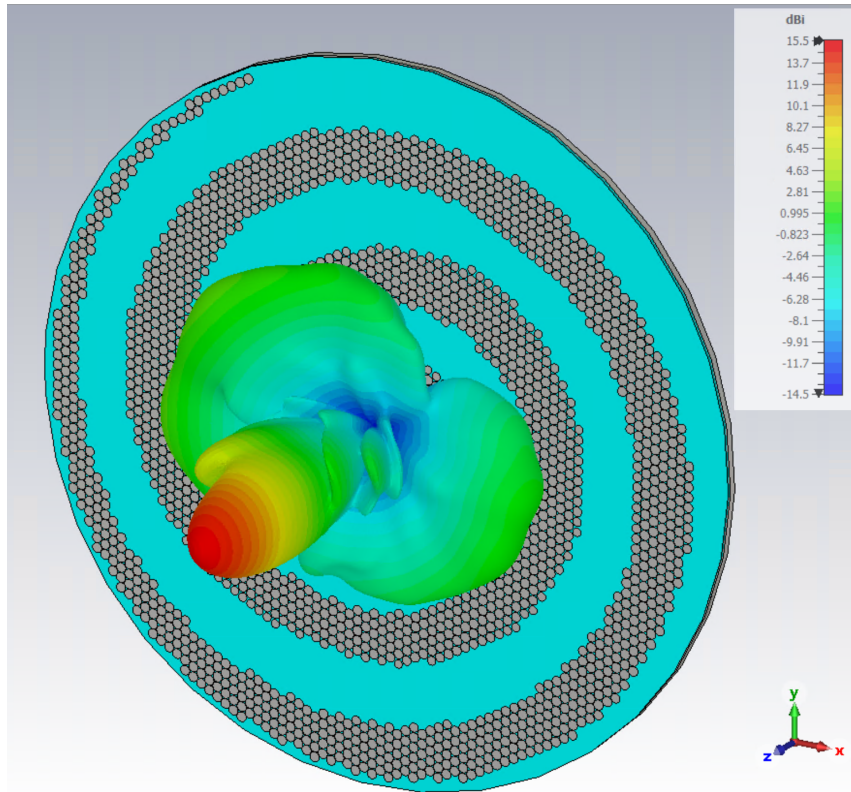
Generally speaking, the radiation results of the designed antenna are not strictly the best that can be achieved but, the optimization of the presented antennas is outside the scope of this thesis. At last, Figure 50 shows the 3D FF radiating results for each reported design.



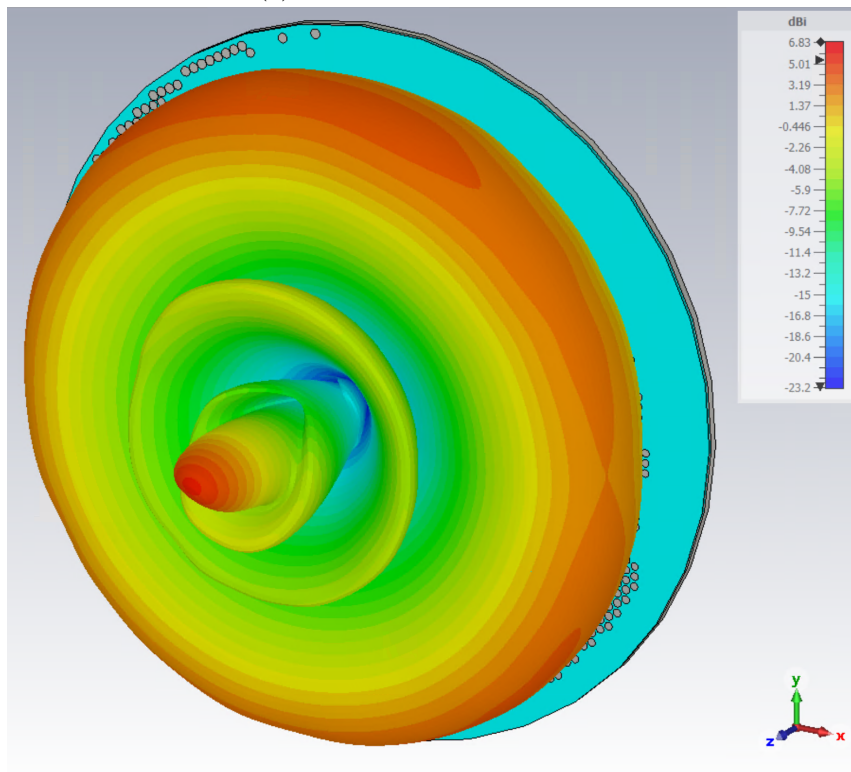
(a) Square isolated case.



(b) Square continuous case.



(c) Hexagonal isolated case.



(d) Hexagonal continuous case.

Figure 50: 3D FF Directivity for each designed MTS antenna.

The faced comparison is extremely important since full-wave CST simulation allows to realistically model and design the structure. Therefore, the extracted results confirm and validate the importance of a design based on isolated cells.

In fact, by the congruence achieved between synthesized and full-wave results for the “isolated” designs it is possible to demonstrate that, by exploiting isolated cells, the coupling effects between adjacent elements are correctly modeled at full-wave level. To conclude, this allows to obtain, already at the synthesis stage, an impedance distribution optimized for “*less idealized*” applications.

From what is reported, the importance of the automatic generation for such complicated structures in full-wave simulation environments can be truly understood.

4.5 Discussion on improvements

Considering the increasing interest in MTS systems, the development of improvements related to the automatic generation method presented in this work could be very useful for future projects.

Firstly, a refinement strictly related to the execution of the automatic code should be discussed. The generation of tricky structures, such as the double anchor profiles, is linked to the execution of numerous instructions because of the combination of multiple geometric shapes. This kind of implementation makes the generation of thousands of those elements problematic in terms of time spent just on generating the MTS structure.

The solution could be reached by changing the generation mode of the cells themselves. In particular, an improvement could be represented by the generation of a single double anchor profile which then would be iteratively *copied*, *rotated*, *scaled* (if necessary), and *translated* in the specific spatial position related to the n -th cell. Considering the CST functioning, this solution is however linked to the complexity increase of the file where input parameters are stored. Indeed, in this case, the rotation angles would no longer be related to the center of the belonging unit cell but each angle should be evaluated starting from the value of the previous one. Moreover, also the sizing of each element would be managed in a more complex way, in fact instead of simply declaring the size of each element, the value of the scale factor should be iteratively declared with respect to the previous element.

The discussed complexity increase would be validated only for complicated elements shape whose generation is linked to long generation time.

Furthermore, considering the introduced and discussed method of MTS synthesis, a very interesting enhancement could be linked to the development of an interface between the automatic code and a dedicated database. More in detail, in previous chapters the automatic generation of the elements that compose the antenna structure was presented as managed by the user’s parameters given as input to the specific functions. As shown, parameters such as the position and dimensions of

the radiating elements can be stored in data files (*.csv*, *.txt*, etc), as done for full structures discussed in Section 4.4.

Thus, the idea could be to organize a database in such a way as to, starting from a specific impedance distribution chosen by the user, generate and return a data file which contains the correct parameters for the specific case of interest. Once the data file is generated, it is provided to the automatic code which, by extracting the input values, would be at that point able to generate the complete MTS antenna structure by implementing the correct impedance distribution.

The discussed improvement could also be enhanced by the development of a *Graphic User Interface (GUI)* which would realize a more user-friendly and intuitive functioning of the automatic code generation. In this case, just the desired impedance profile and specific system parameters, such as the operating frequency, and the substrate features, would be chosen and defined by the user. The exploitation of the correct functions for the desired design will no longer be declared by the user but they would be automatically managed by the execution of the developed app.

5 Conclusions

Full-wave simulation allows considering a lower degree of ideality for the inspection of antenna design performance. This approach is directly linked to the possibility of designing more realistic antenna structures and turns out to be a concrete way to optimize a considered system before its physical realization.

Since crucial differences with ideal numerical methods could be found out in some applications, the current attention and employment of MTS systems validate the need for a full-wave oriented analysis method to design specific systems.

Throughout this thesis work, it was discussed on the technological improvements which the presented MTS systems are related to. Considering the analyzed reduction of structural complexity compared with different high performance solutions, it was demonstrated how, the application of such kinds of antennas, can represent an improvement for different application areas.

Once pointed out the benefits to which Metasurface antennas are linked, the automatic generation of each component of a generic MTS antenna was reported and explained with a step-by-step visualization of the written Matlab functions. Thus, the correct operation of the automatic code was demonstrated by reporting the obtained structures.

It was largely discussed and proven how the antenna radiation features can be controlled by the modelization of the implemented MTS. This characteristic is particularly exploited to impose a certain impedance boundary condition (IBC) that is able to provide a controlled transformation of the propagating surface wave into a leaky wave which is gradually radiated.

As done for the MTS designs presented in Section 4.4.1, the development of an automatic generation code plays a key role in the validation of the numerical approach for MTS synthesis.

The main purpose of the automatic generation was then validated by running the simulation sessions discussed through which it was possible, first, to obtain an optimized design of the feeder structure that would later be exploited in the complete antenna structures, and second, to validate the performance of the MTS antennas through full-wave simulations.

To conclude, according to what was largely discussed and demonstrated, in order to aim for realistic modeling of the interested structures, it can be emphasized the importance of the availability of an easy and guided generation of the MTS distribution within simulation environments able to provide full-wave results.

Bibliography

- [1] Li, Aobo, Singh, Shreya and Sievenpiper, Dan. “Metasurfaces and their applications” *Nanophotonics*, vol. 7, no. 6, 2018, pp. 989-1011.
<https://doi.org/10.1515/nanoph-2017-0120>
- [2] Martini E, Mencagli Jr M, Maci S. 2015 Metasurface transformation for surface wave control. *Phil. Trans. R. Soc.A* 373:20140355.
<http://dx.doi.org/10.1098/rsta.2014.0355>
- [3] Michael Selvanayagam and George V. Eleftheriades, “Discontinuous electromagnetic fields using orthogonal electric and magnetic currents for wavefront manipulation,” *Opt. Express* 21, 14409-14429 (2013)
- [4] Faenzi, M., Minatti, G., González-Ovejero, D. et al. Metasurface Antennas: New Models, Applications and Realizations. *Sci Rep* 9, 10178 (2019). <https://doi.org/10.1038/s41598-019-46522-z>
- [5] D. González-Ovejero, G.Chattopadhyay, and S. Maci, “Multiple beam shared aperture modulated metasurface antennas” in *Proc. IEEE AP-S Soc. Int. Symp.*, Fajardo PR, Jul. 2016.
- [6] Y. B. Li, X. Wan, B. G. Cai, Q. Cheng, T. J. Cui, “Frequency-controls of electromagnetic multi-beam scanning by metasurfaces”, *Scientific Reports*, Vol 4: 6921, 5 November 2014.
- [7] Gonzalez-Ovejero, David; Minatti, Gabriele; Chattopadhyay, Goutam; Maci, Stefano (2017). Multibeam by Metasurface antennas. *IEEE Transactions on Antennas and Propagation*, (), 1–1. doi:10.1109/TAP.2017.2670622
- [8] Jorge Ruiz-García; Marco Faenzi; Adham Mahmoud; Mauro Ettore; Patrick Potier; Philippe Pouliguen; Ronan Sauleau; David González-Ovejero. Multi-beam modulated metasurface antenna for 5G backhaul applications at K-band. *Comptes Rendus. Physique*, Volume 22 (2021) no. S1, pp. 47-52. doi : 10.5802/crphys.62. <https://comptes-rendus.academie-sciences.fr/physique/articles/10.5802/crphys.62/>
- [9] Pozar, David M. *Microwave Engineering*, 4th Edition. Hoboken, NJ :Wiley, 2012.
- [10] W. W. Hansen, BRadiating electromagnetic waveguide,[U.S., Patent 2.402.622, 1940
- [11] C. H. Walter, *Traveling Wave Antennas*. New York: McGraw-Hill, 1965.
- [12] D. R. Jackson and A. A. Oliner, “Leaky-wave antennas,” in *Modern Antenna Handbook*, C. Balanis, Ed. New York, NY, USA: Wiley, 2008.
- [13] F. Monticone and A. Alù, “Leaky-Wave Theory, Techniques, and Applications: From Microwaves to Visible Frequencies,” in *Proceedings of the IEEE*, vol. 103, no. 5, pp. 793-821, May 2015, doi: 10.1109/JPROC.2015.2399419.

- [14] Multiscale EM modeling of metasurfaces and interfaces - Prof. Giuseppe VECCHI - POLITO, at *EXEMI 2018*.
- [15] “*CST Studio Suite 2022*”, Dassault Systemes Simulia.
- [16] https://it.mathworks.com/matlabcentral/fileexchange/67731-hgiddenss-cst_app
- [17] G. Minatti, E. Martini and S. Maci, “Efficiency of Metasurface Antennas,” in *IEEE Transactions on Antennas and Propagation*, vol. 65, no. 4, pp. 1532-1541, April 2017, doi: 10.1109/TAP.2017.2669728.
- [19] Zucchi, Marcello; Righero, Marco; Vecchi, Giuseppe, “Current-Only Metasurface Design with Cell-Level Granularity,” *European Conference on Antenna and Propagation, Florence 2023*
- [20] Zucchi, Marcello; Vernì, Francesco; Righero, Marco; Vecchi, Giuseppe (2022), “Current-Based Automated Design of Realizable Metasurface Antennas with Arbitrary Pattern Constraints,” <https://doi.org/10.36227/techrxiv.20425260.v1>, Aug. 2022.